



Article

# Knock-Out of ACBD3 Leads to Dispersed Golgi Structure, But Unaffected Mitochondrial Functions in HEK293 and HeLa Cells

Tereza Daňhelovská <sup>1</sup>, Lucie Zdražilová <sup>1</sup>, Hana Štufková <sup>1</sup>, Marie Vanišová <sup>1</sup>, Nikol Volfová <sup>1</sup>, Jana Křížová <sup>1</sup>, Ondřej Kuda <sup>2</sup>, Jana Sládková <sup>1</sup> and Markéta Tesařová <sup>1,\*</sup>

- <sup>1</sup> Department of Paediatrics and Inherited Metabolic Disorders, Charles University, First Faculty of Medicine and General University Hospital in Prague, 128 01 Prague, Czech Republic; tereza.danhelovska@vfhn.cz (T.D.); lucie.zdrzilova@lf1.cuni.cz (L.Z.); Hana.Stufkova@vfhn.cz (H.Š.); Marie.Rodinova@vfhn.cz (M.V.); Nikol.Volfova@lf1.cuni.cz (N.V.); Jana.Krizova@vfhn.cz (J.K.); jsladkova@centrum.cz (J.S.)
- <sup>2</sup> Institute of Physiology, Academy of Sciences of the Czech Republic, 142 00 Prague, Czech Republic; Ondrej.Kuda@fgu.cas.cz
- \* Correspondence: marketa.tesarova@lf1.cuni.cz

**Abstract:** The Acyl-CoA-binding domain-containing protein (ACBD3) plays multiple roles across the cell. Although generally associated with the Golgi apparatus, it operates also in mitochondria. In steroidogenic cells, ACBD3 is an important part of a multiprotein complex transporting cholesterol into mitochondria. Balance in mitochondrial cholesterol is essential for proper mitochondrial protein biosynthesis, among others. We generated ACBD3 knock-out (ACBD3-KO) HEK293 and HeLa cells and characterized the impact of protein absence on mitochondria, Golgi, and lipid profile. In ACBD3-KO cells, cholesterol level and mitochondrial structure and functions are not altered, demonstrating that an alternative pathway of cholesterol transport into mitochondria exists. However, ACBD3-KO cells exhibit enlarged Golgi area with absence of stacks and ribbon-like formation, confirming the importance of ACBD3 in Golgi stacking. The glycosylation of the LAMP2 glycoprotein was not affected by the altered Golgi structure. Moreover, decreased sphingomyelins together with normal ceramides and sphingomyelin synthase activity reveal the importance of ACBD3 in ceramide transport from ER to Golgi.

**Keywords:** ACBD3; mitochondria; cholesterol; Golgi; OXPHOS; knock-out



**Citation:** Daňhelovská, T.; Zdražilová, L.; Štufková, H.; Vanišová, M.; Volfová, N.; Křížová, J.; Kuda, O.; Sládková, J.; Tesařová, M. Knock-Out of ACBD3 Leads to Dispersed Golgi Structure, But Unaffected Mitochondrial Functions in HEK293 and HeLa Cells. *Int. J. Mol. Sci.* **2021**, *22*, 7270. <https://doi.org/10.3390/ijms22147270>

Academic Editor: Janusz Blasiak

Received: 28 May 2021

Accepted: 1 July 2021

Published: 6 July 2021

**Publisher's Note:** MDPI stays neutral with regard to jurisdictional claims in published maps and institutional affiliations.



**Copyright:** © 2021 by the authors. Licensee MDPI, Basel, Switzerland. This article is an open access article distributed under the terms and conditions of the Creative Commons Attribution (CC BY) license (<https://creativecommons.org/licenses/by/4.0/>).

## 1. Introduction

Humans express seven highly conserved Acyl-CoA-binding proteins (ACBD1–ACBD7). A common feature of this protein family is the ACB domain, responsible for the binding of long-chain fatty Acyl-CoA esters. ACBD3 is the largest protein of this family, consisting, apart from the ACB domain, of a coiled-coil domain in the middle and a Golgi dynamics (GOLD) domain on the C terminus. The GOLD domain is responsible for multiple protein interactions and may be used to stabilize peripheral membrane proteins at intracellular membranes. As reported in The Human Protein Atlas [1], ACBD3 is highly expressed in some organs of the digestive system, brain, prostate, placenta, and bone marrow; medium expression is characteristic of male and female reproductive tissues (for a complete summary, see Table A1). According to its antibody validation profile, ACBD3 is localized in Golgi (The Human Protein Atlas) and is a membrane-bound or membrane-associated protein. Inferring from sequence similarity, it is probably also localized in mitochondria [1–3]. The MitoCarta predictions for ACBD proteins are summarized in Table A2.

According to published research [4–9], ACBD3 is a protein localized in endoplasmic reticulum (ER), Golgi, mitochondria, plasma membrane, and cytosol. ACBD3 participates in multiple protein–protein interactions and has various functions: a Golgi–ER tether or a Golgi scaffold protein, in vesicle trafficking (sphingolipid transport), mitochondrial

cholesterol transport/steroid synthesis, or in the regulation of cellular iron uptake. Moreover, it serves as a host interaction protein for the replication of multiple members of the picornavirus family (multiple ACBD3–protein interactions and its functions are well summarized in [10]) In this work, we focused on the role of ACBD3 in mitochondria.

The function of ACBD3 in mitochondria has generally been studied in relation to the transport of cholesterol into mitochondria for steroidogenesis [11]. However, mitochondrial cholesterol is not only necessary for synthesis of steroids, oxysterols, and hepatic bile acids; it is also an integral part of mitochondrial membranes. Mitochondrial DNA (mtDNA) exists in nucleoprotein structures called nucleoids, which are associated with mitochondrial membranes and facilitate mtDNA maintenance and gene expression [12]. Nucleoids differ in protein components, depending on their functions—replication, translation, and repair [13]. Membrane-associated replication platforms, containing the major replication proteins, are abundant in cholesterol, and a disruption of the cholesterol homeostasis, for example by gene silencing of *ATAD3* (ATPase family AAA domain-containing protein 3), impairs mtDNA topology and mitochondrial protein synthesis [13–16].

The mechanism of transporting cholesterol into mitochondria is still not well known. Free cholesterol is nearly insoluble in water and therefore depends on transport via cholesterol-binding proteins [17]. In steroidogenic cells, StAR (steroidogenic acute regulatory protein) is involved in the transport of cholesterol from lipid droplets and from the ER to the outer mitochondrial membrane (OMM). StAR is a part of a multiprotein complex, but the exact composition of this complex and the mechanism of cholesterol transport are still debated [11]. The group led by V. Papadopoulos described a multiprotein complex (transduceosome) formed of StAR, VDAC1, TSPO, ACBD3, PKAR1 $\alpha$  (type I PKA), ATAD3, and CYP11A1 (mito cyt P450) [6,18]. The ACBD3 protein was described as an interacting partner between TSPO and PKAR1 $\alpha$  [5], serving as an A-kinase-anchoring protein for PKAR1 $\alpha$ , which has a role in phosphorylation and activation of StAR. Recently, a new role of ACBD3 in the mitochondrial retrograde response, induced by mitochondrial dysfunction, has been described [19]. ACBD3, together with TSPO and PKA, is indispensable in adaptation to stress, via retro-communication with the nucleus [19].

As mentioned above, ACBD3 has an apparently important function in transporting cholesterol into mitochondria. A disruption of cholesterol transport into mitochondria could affect proper mitochondrial replication and protein biosynthesis, and thus lead to secondary mitochondrial defects. The aim of this study was to characterize the impact of a complete absence of the ABCD3 protein on mitochondrial cholesterol level and related changes in mitochondrial energy metabolism: level of mtDNA, representation of mtDNA encoded proteins, mitochondrial function (mitochondrial respiration), production of reactive oxygen species (ROS), and mitochondrial ultrastructure in HEK293 and HeLa cells. In addition, we focused on Golgi structure, the representation of Golgi proteins, and the glycosylation pattern of the LAMP2 glycoprotein. Last but not least, we determined the level of various lipids in ACBD3 knock-out (ACBD3-KO) HEK293 and HeLa cell lines and their isolated mitochondria. Our results emphasize the role of ACBD3 protein in Golgi stacking and suggest the alternative pathway of transporting cholesterol into mitochondria, independent of the ACBD3 protein.

## 2. Results

### 2.1. Localisation of ACBD3 Protein

To reveal the localization of ACBD3 in HEK293 wild-type (WT) and HeLa WT cells, we used the Mitochondria Isolation Kit based on the MACS technology, which yields high-purity mitochondria [20]. In the mitochondrial fraction, we observed approximately 15% of the ACBD3 signal compared to the cell lysate and insignificant contamination of cytosol ( $\beta$ -actin), but the mitochondrial fraction showed an enrichment by ER, in addition to a faint signal of the Golgi protein GM-130 (Figure 1A). Therefore, we are not able to conclude if ACBD3 is localized in the mitochondria from this result. To determine the localization of the ACBD3 protein, we performed confocal microscopy of HEK293 and HeLa WT cells,

focusing on selected organelles (Golgi, ER, and mitochondria) as well. Signal overlay was observed only between ACBD3 and giantin (Figure 1B). These findings suggest that ACBD3 localizes primarily to Golgi in HEK293 and HeLa cells and its interactions with mitochondria might be transient.

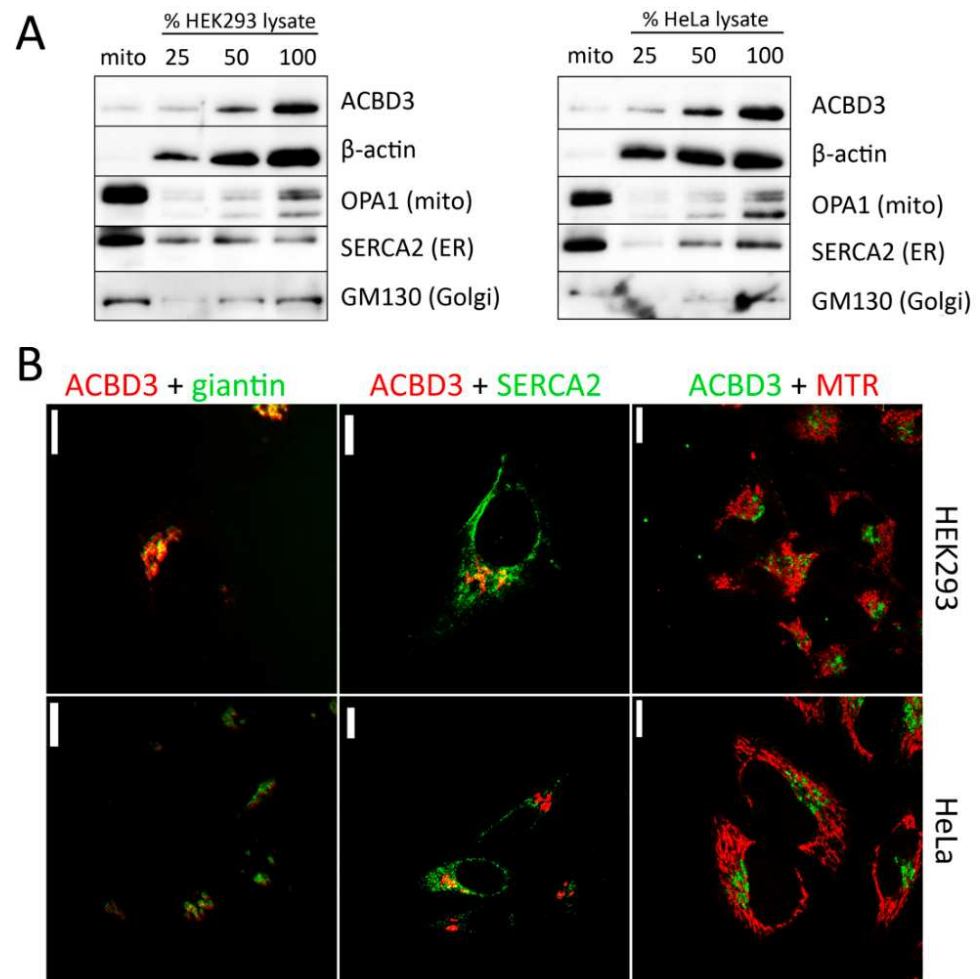


**Figure 1.** Localization of ACBD3 protein in HEK293 and HeLa WT cells. **(A)** Characterization of mitochondrial fraction and whole cell lysate by SDS-PAGE/WB. The mitochondrial fraction reveals only a slight signal of ACBD3, but the mitochondrial fraction is enriched by endoplasmic reticulum (ER, SERCA2 antibody) and also a slight signal of Golgi (GM130). **(B)** Confocal microscopy of HEK293 WT and HeLa WT cells. The cells were immunolabeled by ACBD3 antibody and, where indicated, by specific markers for Golgi (giantin), ER (SERCA2), and mitochondria (MitoTracker Red (MTR)). Overlay of signals was found only between ACBD3 and giantin (Golgi). Scale bar 10  $\mu$ m.

## 2.2. Characterization of ACBD3-KO HEK293 and HeLa Cells

We created three HEK293 ACBD3-KO cell lines and one HeLa ACBD3-KO cell line. Together, all four ACBD3-KO clones (HEK293 ACBD3-KO 24, 59, and 87; HeLa ACBD3-KO B3) showed consistent results across a broad range of analyses. Immunofluorescence images of ACBD3-KO B3 are displayed in Figure A1.

Firstly, we focused on mitochondrial and Golgi ultrastructure, followed by an assessment of the Golgi area, steady-state level of representative Golgi proteins, and the glycosylation of the LAMP2 glycoprotein in HEK293 and HeLa ACBD3-KO. Then, we carried out several well-established analyses to study mitochondrial OXPHOS in ACBD3-KO cells: the representation of OXPHOS protein complexes and selected mitochondrial proteins, mitochondrial respirometry, ROS production, and the relative mtDNA amount. Finally, we performed a lipidomics analysis of ACBD3-KO cells.

### 2.2.1. Mitochondria and Golgi Ultrastructure

Significant changes in mitochondrial ultrastructure were found in multiple cellular disturbances [21,22]. Therefore, we focused on the study of mitochondrial ultrastructure by Transmission Electron Microscopy (TEM). Overall, mitochondrial ultrastructure was not altered in ACBD3-KO cells (Figure 2A,B). In most of the cells, mitochondria exhibited intact structure with normal cristae formation comparable with control samples. However, a significantly increased proportion of mitochondria with abnormal structure was observed in 87-KO (Figure 2A and quantification in Figure 2C). Since the ACBD3 protein primarily acts in Golgi, we also examined the structure of this organelle. We did not see the regular ribbon and stacked cisternae formation, but we observed a significantly increased amount of vesicles in the Golgi area (Figure 2A,B and detail in Figure 2D). This confirms the important role of ACBD3 in maintaining the structure of Golgi.

### 2.2.2. Golgi Assessment (Golgi Area Measurement, Golgi Proteins, and Glycosylation of the LAMP2 Glycoprotein) in ACBD3-KO Cells

Due to altered Golgi structure on TEM (Figure 2D), we performed immunofluorescence labeling of cis- (GM130) and trans-Golgi (TGN46) markers. The ACBD3-KO cells showed an extremely fragmented and disorganized Golgi structure (Figure 3A). The relative Golgi area was notably expanded (Figure 3B) and the cis- and trans-Golgi signals did not co-localize (Figure 3C). Then, we determined the level of selected Golgi proteins involved in the maintenance of Golgi structure. The amount of all analyzed Golgi protein remained in the control range, but the level of  $\beta$ -actin changed (Figures 3D and A2A). Because the Golgi structure was significantly disturbed, we examined the glycosylation pattern of the LAMP2 glycoprotein using the mobility shift assay, but found the pattern comparable with control samples (Figures 3E and A2B).

### 2.2.3. OXPHOS Complexes and Subunits, Mitochondrial Respiration, ROS Production, and Relative mtDNA Amount

We determined the steady-state levels of OXPHOS complexes in isolated mitochondria from ACBD3-KO cell lines. Overall, the amount of OXPHOS protein complexes was not significantly disturbed. We only observed a partial decrease in the complex III level in 59-KO (62% of control value), a mildly decreased amount of complex I in 87-KO (70% of control value), and an increased level of complex IV in B3-KO (184% of control value; Figure 4A,B; quantification in Figure A3A,B). Following the analysis of OXPHOS protein complexes, we determined the amount of selected OXPHOS protein subunits (Figure 4C,D; quantification in Figure A3C,D). We found marked changes in the case of complex IV subunits (encoded by both mtDNA and nuclear DNA) in cell lines 59-KO (COX1 160% of control value and COX5a 134% of control value) and B3-KO (COX2 at 152% of control value and COX5a at 250% of control value), but they had no impact on the assembly of complex IV (Figure 4A,B) and the formation of OXPHOS supercomplexes (data not shown). Altogether, only a mild alteration in the levels of several subunits were found, while in general, the amounts of OXPHOS protein subunits did not significantly change across ACBD3-KO cell lines (Figure 4C,D). Apart from OXPHOS protein subunits, we focused also on proteins of the transduceosome. Selected proteins (VDAC1, TSPO, ACBD1, and ANT) were not altered in ACBD3-KO cells (data not shown). Mitochondrial respiration in most ACBD3-KO cells corresponded with controls in all states, with the exception of B3-KO cells, where the ROUTINE respiration, controlled by cellular energy demand and turnover, was increased in comparison to the control, indicating possible cellular stress (Figure 4E,F). Next, we analyzed ROS production in all ACBD3-KO cell lines to determine oxidative stress. ROS production remained within the control range in all ACBD3-KO cells except 59-KO, where a small amount of ROS-positive cells was detected (Figures A4 and A5). The analysis of mtDNA content did not reveal any alteration across the ACBD3-KO cell lines (Figure 4G). Based on these results, neither mitochondrial OXPHOS, nor the mtDNA amount, seem significantly altered in ACBD3-KO cells.

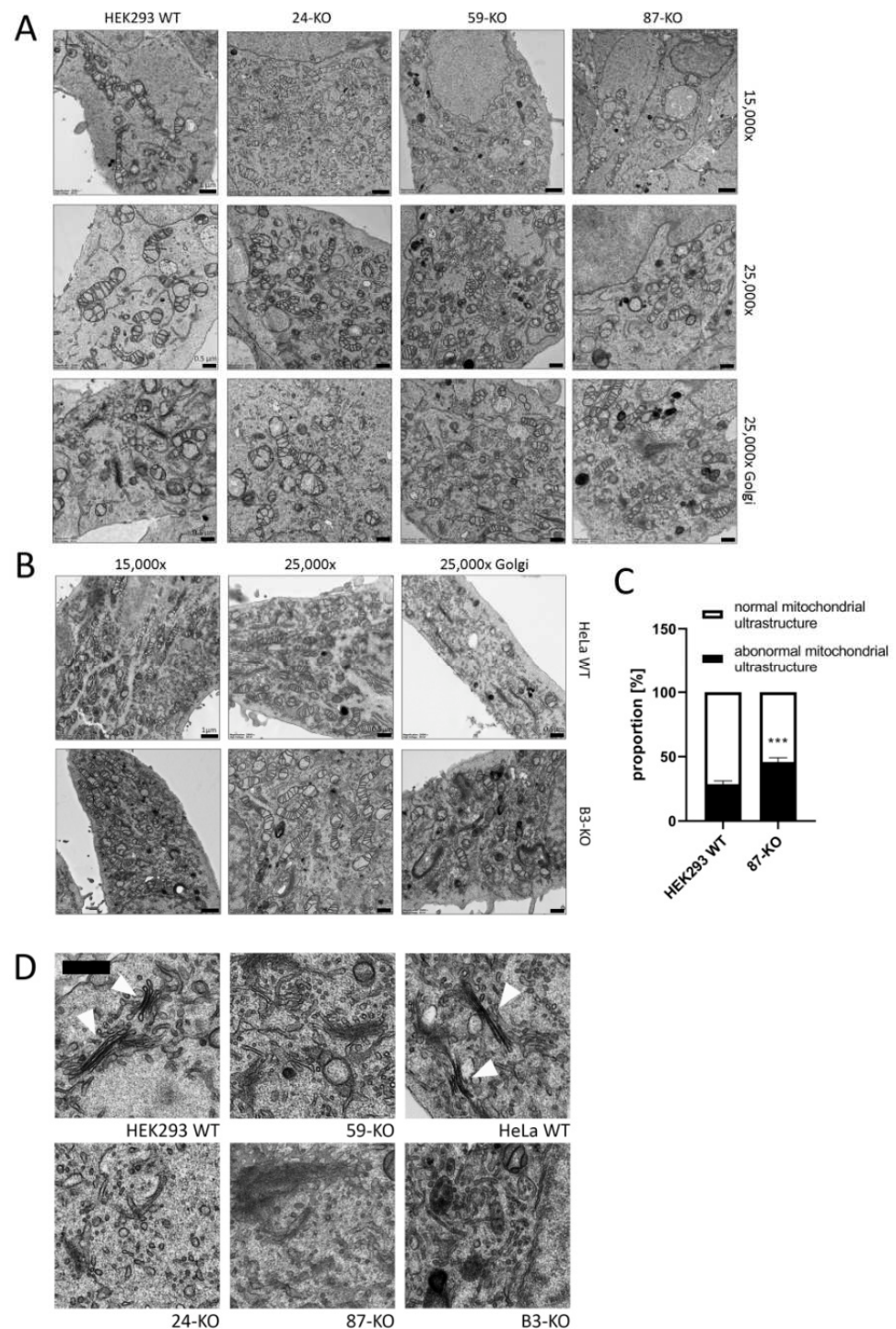


**Figure 2.** Transmission electron microscopy (TEM) of the ultrastructure of mitochondria (15,000 $\times$  (scale bar 1  $\mu$ m) and 25,000 $\times$  (scale bar 0.5  $\mu$ m)) and the Golgi apparatus (25,000 $\times$ ) in (A) HEK293 ACBD3-KO cells and (B) HeLa ACBD3-KO cells. (C) Quantification of the mitochondria with normal and abnormal ultrastructure in HEK293 WT and 87-KO. More than 300 mitochondria from 27 pictures per cell line were used to determine statistical significance by Mann–Whitney t-test. Error bar represents SEM,  $p < 0.001$  (\*\*\*) . (D) Detail of Golgi structure. Arrows point to normal Golgi structure in HEK293 and HeLa WT. In ACBD3-KO cells, normal Golgi structure with stacked cisternae was barely found. However, we detected multiplied vesicles in the Golgi area. Scale bar 0.5  $\mu$ m.

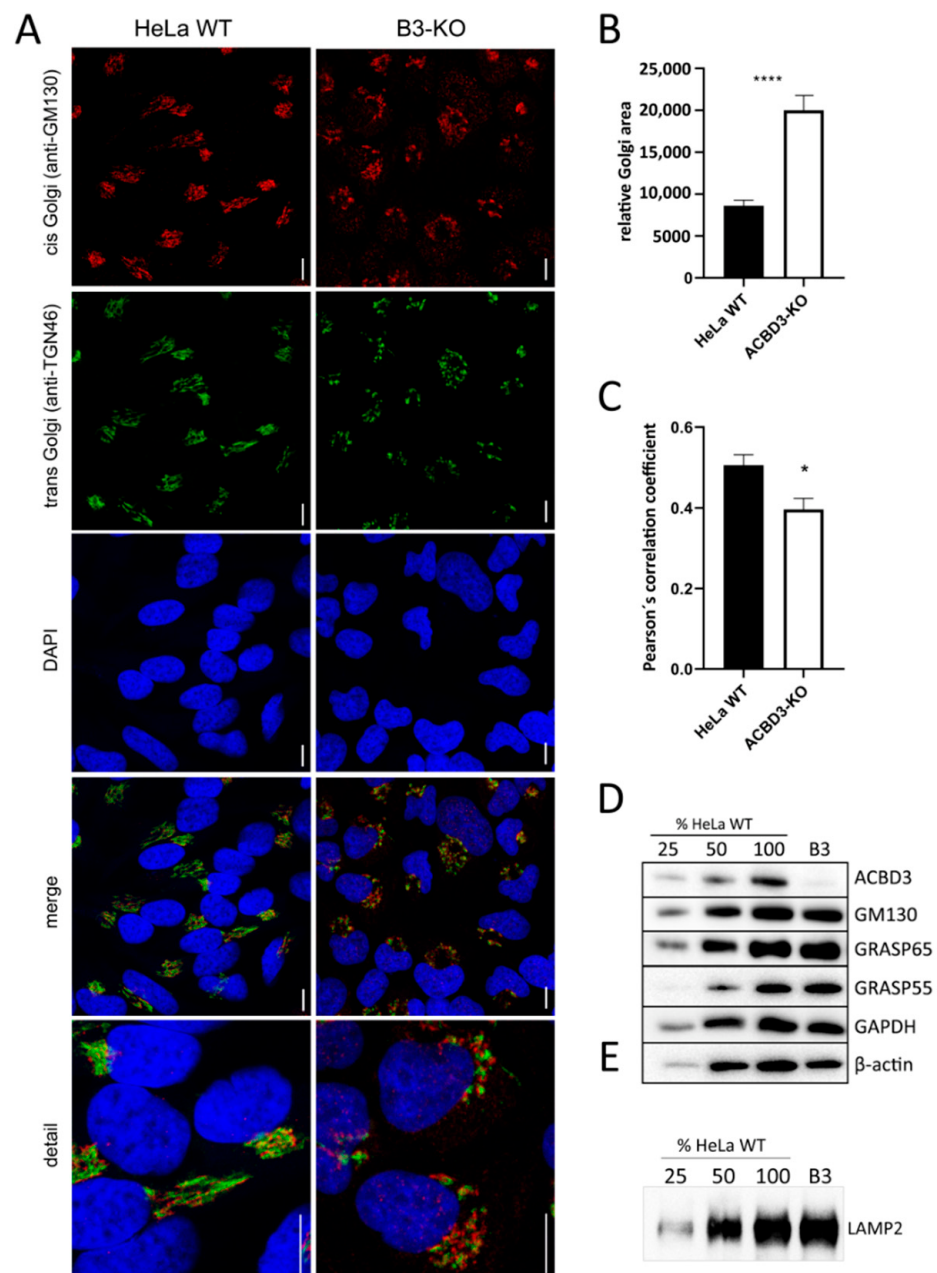


**Figure 3.** Golgi assessment in ACBD3-KO cells. **(A)** Confocal immunofluorescence images of cis-Golgi (GM130) and trans-Golgi markers (TGN-46) in HeLa WT and ACBD3-KO. In ACBD3-KO, Golgi structure is extremely fragmented, whereas control cells exhibit a compact structure, typical for Golgi. Scale bar 10  $\mu$ m. **(B)** Measurement of relative Golgi area in HeLa WT and ACBD3-KO from more than 60 cells was performed using ImageJ. Error bars represent SEM. A Mann–Whitney test was used to determine statistical significance,  $p < 0.0001$  (\*\*\*\*). **(C)** Pearson's correlation coefficient was applied to quantify GM130 and TGN46 colocalization using LAS X software (Leica, Wetzlar, Germany). Error bars represent SEM. A Mann–Whitney test was performed to determine statistical significance,  $p < 0.05$  (\*). **(D)** Steady-state level of selected Golgi proteins in control and ACBD3-KO cells determined by SDS-PAGE/WB. The numbers 25, 50, and 100 demonstrate loading dose of protein. Relative signal intensity was normalized to the intensity of loading control (GAPDH) by densitometric analysis. None of the analyzed Golgi proteins showed any significance change in protein amount but the level of  $\beta$ -actin was altered in ACBD3-KO cells. **(E)** The mobility assay of the LAMP2 glycoprotein did not reveal any alteration in ACBD3-KO cells. The numbers 25, 50, and 100 demonstrate loading dose of protein.

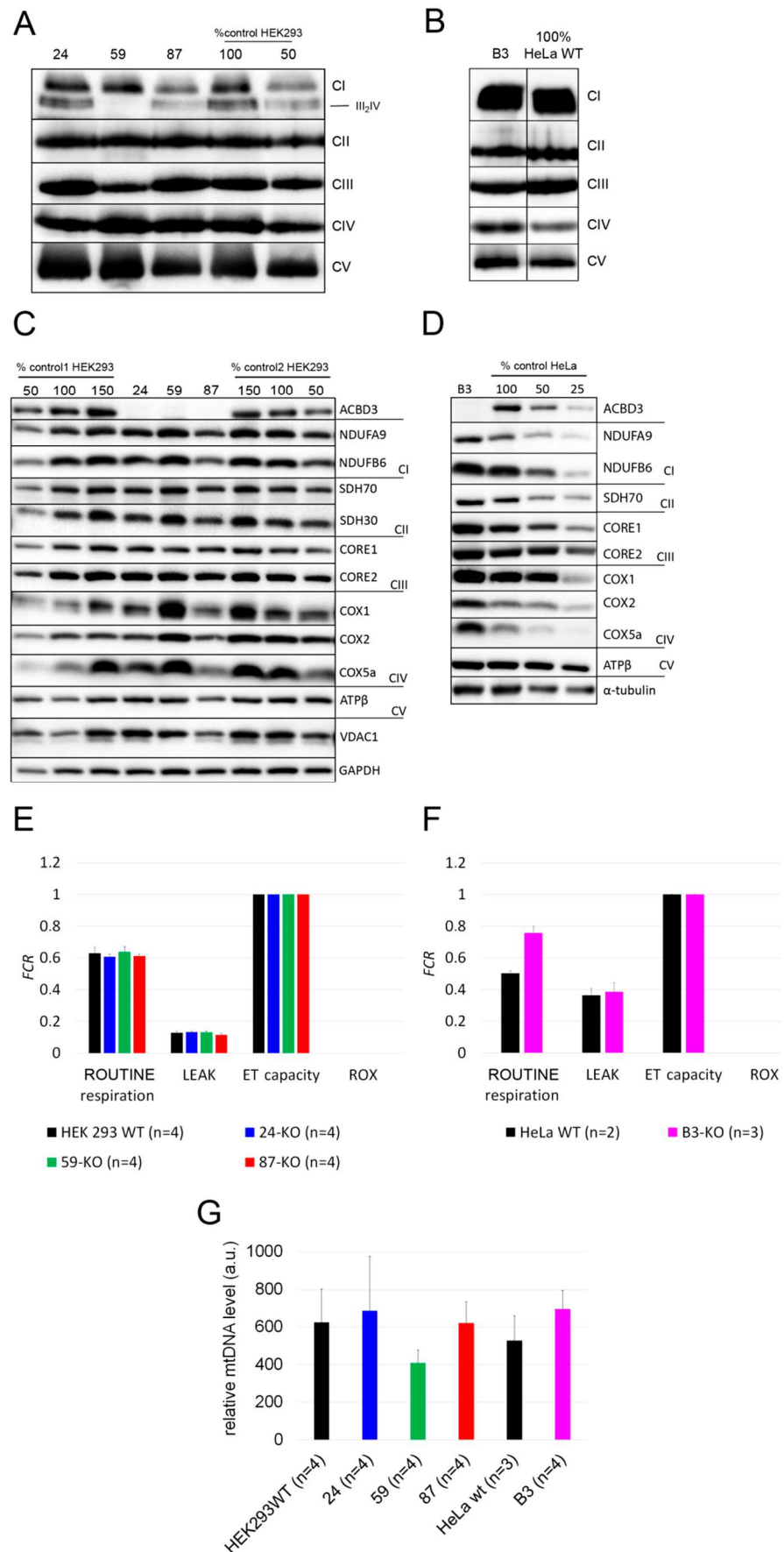


Figure 4. Mitochondrial investigations in ACBD3-KO cells. (A) Steady-state level of OXPHOS protein

complexes in isolated mitochondria from HEK293 and (B) HeLa analyzed by BN-PAGE/WB. The numbers 50 and 100 show the loading dose of protein. Relative signal intensity was normalized to the intensity of complex II by densitometric analysis. (C) Steady-state level of selected OXPHOS protein subunits in HEK293 and (D) HeLa analyzed by SDS-PAGE/WB. The numbers 25, 50, 100, and 150% indicate loading dose of protein. Relative signal intensity of individual antibodies was normalized to the intensity of loading control (GAPDH and  $\alpha$ -tubulin, respectively) by densitometric analysis. (E) High-resolution respirometry in HEK293 and (F) HeLa cell lines. ROUTINE respiration shows physiological respiration, LEAK shows proton leak after the inhibition of ATP synthase by oligomycin. Residual oxygen consumption (ROX) and electron transfer capacity (ET capacity) represent the minimal and maximal nonphysiological values of respiration, which are set on 0.0 and 1.0 in FCR. (G) A comparison of mtDNA level across ACBD3-KO cell lines and controls. 'n' represents the number of independently analyzed samples per each group. Error bars represent SD.

#### 2.2.4. Lipidomics in ACBD3-KO Cells

To evaluate our hypothesis that the ACBD3 protein transports cholesterol into mitochondria and the prediction that its absence will disrupt cholesterol levels in mitochondria, we performed a lipidomics analysis in ACBD3-KO cells as well as in isolated mitochondria (Figure 5A–H, statistics in Table 1). The level of cholesterol did not significantly differ in cells nor in the isolated mitochondria, but the cholesteryl esters were altered significantly. Interestingly, the level of coenzyme Q9 (CoQ9) was significantly lower in both whole cells and mitochondria compared to control samples. Moreover, we also observed significantly decreased levels of sphingomyelins (SM), but normal ceramides and hexosyl ceramides levels in both the cells and the mitochondria compared to controls. Due to the decreased sphingomyelins, we performed an in situ measurement of sphingomyelin synthase (SMS) and glucosylceramide synthase (GCS) activity by quantifying the conversion of C6-NBD-ceramide, a fluorescent ceramide analogue, to C6-NBD-SM (SMS activity) and C6-NBD-GlcCer (GCS activity), respectively, followed by TLC detection [23]. The assay did not reveal any significant changes in SMS and GCS activity across the ACBD3-KO cell lines (Figure 5I, quantification in Figure A6).

**Table 1.** Statistical analysis of lipidomics data from 5A–5H.

		Chol	CE	CoQ9	SM	CER	HexCer	Hex2Cer	Hex3Cer
WT vs. KO	cells	NS	**	**	***	NS	NS	NS	NS
	mitochondria	NS	***	***	**	NS	NS	NS	NS
	HeLa	NS	***	***	NS	NS	NS	NS	NS
	HEK293	NS	NS	***	***	NS	NS	NS	NS
	overall	NS	***	***	***	NS	NS	NS	NS

$p < 0.01$  (\*\*);  $p < 0.001$  (\*\*\*); NS: not significant. Abbreviations: CE: cholesteryl esters, CER: ceramides, Chol: cholesterol, CoQ9: coenzyme Q9, HexCer: hexosylceramides, Hex2Cer: dihexosylceramides, Hex3Cer: trihexosylceramides, KO: knock-out, SM: sphingomyelins, WT: wild type.



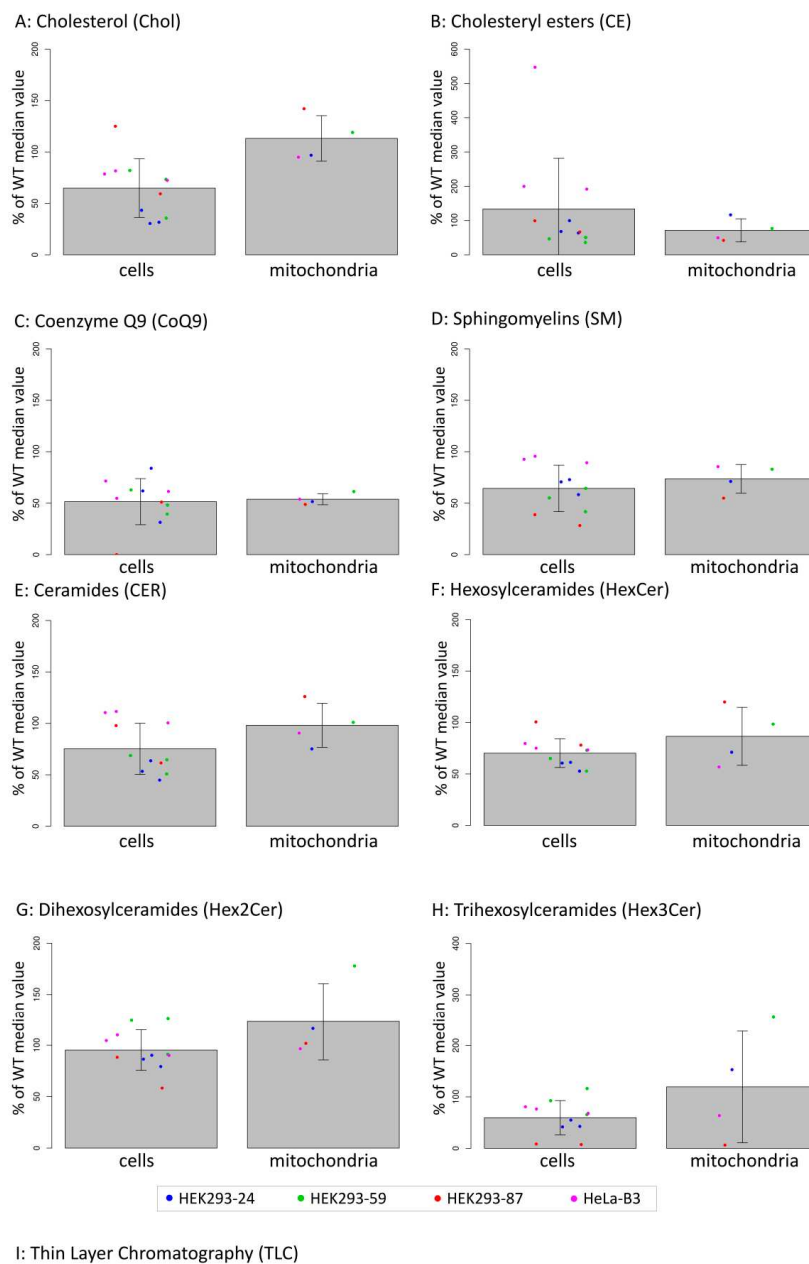


**Figure 5.** (A–H): Lipidomics analysis in whole cells and in isolated mitochondria of ACBD3-KO cells displayed as percentage of control values. Cells were measured in triplicate (duplicate in the case of 87-KO), dots represent individual obtained values, bar charts represent mean values, and errors bars represent SD. Significance of differences between WT and KO in cells and in mitochondria are summarized in Table 1. Linear mixed-effects models were used for statistical analysis. (I) In situ analysis of sphingomyelin synthase (SMS) and glucosylceramide synthase (GCS) activities using fluorescent-labeled ceramide (C6-NBD-Cer). Activities of SMS and GCS are visualized as the amount of synthesized products, sphingomyelin (C6-NBD-SM), and glucosylceramide (C6-NBD-GlcCer), respectively. Quantification of TLC results is shown in Figure A6.

### 3. Discussion

#### 3.1. Altered Golgi Structure in ACBD3-Deficient Cells

In general, ACBD3 is primarily associated with Golgi and to this date, its interactions with several distinct proteins in different parts of Golgi have been described [4,7–9,24–26]. Similarly to others, using immunofluorescence and WB, we showed localization of ACBD3, particularly in Golgi. Functions of these ACBD3-containing protein complexes range from maintenance of the Golgi structure, membrane trafficking, and glycosphingolipid metabolism to regulation of *de novo* fatty acid synthesis or apoptosis [10]. Yue et al. [7] described ACBD3 as a part of multiprotein cisternal adhesion complex (ACBD3-TBC1D22-GRASP55-golgin45), where the exact role of ACBD3 in Golgi stacking remains unclear. Our results from TEM and immunofluorescence imaging show that the absence of ACBD3 significantly affects the structure of the Golgi complex. In ACBD3-KO cell lines, both HeLa- and HEK293-derived, we observed no ribbon-like or stacked structures; instead, we saw an uncommonly increased amount of vesicles and an enlarged Golgi area, confirming previously published data on an ACBD3-downregulated HeLa cell line by Liao et al. [8]. Taken together, the data demonstrate the indispensability of the ACBD3 protein in Golgi stacking. Unlike in a double knock-out of GRASP-55 and GRASP-65 (Golgi ReAssembly Stacking proteins) [27], the depletion of the Golgi structure in ACBD3-KO cells did not affect the level of GRASP55, GRASP65, and GM130 Golgi proteins, participating in the assembly of the apparatus (Figure 3D,E and Figure A2A,B) nor the glycosylation pattern of the LAMP2 glycoprotein and the level of hexosyl ceramides (Figure 5, Table 1). We showed that defects of Golgi maintenance, induced by depletion of ACBD3 protein, did not affect the glycosylation pattern of LAMP2 glycoprotein. Interestingly, another study recently described a disruption of the glycosphingolipid metabolism in an ACBD3-downregulated HeLa cell line [8]. Therefore, it remains unclear whether and to what extent the absence of ACBD3 affects the functions of the Golgi apparatus.

#### 3.2. The Role of ACBD3 in Mitochondrial Cholesterol Transport and Mitochondrial Metabolism

To our knowledge, this is the first study focused on the role of ACBD3 in mitochondrial functions. Based on our results from multiple analyses (representation of OXPHOS protein complexes and subunits, mitochondrial respiration, ROS production, mitochondrial ultrastructure, and mtDNA relative quantification) in ACBD3-deficient HEK293 and HeLa cells, the ACBD3 protein is dispensable for proper function of the OXPHOS complexes and its absence has no notable effect on the level of mitochondrial and cellular cholesterol. We assume there is an alternative pathway of transporting cholesterol into mitochondria. In addition to ACBD3, ACBD1 and ACBD2 are also mitochondrial proteins. ACBD1 was discussed previously as a part of the multiprotein complex transporting cholesterol into mitochondria [28–31], but unlike ACBD3, its role was not described in detail. In C6-2B glioma cells, an ACBD1-dependent formation of mitochondrial pregnenolone was described [32]. The depletion of ACBD1 in MA-10 and R2C Leydig cells led to decreased human chorion gonadotropin-stimulated steroidogenesis and decreased progesterone production, respectively [33,34]. Similarly to ACBD3, ACBD1 also binds TSPO at the outer and inner mitochondrial membrane contact sites and stimulates cholesterol transport into mitochondria. In mitochondria, ACBD1 directly promotes the loading of cholesterol on the CYP11A1 enzyme [35]. Similarly, ACBD2 protein might participate in cholesterol transport into mitochondria. Under ectopic expression of the ACBD2 isoform A, increased basal and hormone-stimulated steroid formation was observed in MA-10 Leydig cells [36].

Although most of the research focusing on cholesterol transport into mitochondria has been carried out in the context of steroidogenesis, recently, a new mechanism of mitochondrial cholesterol transport in non-steroidogenic cells has been described [37]. The authors characterized a new protein, Aster-B, which contains a StAR-related transfer domain and a mitochondrial target sequence. Aster-B, together with the Arf1 GTPase, is indispensable for cholesterol transport from ER to mitochondria in C2C12 cells. Depletion

of Aster-B or Arf1 leads to a significant decrease in mitochondrial cholesterol content, resulting in mitochondrial dysfunction [37].

We were unable to reliably answer the question of if ACBD3 is localized in mitochondria. According to proposed theories, the transduceosome complex probably employs the ACBD3 protein as a tether between TSPO and PKARI $\alpha$ . While the TSPO protein is a transmembrane protein of the OMM, PKA type I is a cytosolic enzyme. Therefore, ACBD3 probably acts as a scaffold between those proteins in close proximity to the OMM, rather than inside the OMM. It is generally accepted that ACBD3 is primarily a Golgi protein, thus its localization in proximity to mitochondria could be transient only after cAMP stimulation. A similar pattern was described in the case of the ACBD2 protein, which is preferentially localized in peroxisomes, but colocalizes with mitochondria upon a cAMP stimulation by dibutyryl-cAMP [36]. Furthermore, we tried to study the impact of ACBD3 protein absence on the other proteins of the transduceosome complex. Unfortunately, our chosen approach did not allow us to uncover the steady-state level of all proteins across both cell types (used antibodies summarized in Table A4).

### 3.3. Lipidomics in ACBD3-KO Cells

We revealed a significantly decreased level of CoQ9 across the ACBD3-KO cell lines by a sensitive mass spectrometry method. In human cells, CoQ9 and CoQ10 are synthesized by the same PDSS1/2 heterotetramer [38] in the first step of the mitochondrial part of the CoQ biosynthesis. To our knowledge, the function of human CoQ9 remains unclear, just as the regulation mechanism specifying if CoQ9 or CoQ10 will be synthesized. Our results suggest that ACBD3 might somehow assist in the regulation of the specificity of PDSS1/2 for chain length formation. A complex study of protein–protein interaction, using BioPlex 2.0, identified the ACAD9 protein as a PDSS1 and PDSS2 interacting partner [39]. The role of ACAD9 in CoQ biosynthesis is not yet known. ACAD9 is also an Acyl-CoA binding protein and seems to have a similar role in the replication of some picornaviruses as ACBD3 [40]. Theoretically, ACAD9 and ACBD3 could have similar but yet unknown functions in the regulation of PDSS1/2. As already mentioned, both CoQ biosynthesis and function in humans still require much research to be carried out.

ACBD3-deficient cells exhibit a decreased level of SM, together with a normal level of ceramides and hexosyl ceramides, as determined by mass spectrometry. The SMS and GCS activities remain comparable to controls. Taken together, this suggests that ceramide is not effectively transported to the Golgi as a substrate for SMS. Transport of ceramides from ER to the Golgi for the synthesis of SM is CERT (ceramide transport protein)-dependent, but it is known that the CERT pathway does not play a major role in the transport of ceramides for GlcCer synthesis [41,42]. We hypothesize that the decreased level of SM, together with a normal SMS activity in ACBD3-KO cells, could be caused by an impaired transport of ceramides from ER to Golgi. These results are in accordance with previously published data [9], indicating for the first time the role of ACBD3 in the recruitment of PPM1L (ER-resident transmembrane protein phosphatase) to the ER–Golgi membrane contact sites, which seems to be indispensable for the activation of CERT protein. We assume that ACBD3 protein is fundamental in the activation of CERT via PPM1L. How ceramides are delivered from the ER to the site of GlcCer synthesis is unknown [41], but according to our finding, the transport is probably ACBD3 independent. Previously, increased SM and GlcCer levels were observed in an ACBD3-downregulated HeLa cell line [8]. This discrepancy could be related to the amount of ACBD3 residual protein in the downregulated HeLa cell line, as discussed previously [43,44].

## 4. Materials and Methods

### 4.1. Cell Culture

Human embryonic kidney cells (HEK293, ATCC<sup>®</sup> CRL-1573<sup>™</sup>) and HeLa (ATCC<sup>®</sup> CCL-2<sup>™</sup>) cells were purchased from the American Type Culture Collection (Rockville, Maryland, MD, USA) and cultivated under standard conditions (37 °C, 5% CO<sub>2</sub> atmosphere) in

high-glucose DMEM (Dulbecco's Modified Eagle Medium; P04-04510, PanBiotech, Aidenbach, Germany) supplemented with 10% (*v/v*) Fetal Bovine Serum (SV30160.03, GE Healthcare, Chicago, IL, USA) and Antibiotic–Antimycotic (XC-A4110/100, Biosera, Nuaille, France).

#### 4.2. Preparation of HEK293 and HeLa ACBD3-KO Cell Lines

ACBD3-KO was introduced into HEK293 and HeLa cells by the CRISPR/CAS9 system (Clustered Regularly Interspaced Short Palindromic Repeats). For preparation of ACBD3-KO cells, a commercial plasmid (404320; Santa Cruz Biotechnology, Dallas, TX, USA) was used and in silico analysis of off-target effects revealed a high specificity of all three gRNAs used for the ACBD3 gene. Cells were transfected using Lipofectamine 300 (Invitrogen, Waltham, MA, USA). Then, 24 h after transfection, cells were diluted into a concentration of 5 cells/mL. This suspension was aliquoted (100  $\mu$ L) into 96-well plates. Wells containing single-cell colonies were identified and further cultivated. Confluent cells in 6-well plates were harvested and characterized by Sodium Dodecyl Sulphate Polyacrylamide Gel Electrophoresis (SDS-PAGE)/Western blot (WB) to confirm complete absence of ACBD3 at the protein level. Cells with no protein levels were sequenced (Sanger sequencing) with the following primers, TGAGTACTTTCAACACTGCATGG, GCCAGACTCACAGTAAAGACAC, GTCAGTTTTCCCTGGGAGCTA, and GTTCTGCAAGTGAACCCCA, to identify nonsense mutations resulting in premature stop codons.

#### 4.3. Isolation of Mitochondria

For Blue Native Polyacrylamide Gel Electrophoresis (BN-PAGE) analysis, mitochondria were isolated by standard differential centrifugation as described previously [45]. For localization of ACBD3 in the cells and for lipidomic analysis, mitochondria were isolated by Mitochondria Isolation Kit (130-094-532; Miltenyi Biotec, Bergisch Gladbach, Germany).

#### 4.4. Electrophoresis and WB

Tricine SDS-PAGE (or glycine SDS-PAGE for LAMP2 detection) was used for separation of proteins according to their molecular weight under denaturing conditions [46]. Cell pellets were resuspended in RIPA buffer (50 mM Tris (pH 7.4), 150 mM NaCl, 1% (*v/v*) Triton X-100, 1% (*w/v*) sodium deoxycholate, 0.1% (*w/v*) SDS, 1 mM EDTA, 1 mM PMSF, and 1% (*v/v*) protease inhibitor cocktail), sonicated and lysed for 20 min at 4 °C. The supernatant obtained after lysis and centrifugation was suspended in sample buffer (50 mM Tris (pH 6.8), 12% (*v/v*) glycerol, 4% (*w/v*) SDS, 0.01% (*w/v*) Bromethanol Blue, and 2% (*v/v*) mercapthoethanol) to a final concentration of 2–5  $\mu$ g/ $\mu$ L. A total of 5–15  $\mu$ g of protein was loaded per lane and separated by 12% (*w/v*) polyacrylamide minigels (MiniProtean<sup>®</sup> 3 System; Bio-Rad, Hercules, CA, USA). BN-PAGE separation [47] was used to analyze the steady-state levels of mitochondrial oxidative phosphorylation system (OXPHOS) protein complexes. The mitochondrial fraction was solubilized with n-dodecyl  $\beta$ -d-maltoside (DDM) at a final 16 mg DDM/mg protein ratio in a buffer containing 1.5 mM aminocaproic acid, 0.05 M Bis-Tris, and 0.5 M EDTA. A total of 15  $\mu$ g of protein was loaded per lane and separated by 6–15% (*w/v*) polyacrylamide gradient gels (MiniProtean<sup>®</sup> 3 System; Bio-Rad).

SDS-PAGE and BN-PAGE gels were transferred onto Immobilon-P PVDF Membrane (Millipore, Burlington, MA, USA) by semi-dry electroblotting using the Hoefer semi-dry transfer unit (Hoefer, Harvard Bioscience, Holliston, MA, USA) or Trans-Blot Turbo Transfer System (Bio-Rad).

For immunodetection, membranes were incubated for 2 h in primary antibodies at room temperature (RT) or overnight at 4 °C in 2% non-fat milk. Particular antibodies for individual experiments are summarized in Table A3. All membranes were detected with peroxidase-conjugated secondary antibodies and SuperSignal<sup>™</sup> West Femto Maximum Sensitivity Substrate or SuperSignal<sup>™</sup> West Pico PLUS Chemiluminescent Substrate (34,096 and 34,577, respectively; Thermo Fisher Scientific, Waltham, MA, USA) using G:Box (Syngene, Cambridge, UK) and analyzed by Quantity One software (Bio-Rad).

#### 4.5. High-Resolution Respirometry

HEK293 and HeLa cells were cultivated to approximately 80% confluence, harvested by incubation (5 min, 37 °C) with TE (Trypsin, 0.05% (*w/v*); EDTA (0.02%, *w/v*)), washed and suspended in mitochondrial respiration medium MiRO5 kit (60101-01, Oroboros Instruments, Innsbruck, Austria), and centrifuged (5 min, 300 g, 24 °C). Cells were resuspended in approximately 500–800 µL MiRO5 and then counted by a Handheld Automated Cell Counter (Millipore). Two million cells were added in a 2 mL chamber with preheated (37 °C) MiRO5 medium and measured in the Oroboros O2k-FluoRespirometer. After cells addition, ROUTINE respiration was analyzed, which is a physiological respiration controlled by cellular energy demand, energy turnover, and the degree of coupling to phosphorylation. Next, ATP synthase inhibitor, oligomycin (25 nM), was added to inhibit the mitochondrial respiration and investigate proton leak. This non-phosphorylating state is a respiration maintained mainly to compensate for the proton leak at a high chemiosmotic potential. Afterwards, the FCCP uncoupler (1 µM titration steps, final conc. 7–10 µM) was added to obtain the maximal electron transfer capacity, meaning oxygen consumption in the noncoupled state at optimum uncoupler concentration. In the electron transfer state, the mitochondrial membrane potential is almost fully collapsed and provides a reference state for flux control ratios. Finally, inhibitors of complex I and III, antimycin A (2.5 µM) and rotenone (0.5 µM), respectively, were added to obtain residual oxygen consumption (ROX), which is due to oxidative side reactions remaining after the inhibition of the electron transfer pathway in cells. ROX state was used as a respiratory and methodological correction factor for other respiratory states. Flux control ratio (*FCR*) is the ratio of oxygen flux in respiratory control states, normalized for maximum flux in a common reference state, to obtain theoretical lower and upper limits of 0.0 and 1.0. *FCR* provides an internal normalization and express respiratory control independent of mitochondrial amount and shows the quality of mitochondrial respiration [48].

#### 4.6. Analysis of mtDNA Content

The relative amount of mtDNA was analyzed by real-time PCR (RT-PCR) as described previously [49]. Briefly, total DNA was isolated from cells using the QIAamp DNA Mini Kit (51306, QIAGEN, Hilden, Germany) according to the manufacturer's instructions. To quantify the mtDNA content, 16S rRNA was used as a mitochondrial target and the GAPDH gene as a nuclear target. Primer sequences were published previously, and PCR conditions were as follows: initial denaturation at 95 °C for 15 min, 42 cycles of 95 °C for 15 s, annealing at 54 °C for 20 s and elongation at 72 °C 30 s, and a final elongation at 72 °C for 7 min using StepOnePlus™ (Applied Biosystems, Foster City, CA, USA). Ten-fold serial dilutions of the genomic DNA (from 100 to 10 ng) from control cell lines were included in each run to generate the calibration curve. The nuclear target was used to quantify nuclear DNA in order to normalize the amount of mtDNA per cell.

#### 4.7. Flow Cytometry Measurement of DHE Stained Cells

Measurements of dihydroethidium (DHE)-stained cells by flow cytometry were performed as described previously [50]. In brief,  $5 \times 10^5$  cells per sample were stained by 10 µM DHE (D23107, Invitrogen) for 30 min at 37 °C and measured by BD FACS CANTO II flow cytometer (BD Biosciences, San Jose, CA, USA) with the FACSDiva Version 6.1.3. software. As a positive control (increased ROS production), 100 µM menadione (M5625, Sigma, St. Louis, MI, USA) was used.

#### 4.8. Confocal and Transmission Electron Microscopy (TEM)

For confocal microscopy, where indicated, cells were stained by 200 nM MitoTracker® Red CMXRos (M7512, Invitrogen) for 30 min at 37 °C before fixation. The cells were fixed in 4% PFA, permeabilized by 0.1% Triton-X100, blocked in 10% iFBS (1 h, RT), and labeled overnight by specific antibodies (summarized in Table A3). Incubations with specific secondary antibodies were performed the next day. Mounted cells (P36931,

Invitrogen) were captured by confocal microscope Leica SP8X, image acquisition using HC PL APO 63x/1.40 OIL CS2 objective, and HyD detectors with gating set to 0.3–6 ns (Leica Microsystems, Wetzlar, Germany).

Measurements of relative Golgi area were performed using ImageJ 1.48 v (Wayne Rasband, National Institutes of Health, Bethesda, Maryland, USA) and correlation coefficients of GM130 and TGN46 signals were determined by the LAS X software (Leica Microsystems). To assess statistical significance, a Mann–Whitney test was calculated by GraphPad Prism version 8.3.0 for Windows (GraphPad Software, San Diego, CA, USA).

For TEM analysis, the cells were fixed using a modification of Luft's method [51]. The cells were incubated in PBS containing 2% potassium permanganate for 15 min, washed with PBS, and dehydrated with an ethanol series. The cells were subsequently embedded in Durcupan Epon (Electron Microscopy Sciences, Hatfield, PA, USA), sectioned on an Ultracut microtome (Reichert, Depew, NY, USA) to thicknesses ranging from 600 to 900 Å, and finally stained with lead citrate and uranyl acetate. A Jeol JEM 1400 Plus transmission electron microscope (JEOL, Tokyo, Japan) was used for image acquisition.

Mitochondria of a normal size and cristae formation were counted as 'normal', and mitochondria with atypical ultrastructure were counted as 'abnormal'. Overall, more than 300 mitochondria from 27 TEM pictures were categorized. Disputable mitochondria were excluded from the analysis. Significance was determined by Mann–Whitney t-test, using GraphPad Prism.

#### 4.9. Lipidomics

For the lipidomics analysis, two types of input material were used—cells and mitochondria. The cellular material was obtained from a confluent 6-well plate (in triplicate for each ACBD3-KO clone), rinsed twice with PBS, scraped into 1 mL PBS, and stored at 80 °C for a downstream analysis. In the case of mitochondria, the organelles were isolated by the Mitochondrial Isolation Kit (Miltenyi Biotec) from  $10^7$  cells. One sample for each ACBD3-KO clone was used. Overall, ACBD3-KO mitochondria were analyzed in quadruplicate. For a quantification of absolute values from the MS analysis, protein concentration of each sample was used (BCA assay).

Samples were processed via LC–MS workflow LIMeX (LIpids, Metabolites, and eXposome compounds) for simultaneous extraction of complex lipids, polar metabolites, and exposome compounds that combines an LC–MS untargeted and targeted analysis. The extraction of metabolites was carried out using a biphasic solvent system of cold methanol, methyl tert-butyl ether (MTBE), and 10% methanol [52–55].

Due to repeated measurements, linear mixed-effects models with interactions were used to analyze the data. The subject of the patient was considered as a random effect. *p*-values less than 5% were considered as statistically significant. Analyses were conducted using the R statistical package version 3.6.3. (R Core Team (2020), Vienna, Austria).

#### 4.10. Sphingomyelin Synthase Activity

The activity of sphingomyelin synthase (SMS) was measured as described previously [23]. In short,  $1.5 \times 10^6$  cells were incubated with 2.5 μM C6-NBD-ceramide (144090, Abcam, Cambridge, UK) for 1 h at 37 °C. Lipids were extracted by the Folch method and separate by thin-layer chromatography (TLC). The same amount of protein (determined by BCA assay) was used for individual spotted samples. Visualization of the fluorescence-labeled sphingolipid species was performed by G:box (Syngene) and quantified by Quantity One software (Bio-Rad).

## 5. Conclusions

Herein, using ACBD3-KO HEK293 and HeLa cells, we confirm the importance of the ACBD3 protein in Golgi structure maintenance, but the consequences of its absence on proper Golgi function remain unclear. We observed a decreased level of SM, together with a normal SMS activity and ceramide level, which we suggest to be caused by an impaired

transport of ceramides from ER to Golgi (CERT pathway). Further analysis is required to confirm our hypothesis. We also show that in HEK293 and HeLa cells, ACBD3 is not vital for cholesterol homeostasis in mitochondria or for the function of the mitochondrial oxidative phosphorylation system. We speculate about the existence of an alternative mechanism for mitochondrial cholesterol transport, independent of ACBD3. One such mechanism could be the recently described novel pathway of cholesterol transport [37]. Altogether, the exact mechanism of cholesterol transport into mitochondria remains largely unknown, and further investigation is required to gain proper insight.

**Author Contributions:** Conceptualization, T.D. and M.T.; methodology, T.D. and M.T.; formal analysis, T.D. (consulted with statistician, see acknowledgements); investigation, T.D., L.Z., H.Š., M.V., N.V., J.K., O.K. and J.S.; resources, T.D., M.T. and O.K.; writing—original draft preparation, T.D.; writing—review and editing, T.D., M.T. and O.K.; visualization, T.D.; supervision, M.T.; project administration, T.D. and M.T.; funding acquisition, M.T., T.D. and O.K. All authors have read and agreed to the published version of the manuscript.

**Funding:** This research was funded by Charles University (grant numbers GAUK 542217, SVV260367, Progress Q26/LF1) and the Ministry of Health of the Czech Republic (grant numbers AZV 17-30965A, RVO VFN 64165). O.K. was supported by the Czech Academy of Sciences (Lumina quaeruntur LQ200111901).

**Data Availability Statement:** The data presented in this study are available upon request from the corresponding author.

**Acknowledgments:** We would like to acknowledge J. Živný from the Institute of Pathological Physiology (First Faculty of Medicine, Charles University, Prague, the Czech Republic) for his assistance with the flow cytometry analysis, and R. Dobrovolný and A. Befecadu from the Department of Pediatrics and Inherited Metabolic Disorders (First Faculty of Medicine, Charles University, Prague, the Czech Republic) for their assistance with the confocal microscopy and TLC, respectively. Last but not least, we would like to acknowledge J. Zeman for critical review of the manuscript and V. Čapek for statistical analysis.

**Conflicts of Interest:** The authors declare no conflict of interest. The funders had no role in the design of the study; in the collection, analyses, or interpretation of data; in the writing of the manuscript, or in the decision to publish the results.

## Appendix A

**Table A1.** Expression level of ACBD3 protein in different organs and tissues according to The Human Protein Atlas (available on 28 May 2021 at <https://www.proteinatlas.org/>).

Level of Expression	Organs/Tissues
high	digestive system duodenum, small intestine, colon, gallbladder, pancreas, and appendix
	brain cerebral cortex and hippocampus
	others prostate, placenta, and bone marrow
medium	male tissues testis, epididymis, and seminal vesicles
	female tissues vagina, fallopian tube, endometrium, cervix, uterine, and breast
	endocrine tissues thyroid and adrenal gland
	brain cerebellum and caudate
	digestive system salivary gland, esophagus, stomach, and rectum
	lung nasopharynx, bronchus, and lung
	others kidney and urinary bladder, smooth muscle, skin, lymph node, and tonsil
low	others adipose and soft tissues, liver, ovary, skeletal muscle, spleen, and oral mucosa

**Table A2.** Expression level of ACBDs proteins according to MitoCarta 2.0.

	Training Dataset	MSMS NUM TISSUES **
ACBD1	Possible mito *	12/14
ACBD2	Mito	14/14
ACBD3	Possible mito *	0
ACBD4	Non mito	0
ACBD5	Non mito	0
ACBD6	Non mito	0
ACBD7	Non mito	0

\* Indicating evidence based on NCBI GO mitochondrial annotation or MitoP2 database, but not in mito. \*\* Number 0–14 tissues where gene products were found by MS/MS.

**Table A3.** Summary of antibodies used in experiments.

Figure	Antibody	Company	Catalog Number	Dilution	Method
1A	ACBD3	Atlas Antibodies	HPA015594	1:2000	tricine SDS-PAGE
	$\beta$ -actin	Cell Signaling Technology	4970	1:2000	tricine SDS-PAGE
	OPA1	BD Transduction Laboratories	612607	1:1000	tricine SDS-PAGE
	SERCA2	Abcam	2861	1:1000	tricine SDS-PAGE
	GM130	Sigma	G7295	1:3000	tricine SDS-PAGE
1B	ACBD3	Atlas Antibodies	HPA015594	1:500	ICC
	Giantin	Abcam	37266	1:200	ICC
	SERCA2	Abcam	2861	1:200	ICC
3A	GM130	Abcam	52649	1:250	ICC
	TGN46	Biorad	AHP500G	1:250	ICC
3D, A2A	ACBD3	Atlas Antibodies	HPA015594	1:2000	tricine SDS-PAGE
	GM130	Abcam	52649	1:5000	tricine SDS-PAGE
	GRASP65	Abcam	174834	1:1000	tricine SDS-PAGE
	GRASP55	ProteinTech	10598-1-AP	1:5000	tricine SDS-PAGE
	GAPDH	Abcam	8245	1:13,000	tricine SDS-PAGE
	$\beta$ -actin	Cell Signaling Technology	4970	1:2000	tricine SDS-PAGE
3E, A2B	LAMP2	Santa Cruz Biotechnology	18822	1:500	glycine SDS-PAGE
4A, 4B	NDUFA9	Abcam	14713	1:1000	BN-PAGE
	SDH70	Abcam	14715	1:10,000	BN-PAGE
	CORE2	Abcam	14745	1:8000	BN-PAGE
	COX2	Abcam	110258	1:10,000	BN-PAGE
	ATP $\beta$	Abcam	14730	1:4000	BN-PAGE



**Table A3.** *Cont.*

Figure	Antibody	Company	Catalog Number	Dilution	Method
4C, 4D	ACBD3	Atlas Antibodies	HPA015594	1:2000	tricine SDS-PAGE
	NDUFA9	Abcam	14713	1:2500	tricine SDS-PAGE
	NDUFB6	Abcam	110244	1:4000	tricine SDS-PAGE
	SDH70	Abcam	14715	1:20,000	tricine SDS-PAGE
	SDH30	Abcam	14714	1:1000	tricine SDS-PAGE
	CORE1	Abcam	110252	1:5000	tricine SDS-PAGE
	CORE2	Abcam	14745	1:20,000	tricine SDS-PAGE
	COX1	Abcam	14705	1:4000	tricine SDS-PAGE
	COX2	Abcam	110258	1:10,000	tricine SDS-PAGE
	COX5a	Abcam	110262	1:2000	tricine SDS-PAGE
	ATP $\beta$	Abcam	14730	1:2000	tricine SDS-PAGE
	VDAC1	Abcam	14734	1:2000	tricine SDS-PAGE
	GAPDH	Abcam	8245	1:13,000	tricine SDS-PAGE
	$\alpha$ -tubulin	Cell Signaling Technology	2125	1:2000	tricine SDS-PAGE
A1	ACBD3	Atlas Antibodies	HPA015594	1:500	ICC

Abbreviations: ICC—immunocytochemistry, SDS-PAGE—sodium dodecyl sulphate polyacrylamide gel electrophoresis, BN-PAGE—blue native polyacrylamide gel electrophoresis.

**Table A4.** Summary of antibodies used in experiments.

	Antibody	Company	Catalog Number	Results from SDS-PAGE in HEK293/HeLa
Not shown	StAR	Abcam	58013	↓↓↓/↓↓↓
	VDAC1	Abcam	14734	not changed/not changed
	TSPO	Cell Signaling	9530	↓↓↓/not changed
	ACBD1	Atlas Antibodies	HPA051428	↓↓↓/↓↓↓
		Abcam	16806	↓↓↓/not changed
ATAD3	Abcam	112572	↓↓↓/NA	

Annotation: ↓↓↓—low specificity of the antibody; NA—not analyzed.

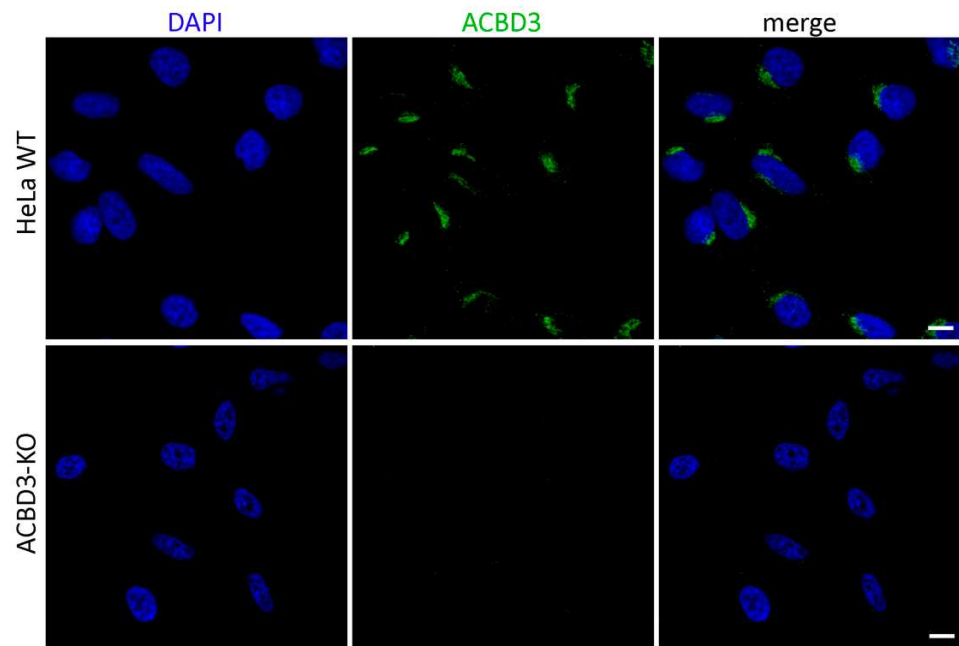


**Figure A1.** Confocal immunofluorescence images of ACBD3 antibody in HeLa WT and ACBD3-KO cell lines. Scale bar 10  $\mu$ m.

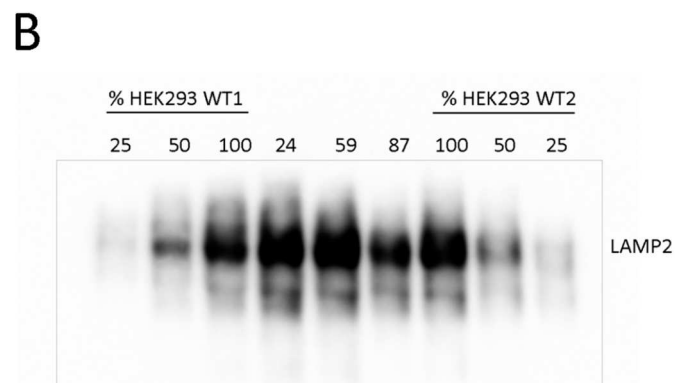
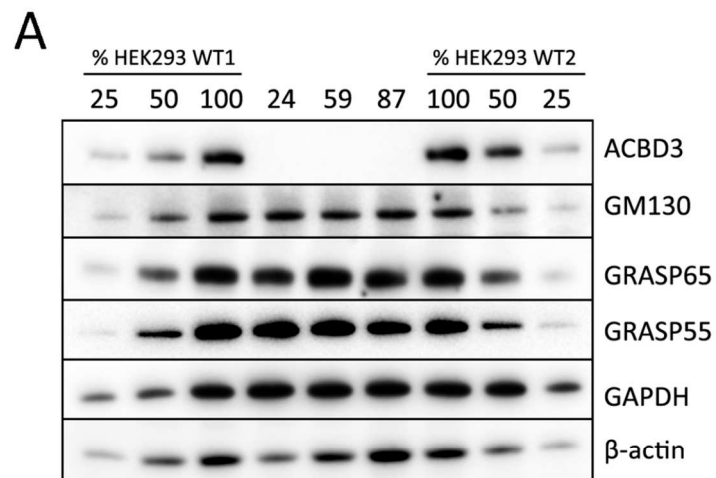


**Figure A2.** (A) Western blots of selected Golgi proteins in HEK293 ACBD3-KO cells. (B) Glycosylation of LAMP2 glycoprotein in HEK293 ACBD3-KO cells.

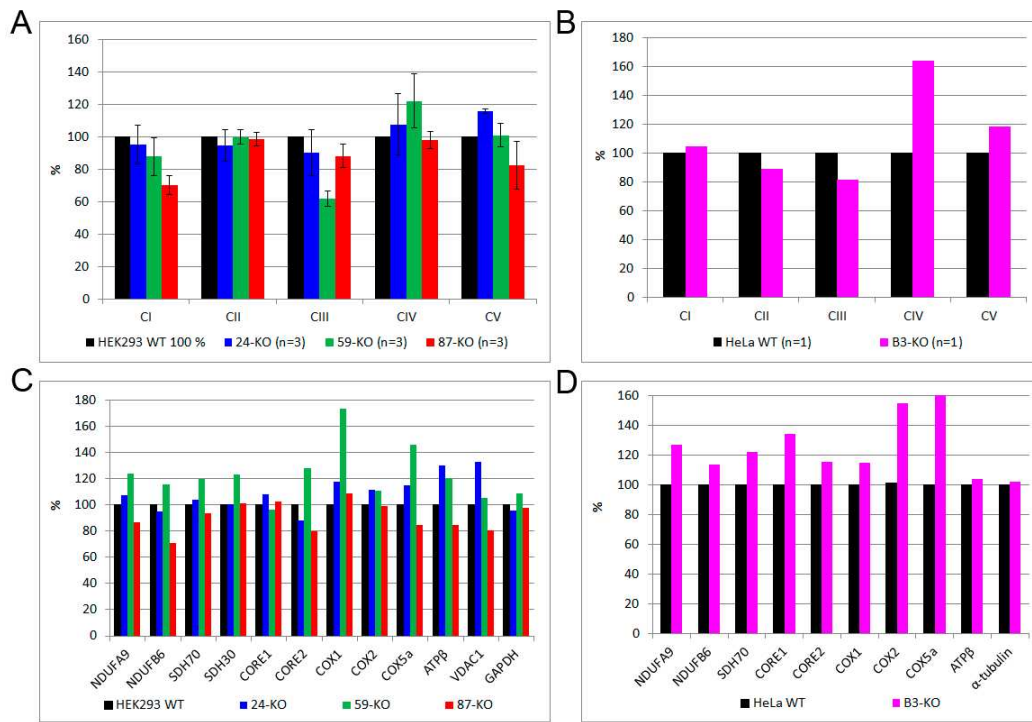


**Figure A3.** Quantification of Western blots from Figure 4. (A) BN-PAGE/WB of HEK293 ACBD3-KO, (B) BN-PAGE/WB of HeLa ACBD3-KO, (C) SDS-PAGE/WB of HEK293 ACBD3-KO, and (D) SDS-PAGE/WB of HeLa ACBD3-KO. ‘n’ represents number of independent analyses per sample.

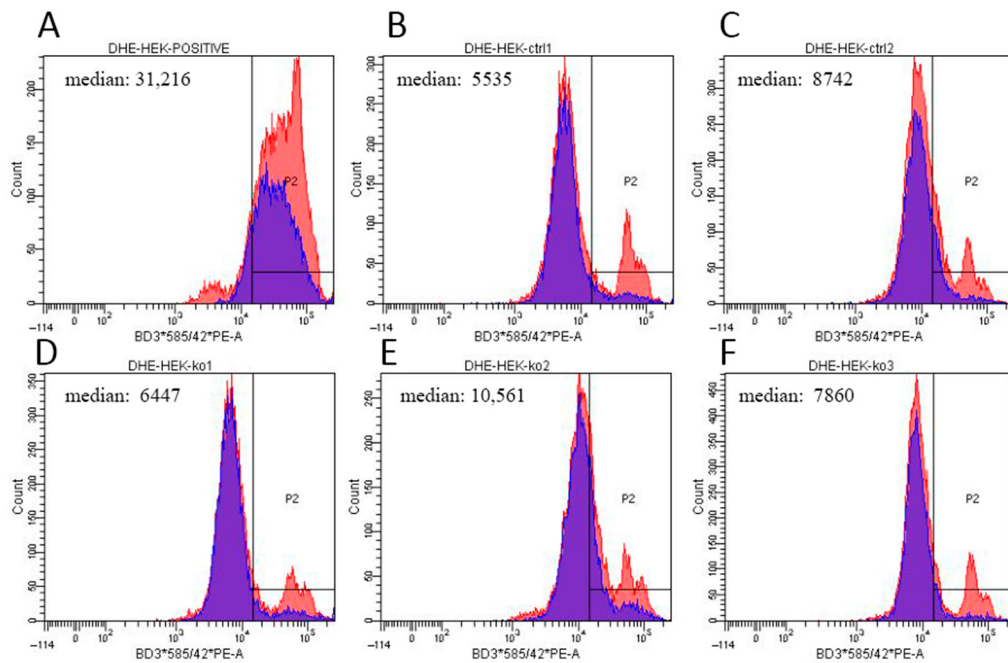


**Figure A4.** ROS detection by flow cytometry after DHE staining. Histogram plots show the fluorescent signal distribution in (A) a positive control treated with 100  $\mu$ M menadione, two control cell lines ((B) HEK293 WT1 and (C) WT2), and ACBD3-KO cell lines (D) 24-KO, (E) 59-KO, and (F) 87-KO. *x*-axis: fluorescence intensity; *y*-axis: cell count. Blue populations represents cells without ROS-positive signal in control samples; medians are figured in each plot. Slight increase in ROS production was observed in ACBD3-KO cell line 59 (median 10,561). ROS production in the other two ACBD3-KO cell lines remained in control range.

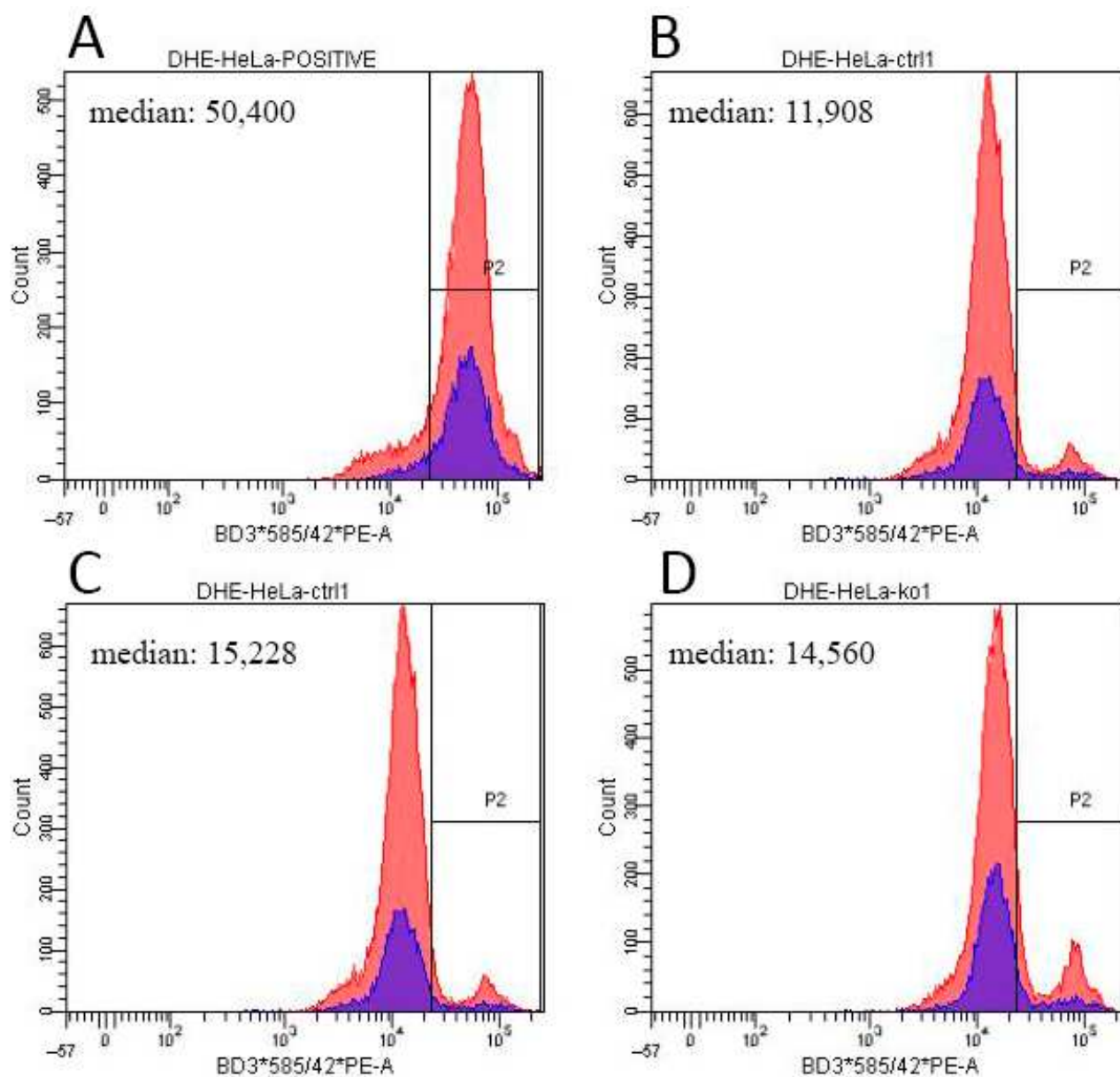


**Figure A5.** ROS detection by flow cytometry after DHE staining. Histogram plots show the fluorescent signal distribution in (A) a positive control treated with 100  $\mu$ M menadione, two control cell lines ((B) HeLa WT1 and (C) WT2), and ACBD3-KO cell line (D) B3-KO. *x*-axis: fluorescence intensity; *y*-axis: cell count. In case of HeLa ABCD3-KO, ROS production remained similar to controls.

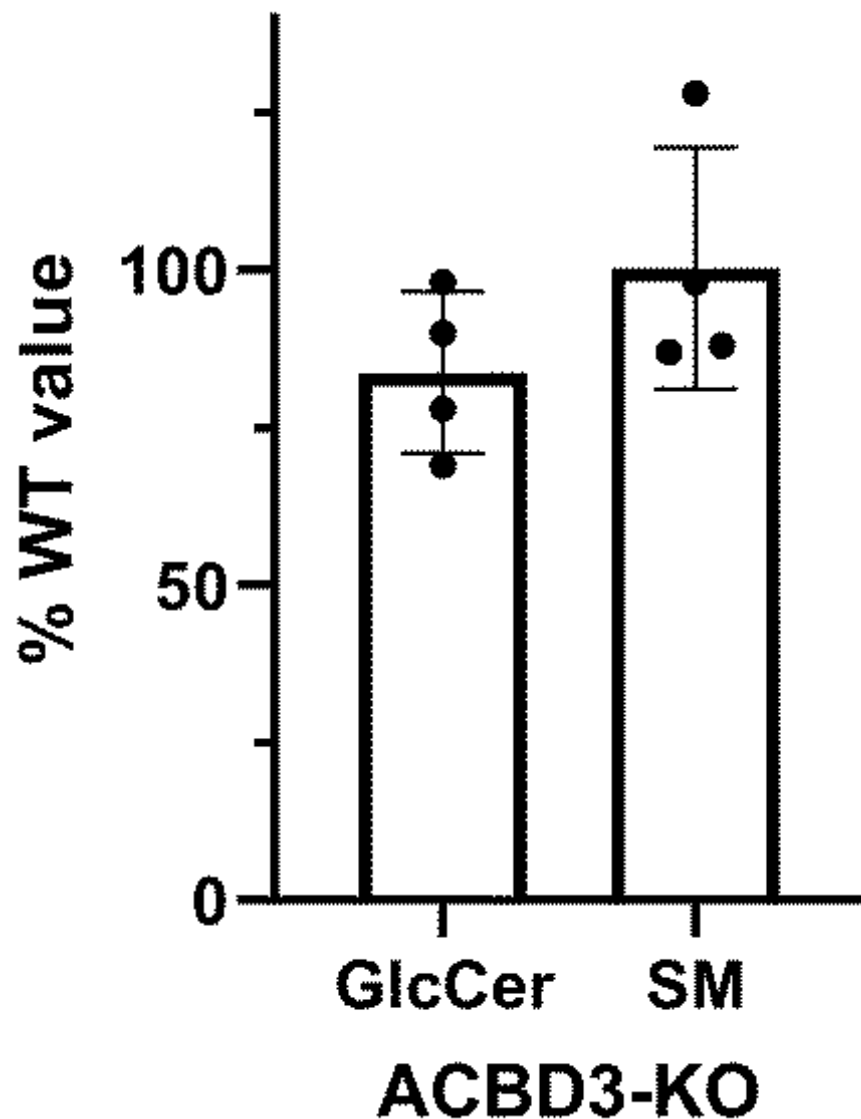


**Figure A6.** Quantification TLC results from Figure 5I. Relative signal intensity of glucosylceramide synthase (GlcCer) activity and sphingomyelin synthase (SM) activity were normalized to the intensity of ceramide by a densitometric analysis. Each dot represents value for particular ACBD3-KO. Values are displayed as a percentage of control value.

## References

- Uhlen, M.; Fagerberg, L.; Hallstrom, B.M.; Lindskog, C.; Oksvold, P.; Mardinoglu, A.; Sivertsson, A.; Kampf, C.; Sjostedt, E.; Asplund, A.; et al. Tissue-Based Map of the Human Proteome. *Science* **2015**, *347*, 1260419. [[CrossRef](#)]
- The UniProt Consortium UniProt: A Worldwide Hub of Protein Knowledge. *Nucleic Acids Res.* **2019**, *47*, D506–D515. [[CrossRef](#)]
- Binder, J.X.; Pletscher-Frankild, S.; Tsafou, K.; Stolte, C.; O'Donoghue, S.I.; Schneider, R.; Jensen, L.J. COMPARTMENTS: Unification and Visualization of Protein Subcellular Localization Evidence. *Database J. Biol. Databases Curation* **2014**, *2014*. [[CrossRef](#)] [[PubMed](#)]
- Sohda, M.; Misumi, Y.; Yamamoto, A.; Yano, A.; Nakamura, N.; Ikehara, Y. Identification and Characterization of a Novel Golgi Protein, GCP60, That Interacts with the Integral Membrane Protein Giantin. *J. Biol. Chem.* **2001**, *276*, 45298–45306. [[CrossRef](#)]
- Li, H.; Degenhardt, B.; Tobin, D.; Yao, Z.X.; Tasken, K.; Papadopoulos, V. Identification, Localization, and Function in Steroidogenesis of PAP7: A Peripheral-Type Benzodiazepine Receptor- and PKA (RIalpha)-Associated Protein. *Mol. Endocrinol. Baltim. Md* **2001**, *15*, 2211–2228. [[CrossRef](#)]
- Liu, J.; Rone, M.B.; Papadopoulos, V. Protein-Protein Interactions Mediate Mitochondrial Cholesterol Transport and Steroid Biosynthesis. *J. Biol. Chem.* **2006**, *281*, 38879–38893. [[CrossRef](#)]

7. Yue, X.; Bao, M.; Christiano, R.; Li, S.; Mei, J.; Zhu, L.; Mao, F.; Yue, Q.; Zhang, P.; Jing, S.; et al. ACBD3 Functions as a Scaffold to Organize the Golgi Stacking Proteins and a Rab33b-GAP. *FEBS Lett.* **2017**, *591*, 2793–2802. [[CrossRef](#)] [[PubMed](#)]
8. Liao, J.; Guan, Y.; Chen, W.; Shi, C.; Yao, D.; Wang, F.; Lam, S.M.; Shui, G.; Cao, X. ACBD3 Is Required for FAPP2 Transferring Glucosylceramide through Maintaining the Golgi Integrity. *J. Mol. Cell Biol.* **2019**, *11*, 107–117. [[CrossRef](#)]
9. Shinoda, Y.; Fujita, K.; Saito, S.; Matsui, H.; Kanto, Y.; Nagaura, Y.; Fukunaga, K.; Tamura, S.; Kobayashi, T. Acyl-CoA Binding Domain Containing 3 (ACBD3) Recruits the Protein Phosphatase PPM1L to ER-Golgi Membrane Contact Sites. *FEBS Lett.* **2012**, *586*, 3024–3029. [[CrossRef](#)] [[PubMed](#)]
10. Islinger, M.; Costello, J.L.; Kors, S.; Soupene, E.; Levine, T.P.; Kuypers, F.A.; Schrader, M. The Diversity of ACBD Proteins—From Lipid Binding to Protein Modulators and Organelle Tethers. *Biochim. Biophys. Acta BBA Mol. Cell Res.* **2020**, *1867*, 118675. [[CrossRef](#)]
11. Elustondo, P.; Martin, L.A.; Karten, B. Mitochondrial Cholesterol Import. *Biochim. Biophys. Acta BBA Mol. Cell Biol. Lipids* **2017**, *1862*, 90–101. [[CrossRef](#)]
12. Hensen, F.; Cansiz, S.; Gerhold, J.M.; Spelbrink, J.N. To Be or Not to Be a Nucleoid Protein: A Comparison of Mass-Spectrometry Based Approaches in the Identification of Potential MtDNA-Nucleoid Associated Proteins. *Biochimie* **2014**, *100*, 219–226. [[CrossRef](#)] [[PubMed](#)]
13. Gerhold, J.M.; Cansiz-Arda, Ş.; Löhmus, M.; Engberg, O.; Reyes, A.; van Rennes, H.; Sanz, A.; Holt, I.J.; Cooper, H.M.; Spelbrink, J.N. Human Mitochondrial DNA-Protein Complexes Attach to a Cholesterol-Rich Membrane Structure. *Sci. Rep.* **2015**, *5*. [[CrossRef](#)] [[PubMed](#)]
14. He, J.; Cooper, H.M.; Reyes, A.; Di Re, M.; Sembongi, H.; Litwin, T.R.; Gao, J.; Neuman, K.C.; Fearnley, I.M.; Spinazzola, A.; et al. Mitochondrial Nucleoid Interacting Proteins Support Mitochondrial Protein Synthesis. *Nucleic Acids Res.* **2012**, *40*, 6109–6121. [[CrossRef](#)] [[PubMed](#)]
15. He, J.; Mao, C.-C.; Reyes, A.; Sembongi, H.; Di Re, M.; Granycome, C.; Clippingdale, A.B.; Fearnley, I.M.; Harbour, M.; Robinson, A.J.; et al. The AAA+ Protein ATAD3 Has Displacement Loop Binding Properties and Is Involved in Mitochondrial Nucleoid Organization. *J. Cell Biol.* **2007**, *176*, 141–146. [[CrossRef](#)]
16. Peralta, S.; Goffart, S.; Williams, S.L.; Diaz, F.; Garcia, S.; Nissanka, N.; Area-Gomez, E.; Pohjoismäki, J.; Moraes, C.T. ATAD3 Controls Mitochondrial Cristae Structure in Mouse Muscle, Influencing MtDNA Replication and Cholesterol Levels. *J. Cell Sci.* **2018**, *131*. [[CrossRef](#)]
17. Mesmin, B.; Maxfield, F.R. Intracellular Sterol Dynamics. *Biochim. Biophys. Acta BBA Mol. Cell Biol. Lipids* **2009**, *1791*, 636–645. [[CrossRef](#)] [[PubMed](#)]
18. Rone, M.B.; Midzak, A.S.; Issop, L.; Rammouz, G.; Jagannathan, S.; Fan, J.; Ye, X.; Blonder, J.; Veenstra, T.; Papadopoulos, V. Identification of a Dynamic Mitochondrial Protein Complex Driving Cholesterol Import, Trafficking, and Metabolism to Steroid Hormones. *Mol. Endocrinol.* **2012**, *26*, 1868–1882. [[CrossRef](#)]
19. Desai, R.; East, D.A.; Hardy, L.; Faccenda, D.; Rigon, M.; Crosby, J.; Alvarez, M.S.; Singh, A.; Mainenti, M.; Hussey, L.K.; et al. Mitochondria Form Contact Sites with the Nucleus to Couple Prosurvival Retrograde Response. *Sci. Adv.* **2020**, *6*. [[CrossRef](#)] [[PubMed](#)]
20. Hornig-Do, H.-T.; Günther, G.; Bust, M.; Lehnartz, P.; Bosio, A.; Wiesner, R.J. Isolation of Functional Pure Mitochondria by Superparamagnetic Microbeads. *Anal. Biochem.* **2009**, *389*, 1–5. [[CrossRef](#)]
21. Brantová, O.; Tesařová, M.; Hansíková, H.; Elleder, M.; Zeman, J.; Sládková, J. Ultrastructural Changes of Mitochondria in the Cultivated Skin Fibroblasts of Patients with Point Mutations in Mitochondrial DNA. *Ultrastruct. Pathol.* **2006**, *30*, 239–245. [[CrossRef](#)]
22. Cesnekova, J.; Rodinova, M.; Hansikova, H.; Zeman, J.; Stiburek, L. Loss of Mitochondrial AAA Proteases AFG3L2 and YME1L Impairs Mitochondrial Structure and Respiratory Chain Biogenesis. *Int. J. Mol. Sci.* **2018**, *19*, 3930. [[CrossRef](#)]
23. Bilal, F.; Pérès, M.; Andrieu-Abadie, N.; Levade, T.; Badran, B.; Daher, A.; Ségui, B. Method to Measure Sphingomyelin Synthase Activity Changes in Response to CD95L. In *CD95*; Humana Press: New York, NY, USA, 2017; Volume 1557, pp. 207–212. [[CrossRef](#)]
24. Sbodio, J.I.; Hicks, S.W.; Simon, D.; Machamer, C.E. GCP60 Preferentially Interacts with a Caspase-Generated Golgin-160 Fragment. *J. Biol. Chem.* **2006**, *281*, 27924–27931. [[CrossRef](#)]
25. Klima, M.; Tóth, D.J.; Hexnerova, R.; Baumlova, A.; Chalupska, D.; Tykvart, J.; Rezabkova, L.; Sengupta, N.; Man, P.; Dubankova, A.; et al. Structural Insights and in Vitro Reconstitution of Membrane Targeting and Activation of Human PI4KB by the ACBD3 Protein. *Sci. Rep.* **2016**, *6*. [[CrossRef](#)]
26. Chen, Y.; Patel, V.; Bang, S.; Cohen, N.; Millar, J.; Kim, S.F. Maturation and Activity of Sterol Regulatory Element Binding Protein 1 Is Inhibited by Acyl-CoA Binding Domain Containing 3. *PLoS ONE* **2012**, *7*, e49906. [[CrossRef](#)]
27. Bekier, M.E.; Wang, L.; Li, J.; Huang, H.; Tang, D.; Zhang, X.; Wang, Y. Knockout of the Golgi Stacking Proteins GRASP55 and GRASP65 Impairs Golgi Structure and Function. *Mol. Biol. Cell* **2017**, *28*, 2833–2842. [[CrossRef](#)] [[PubMed](#)]
28. Miller, W.L. Steroid Hormone Synthesis in Mitochondria. *Mol. Cell. Endocrinol.* **2013**, *379*, 62–73. [[CrossRef](#)]
29. Midzak, A.; Rone, M.; Aghazadeh, Y.; Culty, M.; Papadopoulos, V. Mitochondrial Protein Import and the Genesis of Steroidogenic Mitochondria. *Mol. Cell. Endocrinol.* **2011**, *336*, 70–79. [[CrossRef](#)] [[PubMed](#)]
30. Desai, R.; Campanella, M. Exploring Mitochondrial Cholesterol Signalling for Therapeutic Intervention in Neurological Conditions. *Br. J. Pharmacol.* **2019**, *176*, 4284–4292. [[CrossRef](#)] [[PubMed](#)]

31. Midzak, A.; Papadopoulos, V. Adrenal Mitochondria and Steroidogenesis: From Individual Proteins to Functional Protein Assemblies. *Front. Endocrinol.* **2016**, *7*. [[CrossRef](#)]
32. Papadopoulos, V.; Guarneri, P.; Kreuger, K.E.; Guidotti, A.; Costa, E. Pregnenolone Biosynthesis in C6-2B Glioma Cell Mitochondria: Regulation by a Mitochondrial Diazepam Binding Inhibitor Receptor. *Proc. Natl. Acad. Sci. USA* **1992**, *89*, 5113–5117. [[CrossRef](#)] [[PubMed](#)]
33. Boujrad, N.; Hudson, J.R.; Papadopoulos, V. Inhibition of Hormone-Stimulated Steroidogenesis in Cultured Leydig Tumor Cells by a Cholesterol-Linked Phosphorothioate Oligodeoxynucleotide Antisense to Diazepam-Binding Inhibitor. *Proc. Natl. Acad. Sci. USA* **1993**, *90*, 5728–5731. [[CrossRef](#)]
34. Garnier, M.; Boujrad, N.; Ogwuegbu, S.O.; Hudson, J.R.; Papadopoulos, V. The Polypeptide Diazepam-Binding Inhibitor and a Higher Affinity Mitochondrial Peripheral-Type Benzodiazepine Receptor Sustain Constitutive Steroidogenesis in the R2C Leydig Tumor Cell Line. *J. Biol. Chem.* **1994**, *269*, 22105–22112. [[CrossRef](#)]
35. Papadopoulos, V.; Brown, A.S. Role of the Peripheral-Type Benzodiazepine Receptor and the Polypeptide Diazepam Binding Inhibitor in Steroidogenesis. *J. Steroid Biochem. Mol. Biol.* **1995**, *53*, 103–110. [[CrossRef](#)]
36. Fan, J.; Li, X.; Issop, L.; Culty, M.; Papadopoulos, V. ACBD2/ECI2-Mediated Peroxisome-Mitochondria Interactions in Leydig Cell Steroid Biosynthesis. *Mol. Endocrinol.* **2016**, *30*, 763–782. [[CrossRef](#)] [[PubMed](#)]
37. Andersen, J.-P.; Zhang, J.; Sun, H.; Liu, X.; Liu, J.; Nie, J.; Shi, Y. Aster-B Coordinates with Arf1 to Regulate Mitochondrial Cholesterol Transport. *Mol. Metab.* **2020**, *42*, 101055. [[CrossRef](#)] [[PubMed](#)]
38. Saiki, R.; Nagata, A.; Kainou, T.; Matsuda, H.; Kawamukai, M. Characterization of Solanesyl and Decaprenyl Diphosphate Synthases in Mice and Humans. *FEBS J.* **2005**, *272*, 5606–5622. [[CrossRef](#)] [[PubMed](#)]
39. Huttlin, E.L.; Bruckner, R.J.; Paulo, J.A.; Cannon, J.R.; Ting, L.; Baltier, K.; Colby, G.; Gebreab, F.; Gygi, M.P.; Parzen, H.; et al. Architecture of the Human Interactome Defines Protein Communities and Disease Networks. *Nature* **2017**, *545*, 505–509. [[CrossRef](#)] [[PubMed](#)]
40. Greninger, A.L.; Knudsen, G.M.; Betegon, M.; Burlingame, A.L.; DeRisi, J.L. The 3A Protein from Multiple Picornaviruses Utilizes the Golgi Adaptor Protein ACBD3 To Recruit PI4KIII $\beta$ . *J. Virol.* **2012**, *86*, 3605–3616. [[CrossRef](#)]
41. Kumagai, K.; Hanada, K. Structure, Functions and Regulation of CERT, a Lipid-transfer Protein for the Delivery of Ceramide at the ER–Golgi Membrane Contact Sites. *FEBS Lett.* **2019**, *593*, 2366–2377. [[CrossRef](#)]
42. Yamaji, T.; Hanada, K. Establishment of HeLa Cell Mutants Deficient in Sphingolipid-Related Genes Using TALENs. *PLoS ONE* **2014**, *9*, e88124. [[CrossRef](#)]
43. Housden, B.E.; Muhar, M.; Gemberling, M.; Gersbach, C.A.; Stainier, D.Y.R.; Seydoux, G.; Mohr, S.E.; Zuber, J.; Perrimon, N. Loss-of-Function Genetic Tools for Animal Models: Cross-Species and Cross-Platform Differences. *Nat. Rev. Genet.* **2017**, *18*, 24–40. [[CrossRef](#)] [[PubMed](#)]
44. Zimmer, A.M.; Pan, Y.K.; Chandrapalan, T.; Kwong, R.W.M.; Perry, S.F. Loss-of-Function Approaches in Comparative Physiology: Is There a Future for Knockdown Experiments in the Era of Genome Editing? *J. Exp. Biol.* **2019**, *222*, jeb175737. [[CrossRef](#)] [[PubMed](#)]
45. Stiburek, L.; Vesela, K.; Hansikova, H.; Pecina, P.; Tesarova, M.; Cerna, L.; Houstek, J.; Zeman, J. Tissue-Specific Cytochrome c Oxidase Assembly Defects Due to Mutations in SCO<sub>2</sub> and SURF1. *Biochem. J.* **2005**, *392*, 625–632. [[CrossRef](#)]
46. Schagger, H.; von Jagow, G. Tricine-Sodium Dodecyl Sulfate-Polyacrylamide Gel Electrophoresis for the Separation of Proteins in the Range from 1 to 100 KDa. *Anal. Biochem.* **1987**, *166*, 368–379. [[CrossRef](#)]
47. Schagger, H.; von Jagow, G. Blue Native Electrophoresis for Isolation of Membrane Protein Complexes in Enzymatically Active Form. *Anal. Biochem.* **1991**, *199*, 223–231. [[CrossRef](#)]
48. Gnaiger, E. Mitochondrial Pathways and Respiratory Control: An Introduction to OXPHOS Analysis. In *Mitochondr Physiol Network 19.12*, 5th ed.; Oroboros MiPNet Publications: Innsbruck, Austria, 2020. [[CrossRef](#)]
49. Pejznochova, M.; Tesarova, M.; Hansikova, H.; Magner, M.; Honzik, T.; Vinsova, K.; Hajkova, Z.; Havlickova, V.; Zeman, J. Mitochondrial DNA Content and Expression of Genes Involved in MtDNA Transcription, Regulation and Maintenance during Human Fetal Development. *Mitochondrion* **2010**, *10*, 321–329. [[CrossRef](#)] [[PubMed](#)]
50. Ondruskova, N.; Honzik, T.; Vondrackova, A.; Stranecky, V.; Tesarova, M.; Zeman, J.; Hansikova, H. Severe Phenotype of ATP6AP1-CDG in Two Siblings with a Novel Mutation Leading to a Differential Tissue-Specific ATP6AP1 Protein Pattern, Cellular Oxidative Stress and Hepatic Copper Accumulation. *J. Inherit. Metab. Dis.* **2020**, *43*, 694–700. [[CrossRef](#)]
51. Luft, J.H. Permanganate; a New Fixative for Electron Microscopy. *J. Biophys. Biochem. Cytol.* **1956**, *2*, 799–802. [[CrossRef](#)]
52. Janovska, P.; Melenovsky, V.; Svobodova, M.; Havlenova, T.; Kratochvilova, H.; Haluzik, M.; Hoskova, E.; Pelikanova, T.; Kautzner, J.; Monzo, L.; et al. Dysregulation of Epicardial Adipose Tissue in Cachexia Due to Heart Failure: The Role of Natriuretic Peptides and Cardiopilin. *J. Cachexia Sarcopenia Muscle* **2020**, *11*, 1614–1627. [[CrossRef](#)]
53. Paluchova, V.; Oseeva, M.; Brezinova, M.; Cajka, T.; Bardova, K.; Adamcova, K.; Zacek, P.; Brejchova, K.; Balas, L.; Choudounska, H.; et al. Lipokine 5-PAHSA Is Regulated by Adipose Triglyceride Lipase and Primes Adipocytes for De Novo Lipogenesis in Mice. *Diabetes* **2020**, *69*, 300–312. [[CrossRef](#)] [[PubMed](#)]

54. Paluchova, V.; Vik, A.; Cajka, T.; Brezinova, M.; Brejchova, K.; Bugajev, V.; Draberova, L.; Draber, P.; Buresova, J.; Kroupova, P.; et al. Triacylglycerol-Rich Oils of Marine Origin Are Optimal Nutrients for Induction of Polyunsaturated Docosahexaenoic Acid Ester of Hydroxy Linoleic Acid (13-DHAHLA) with Anti-Inflammatory Properties in Mice. *Mol. Nutr. Food Res.* **2020**, *64*, e1901238. [[CrossRef](#)] [[PubMed](#)]
55. Sistilli, G.; Kalendova, V.; Cajka, T.; Irodenko, I.; Bardova, K.; Oseeva, M.; Zacek, P.; Kroupova, P.; Horakova, O.; Lackner, K.; et al. Krill Oil Supplementation Reduces Exacerbated Hepatic Steatosis Induced by Thermoneutral Housing in Mice with Diet-Induced Obesity. *Nutrients* **2021**, *13*, 437. [[CrossRef](#)] [[PubMed](#)]




RESEARCH ARTICLE

Open Access



# Multisystem mitochondrial diseases due to mutations in mtDNA-encoded subunits of complex I

Tereza Danhelovska<sup>1</sup>, Hana Kolarova<sup>1</sup>, Jiri Zeman<sup>1</sup>, Hana Hansikova<sup>1</sup>, Manuela Vaneckova<sup>2</sup>, Lukas Lambert<sup>2</sup>, Vendula Kucerova-Vidrova<sup>1</sup>, Kamila Berankova<sup>1</sup>, Tomas Honzik<sup>1</sup> and Marketa Tesarova<sup>1\*</sup> 

## Abstract

**Background:** Maternally inherited complex I deficiencies due to mutations in *MT-ND* genes represent a heterogeneous group of multisystem mitochondrial disorders (MD) with a unfavourable prognosis. The aim of the study was to characterize the impact of the mutations in *MT-ND* genes, including the novel m.13091 T > C variant, on the course of the disease, and to analyse the activities of respiratory chain complexes, the amount of protein subunits, and the mitochondrial energy-generating system (MEGS) in available muscle biopsies and cultivated fibroblasts.

**Methods:** The respiratory chain complex activities were measured by spectrophotometry, MEGS were analysed using radiolabelled substrates, and protein amount by SDS-PAGE or BN-PAGE in muscle or fibroblasts.

**Results:** In our cohort of 106 unrelated families carrying different mtDNA mutations, we found heteroplasmic mutations in the genes *MT-ND1*, *MT-ND3*, and *MT-ND5*, including the novel variant m.13091 T > C, in 13 patients with MD from 12 families. First symptoms developed between early childhood and adolescence and progressed to multisystem disease with a phenotype of Leigh or MELAS syndromes. MRI revealed bilateral symmetrical involvement of deep grey matter typical of Leigh syndrome in 6 children, cortical/white matter stroke-like lesions suggesting MELAS syndrome in 3 patients, and a combination of cortico-subcortical lesions and grey matter involvement in 4 patients. MEGS indicated mitochondrial disturbances in all available muscle samples, as well as a significantly decreased oxidation of [1-<sup>14</sup>C] pyruvate in fibroblasts. Spectrophotometric analyses revealed a low activity of complex I and/or complex I + III in all muscle samples except one, but the activities in fibroblasts were mostly normal. No correlation was found between complex I activities and mtDNA mutation load, but higher levels of heteroplasmy were generally found in more severely affected patients.

**Conclusions:** Maternally inherited complex I deficiencies were found in 11% of families with mitochondrial diseases in our region. Six patients manifested with Leigh, three with MELAS. The remaining four patients presented with an overlap between these two syndromes. MEGS, especially the oxidation of [1-<sup>14</sup>C] pyruvate in fibroblasts might serve as a sensitive indicator of functional impairment due to *MT-ND* mutations. Early onset of the disease and higher level of mtDNA heteroplasmy were associated with a worse prognosis.

**Keywords:** mtDNA, *MT-ND* genes, Complex I, Leigh syndrome, MELAS syndrome, MEGS, Mitochondria

\* Correspondence: [marketa.tesarova@lf1.cuni.cz](mailto:marketa.tesarova@lf1.cuni.cz)

<sup>1</sup>Department of Pediatrics and Adolescent Medicine, First Faculty of Medicine, Charles University and General University Hospital in Prague, Ke Karlovu 2, 128 08 Praha 2, Prague, Czech Republic

Full list of author information is available at the end of the article



## Background

Disturbances of the respiratory chain complex I (CI, NADH:coenzyme Q oxidoreductase, EC 1.6.5.3) represent the most common cause of multisystem mitochondrial disorders (MD), accounting for nearly one-third of patients [1]. CI consists of 45 protein subunits with different functions necessary for enzyme assembly, stabilization, and regulation [2], encoded by genes in nuclear or mitochondrial DNA (mtDNA). Many mutations in these genes have already been described including in 22 genes for structural proteins and 11 genes for non-structural proteins encoded by nuclear DNA (Additional file 1: Table S1), and in all 7 mtDNA genes (*MT-ND1–6* and *MT-ND4L*) for structural subunits of CI. With respect to maternally inherited mutations, 28 different mutations sites have been confirmed, and another 113 sites in *MT-ND* genes have been published ([www.mitomap.org](http://www.mitomap.org)).

Clinically, CI deficiency represents a heterogeneous group of MDs with an early, neonatal onset of fatal lactic acidosis; infantile onset of progressive mitochondrial encephalopathy with Leigh syndrome (LS); onset of Mitochondrial Encephalopathy, Lactic Acidosis and Stroke-like episodes (MELAS) syndrome during childhood, or adult-onset encephalomyopathic syndromes with various severities. Leber Hereditary Optic Neuropathy (LHON) syndrome with acute or subacute loss of vision usually starts during the second or third decade of life. In addition, several studies have also documented the LHON/MELAS overlap syndromes [3–5].

The prognosis in patients with maternally inherited complex I deficiencies is unfavourable and hardly predictable. In the cohort of 13 patients with MD due to 8 different mtDNA mutations in *MT-ND1*, *MT-ND3* and *MT-ND5* genes, including one novel variant m.13091 T > C in *MT-ND5* gene, we characterized the impact of the mutations in *MT-ND* genes on the course of the disease and we analysed their biochemical consequences in available muscle biopsies and cultivated skin fibroblasts.

## Material and methods

### Patients

Our laboratory serves as the diagnostic centre for MD in the Czech Republic, a country with 10.5 million inhabitants. During the last 25 years, different maternally inherited mtDNA mutations have been diagnosed in 106 unrelated families and sporadic large-scale deletions in mtDNA in 25 patients with Kearns-Sayre/Pearson syndromes. mtDNA mutations in genes for structural subunits of CI were present in 47 families, including 12 families with 13 patients with multisystem diseases due to heteroplasmic mtDNA mutations in *MT-ND1*, *MT-ND3* and *MT-ND5*, and 35 families with CI deficiency and LHON syndrome with tissue-specific optic nerve

involvement due to homoplasmic mutations in m.3460G > A in *MT-ND1*, m.11777G > A in *MT-ND4* and m.14484 T > C in *MT-ND6*.

## Methods

### Analysis of mtDNA

In patients 1–8 and 10, total genomic DNA isolated from muscle biopsy or cultivated skin fibroblasts (P2) and mtDNA (NC\_012920) was sequenced as described previously [6]. In patients 9 and 11–13, the mtDNA mutation m.13513G > A was detected by PCR-RFLP using mismatch primers (F: 5'-GTTTTCGGTTTCGA TGATGTGAT-3'; R: 5'-AACCATACC-TCTCAC TTCAACCTCCC-3') and Bsp143I endonuclease (Thermo Fisher Scientific, Waltham, Massachusetts, USA). Levels of heteroplasmy in available tissues were determined by mutation-specific PCR-RFLP analyses. Digested products were separated on an Agilent 2100 Bioanalyzer using High Sensitivity DNA kits. For each sample, the intensities of the individual restriction fragments were determined using Agilent 2100 Expert Software (Agilent Technologies, Santa Clara, California, USA). The level of heteroplasmy was calculated as the percentage of fragment intensity corresponding to the mutated mtDNA molecule. The detection limit of this method is 3%.

### Isolation of mitochondria

Samples obtained by muscle biopsy were transported on ice (at 4 °C) and mitochondria were isolated immediately according to standard differential centrifugation procedures [7] in a buffer containing 150 mM KCl, 50 mM Tris/HCl, 2 mM EDTA and 2 µg/ml aprotinin (pH 7.5) at 4 °C. The homogenate was centrifuged for 10 min at 4 °C and 600 g, the supernatant was filtered through a 100 µm nylon membrane, and mitochondria were obtained by centrifugation for 10 min at 4 °C and 10,000 g. The mitochondrial pellet was washed and resuspended to a final protein concentration of 20–25 mg/ml [8].

### Spectrophotometry

The activities of respiratory chain complexes (complex I – NADH:coenzyme Q oxidoreductase, CI, EC 1.6.5.3; complex I + III – NADH:cytochrome *c* oxidoreductase, CI + III; complex II – succinate:coenzyme Q oxidoreductase, CII, EC 1.3.5.1; complex II + III – succinate:cytochrome *c* oxidoreductase, CII + III; complex III – coenzyme Q:cytochrome *c* oxidoreductase, CIII, EC 7.1.1.8; complex IV – cytochrome *c* oxidase, CIV, EC 1.9.3.1) were measured according to [9]. The activity of citrate synthase (CS, EC 2.3.3.1), serving as the control enzyme to avoid assay variability, was measured according to [10]. Protein concentrations were measured by the Lowry method [11].

### Electrophoresis

Blue Native Polyacrylamide Gel Electrophoresis (BN-PAGE) separation [12] of mitochondrial membrane complexes on polyacrylamide 4–14% or 6–15% (w/v) gradient gels (MiniProtean<sup>®</sup> 3 System; Bio-Rad, Hercules, California, USA), followed by immunoblot analysis was used to analyse the steady-state levels of oxidative phosphorylation system complexes [13]. Primary detection of BN-PAGE blots was performed using mouse monoclonal antibodies against the CI subunit NDUFA9 (1:2000), complex II subunit SDH70 protein (1: 6666), complex III subunit Core 2 (1:20000), complex IV subunit COX1 (1:3000) and ATP synthase subunit alpha (1:2000) (Abcam, Cambridge, UK). Sodium Dodecyl Sulfate Polyacrylamide Gel Electrophoresis (SDS-PAGE) was performed on 12% (w/v) polyacrylamide minigels (Mini-Protean<sup>®</sup> 3 System) according to Schägger and von Jagow [14]. Primary antibodies against the CI subunits ND5 (1: 2000), NDUFA9 (1:4000), and NDUF6 (1:3000); complex II subunit SDH70 (1:20000); complex III subunits Core 1 (1:2000) and Core 2 (1:40000); complex IV subunit COX2 (1:10000) (all from Abcam) and control cytosol marker  $\beta$ -tubulin (1:4000; Sigma, St. Louis, Missouri, USA) were used for the detection of SDS-PAGE membranes. The immunoblots were detected with peroxidase-conjugated secondary antibodies and Super-Signal West Femto Maximum Sensitivity Substrate (Thermo Fisher Scientific) using G:Box (Syngene, Cambridge, UK) and analysed by Quantity One software (Bio-Rad).

### MEGS analysis

The analysis of the mitochondrial energy-generating system (MEGS) was performed in 10 incubations containing <sup>14</sup>C-labelled pyruvate, malate and succinate, donors and acceptors of Acetyl-CoA and inhibitors of TCA cycle, according to Janssen [15]. Briefly, each incubation contains the buffer for MEGS (30 mM KH<sub>2</sub>PO<sub>4</sub> pH 7.4; 75 mM KCl; 8 mM Tris; 1.6 mM EDTA; 5 mM MgCl<sub>2</sub>; 0.2 mM p<sub>1</sub>,p<sub>5</sub>-di (adenosine-5') pentaphosphate (myoadenylate kinase inhibitor), and where indicated, 2 nM ADP; 1 mM pyruvate; 1 mM malate; 1 mM succinate (all from Sigma); with combinations of [1-<sup>14</sup>C] pyruvate (PerkinElmer, Waltham, Massachusetts, USA); [U-<sup>14</sup>C] malate (PerkinElmer) and [1,4-<sup>14</sup>C] succinate (Moravek Biochemicals, Brea, California, USA); 5 mM L-carnitine; 2 mM acetyl-D,L-carnitine; 2 mM sodium arsenite; 5 mM malonate; 2  $\mu$ M CCCP and 40  $\mu$ M atractyloside (all from Sigma). The composition of individual incubations is summarized in Additional file 1: Table S2. Incubations were performed in a shaking water bath at 37 °C in 0.2 ml glass incubation vials with caps and rubber septa. The measurement was started by adding 5  $\mu$ l of whole cell lysate of fibroblasts and stopped after 20 min by

50  $\mu$ l 3 M HClO<sub>4</sub>. The CO<sub>2</sub> produced was trapped on a filter paper (saturated by 1 M NaOH) in each cap for 1 h at 4 °C; the filter paper was then transferred to a scintillation vial with 3 ml BCS solution (Amersham, Little Chalfont, UK) and <sup>14</sup>CO<sub>2</sub> was counted after 24 h in the Beckman Coulter LS6500 (Beckman Coulter, Brea, California, USA). Due to repeated measurements, the data related to protein amounts were analysed using a logistic regression model with mixed effects, where the studied reaction was perceived as a disease predictor and patient subjects or controls as a random effect. *P*-values less than 0.05 were considered statistically significant. Analysis was performed in R 3.5.1 statistical package, R Core Team (2018).

### Results

Multisystem MDs caused by mtDNA mutations in genes for structural subunits of CI were diagnosed in 13 patients from 12 families (P1 and P2 were cousins; their mothers are sisters), representing 11% of families with reported mtDNA mutations in our geographical region. Altogether, 8 different heteroplasmic mtDNA mutations in the genes *MT-ND1*, *MT-ND3*, and *MT-ND5* were found, including one novel variant m.13091 T > C (p.Met252Thr) in *MT-ND5*. The mutations and the levels of mtDNA heteroplasmy in muscle biopsies, cultivated fibroblasts, and other tissues are shown in Table 1. The most frequent were mutations in *MT-ND5* (69%). The same mtDNA mutations as in patients were also found in six mothers (of P1, P4, P5, P8, P10, and P11) and in two sisters (of P4 and P10) at least in one out of three or four examined tissues (blood, urinary sediment, buccal smear or hair follicles). All were asymptomatic, except the mother of P8 who had repeated attacks of migraine. No mutations were detected in the other six mothers; the mother of P2 was not analysed.

### Clinical data

Clinical data are outlined in Table 1. The onset of the disease varied from the neonatal period to 17 years, and three main phenotypes were observed: 1) Six children developed LS (P1, P2, P4, P6, P9, and P13) associated with a worse prognosis, because four of them died between the age of 16 months and 7 years. Two surviving children with LS (P6 and P13) are 6.5-year-old girls. 2) Five children developed MELAS syndrome (P3, P5, P8, P11, and P12) with a history of stroke-like episodes, and 3) the last two children (P7 and P10) had LHON-like onset of the disease with optic neuropathy at the age of 12 years and 6 years, respectively. Nevertheless, both of them later developed multisystem symptoms and transitioned to MELAS syndrome or LHON/MELAS overlap syndrome. In addition, P9 and P11 also had MELAS syndrome with some degree of optic neuropathy with

**Table 1** Clinical and laboratory data in 13 patients with complex I deficiency

Patient	1	2	3	4	5	6	7	8	9	10	11	12	13
mtDNA gene mutation	m. 3697 G>A	m. 3946 G>A	m. 10158 T>C	m. 12706 T>C	m. 13046 T>C	m. 13042 G>A	m. 13091 T>C	m. 13513 G>A					
muscle mtDNA heteroplasmy [%]	93	53	95	83	70	96	61	67	48	97	np	np	np
fibroblasts mtDNA heteroplasmy [%]	81	79	85	np	43	65	np	65	40	4	np	np	np
blood mtDNA heteroplasmy [%]	93	96	90	3	27	96	4	58	44	35	21	64	64
hair follicles mtDNA heteroplasmy [%]	93	np	94	np	44	90	12	np	66	86	9	4	4
urinary sediment mtDNA heteroplasmy [%]	96	np	np	47	71	89	52	np	81	92	74	80	80
buccal smear mtDNA heteroplasmy [%]	93	np	92	np	34	93	30	np	55	68	5	71	71
median for all tissues	93	88	53	92	47	92	44	30	65	52	77	15	68
age at onset (week, months, years)	1 w	1 w	9 y	4 m	17 y	6 m	12 y	10 y	1 m	6 y	10 y	10 y	5 m
first symptom	hypotony	hypotony	stroke-like episode	hypotony	Wernicke aphasia	hypotony	optic neuropathy	migraine	hypotony	optic neuropathy	stroke-like episode	hearing loss	nystagmus
failure to thrive	+	-	+	+	-	-	-	-	+	-	-	+	-
initial hypotony/ later spasticity	+/+	+/+	+/+	+/+	-/-	+/+	-/-	-/-	+/+	-/-	-/-	+/+	+/-
delayed motor development	+	+	+	+	-	+	-	-	+	-	-	+	-
cerebellar symptoms	+	-	+	+	+	+	-	-	+	+	+	+	-
strabismus	+	+	+	+	-	+	-	+	+	+	+	+	+
epilepsy	+	-	+	+	+	-	+	+	+	+	+	+	-
migraine	-	-	-	-	-	-	+	+	-	+	+	+	-
optic atrophy	-	-	-	-	-	+	+	+	-	+	+	+	-
ptosis	-	-	-	-	-	+	-	-	+	+	+	+	+
CPEO	-	-	-	-	-	+	-	-	-	+	-	+	+
visual impairment	+	+	-	-	+	+	+/+	-	+	+	-	+	+
hearing loss	+	+	+	+	+	-	-	-	+	+	+	+	-
peripheral neuropathy	-	-	+	+	-	-	-	-	-	-	+	-	-

**Table 1** Clinical and laboratory data in 13 patients with complex I deficiency (Continued)

Patient	1	2	3	4	5	6	7	8	9	10	11	12	13
mental insufficiency	+	+	+	+	-	-	-	-	+	+	-	+	-
psychiatric disturbances			+		+	-	+	-		+	+		-
present age (years)	died at 7	died at 1.8	31	died at 1.3	died at 42	6.5	17	31	died at 3.3	20.5	25	22	6.5
creatine kinase [controls < 2.5 ukat/l]	1-2.4	0.8	1	0.66	2-3.8	np	1-190	1-1.7	0.6	np	0.6-2	1.5-14	2-10
blood-lactate [controls < 2.3 mmol/l]	2-6	3-6	2.7-4.4	3-7	3-8	2.8-5	1.5-13	1.2-2.6	2-3.4	8.6	2-5	2-5	2.4-4
CSF-lactate [controls < 2.1 mmol/l]	3	4	7	5.6	4.5	3.9	4.3	4.2	3.6	14	6.2	np	4.3
age at MRI (months, years)	2 y	7 m	14 y		36 y	20 m	17 y	32 y	34 m	9 y	25y	18 y	3 y
MRI - bilateral deep gray matter lesions <sup>a</sup>	+	+	+	+	-	+	+	-	+	+	-	+	+
MRI -stroke-like lesions <sup>b</sup>	+	-	+	-	+	-	+	+	-	-	+	+	-
MRI -periventricular atrophy	++	+	++	-	++	-	-	+	+	-	+	+	-

**Abbreviations:** CPEO chronic progressive external ophthalmoplegia, PM psychomotor, CSF cerebrospinal fluid (CSF lactate in P10 analysed at stroke-like episode); np - not performed  
<sup>a</sup>Compatible with Leigh syndrome (see Fig. 1), <sup>b</sup>compatible with MELAS syndrome (see Fig. 1)

alterations in Best Corrected Visual Acuity (BCVA), and P12 had limited size of the optic discs. Hypertrophic cardiomyopathy (HCMP) with Wolf-Parkinson-White (WPW) syndrome was present in P9 and P13. Most patients also exhibited intermittent or permanent increases of lactate in the blood (B-lactate 1.2–13 mmol/l, controls < 2.3 mmol/l) and the cerebrospinal fluid (CSF-lactate 3–14 mmol/l, controls < 2.3 mmol/l).

Brain MRI was performed in all patients, albeit at different ages (Table 1). In 6 of them (P2, P4, P6, P9, P10, and P13), symmetric signal changes in deep grey matter structures, including the basal ganglia and the brainstem, characteristic for LS, were found. Signal changes in the

cortex and white matter of the hemispheres and the cerebellum resembling stroke-like lesions of MELAS syndrome were found in 3 patients (P5, P8, and P11), and the combination of both changes typical for LS and stroke-like lesions was present in 4 patients (P1, P3, P7, and P12). In addition, moderate to severe periventricular atrophy was found in three patients (P1, P3, and P5). Brain MRI images of all patients, except P4, are shown in Fig. 1.

#### Biochemical measurement

In isolated muscle mitochondria, the activity of CI/CS was decreased or borderline low in 8 of 10 analysed

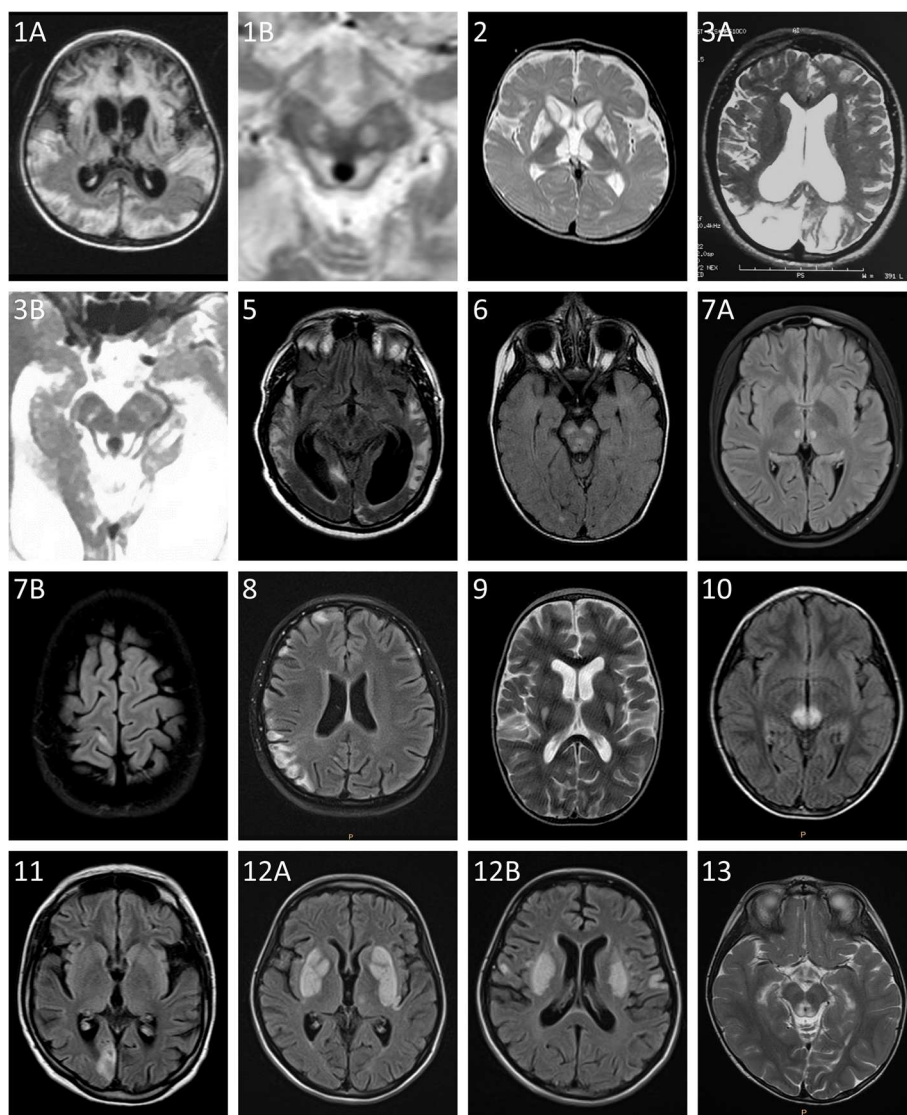


**Fig. 1** MRI of the brain in P1–P3 and P5–P12 with complex I deficiency. Signal changes in basal ganglia or brainstem characteristic for Leigh syndrome are present in patients P2, P6, P9, P10 and P13. Signal changes in the cortex and white matter of the hemispheres or cerebellum with stroke-like lesion are present in patients P5, P8, P11, and the combination of both changes are visible in patients P1, P3, P7 and P12. Moderate to severe periventricular atrophy was found in patients P1, P3 and P5.

patients (P3–P8, P10, and P11), and the activity of the respiratory chain CI + III/CS was low in 9 of 10 analysed patients (P3–P11). Activities of other oxidative phosphorylation (OXPHOS) complexes were altered in some patients. CII + III/CS was increased in 3 patients, CIII/CS was elevated in 3 patients, and CIV/CS was altered in 4 patients (3 increased, 1 decreased), see Table 2. We observed no significant correlation between enzymatic activities and the heteroplasmy of mtDNA mutations. The activities of CI in cultivated fibroblasts were within the reference range (data not shown).

SDS-PAGE/Western blots (WB) in cultivated fibroblasts of patients with *MT-ND5* mutations revealed slightly increased amounts of the ND5 subunit (Fig. 2a and c) in three patients (P5, P7 and P9). We noted mild alterations in the amount of selected OXPHOS protein subunits in comparison to age-related controls, but they were not uniform across the group of patients.

The MEGS analysis in cultivated skin fibroblasts from 8 patients (P1, P2, P4, P6, P7, and P9–P11) revealed decreased oxidation rates in 4 incubations containing [1-<sup>14</sup>C] pyruvate (Fig. 3). Oxidation rates of the other 2 incubations containing [1-<sup>14</sup>C] pyruvate and incubations containing [U-<sup>14</sup>C] malate and [1,4-<sup>14</sup>C] succinate were similar to controls. MEGS analyses were also performed in muscle postnuclear homogenate in 4 patients (P4, P5, P7 and P9). In all samples, MEGS revealed disruption at the level of the respiratory chain (data not shown).

**The novel variant**

The novel variant m.13091 T > C (p.Met252Thr) in the *MT-ND5* gene was found in P8 (Table 1). She

was born at term to healthy parents and was asymptomatic until the age of 10 years, when frequent attacks of migraine started. At the age of 26 years, she developed repeated stroke-like episodes with secondary epilepsy. She has had no ptosis or chronic ophthalmoplegia. Cardiologic examination and audiometry were uneventful, but the CSF-lactate was elevated (4.2 mmol/l, controls < 2.3 mmol/l) and both optic nerves appeared pale on ophthalmoscopy. Perimetric investigation revealed multiple bilateral scotomas, and visual evoked potentials showed reduced amplitudes with prolonged P100 wave latencies. Ophthalmological assessment revealed bilateral pallor of the optic discs and decreased retinal nerve fibre layer thickness in all four quadrants (OCT Spectralis, Heidelberg Engineering, Germany). Nevertheless, the patient’s visual acuity was normal, bilaterally (Best Corrected Visual Acuity 1.0). Muscle biopsy revealed a mild focal subsarcolemmal accumulation of SDH product (3%) with a decreased activity of CI + III in isolated mitochondria (Table 2), while the activities of CI and other respiratory chain complexes were within the control range, except for the increased activity of respiratory chain CII + III (probably as the compensatory impact of CI + III deficiency). BN-PAGE revealed decreased amounts of CI in muscle to approx. 74%; the amount of other OXPHOS complexes remained unchanged (Fig. 2b and d) except ATP synthase, where we observed a mildly increased amount of free F<sub>1</sub> domain in comparison to control. Both the patient’s mother and sister suffer from migraines. However, in the patient’s mother, only a 12% mutational

**Table 2** The activities of respiratory chain complexes in isolated muscle mitochondria

Patient	Individual respiratory chain complexes activities in isolated muscle mitochondria											
	CI/CS		CI + III/CS		CII/CS		CII + III/CS		CIII/CS		CIV/CS	
	patient	age related control range	patient	age related control range	patient	age related control range	patient	age related control range	patient	age related control range	patient	age related control range
1	0.50	0.45–1.05	0.18	0.17–0.31	0.09	0.07–0.27	0.33	0.17–0.47	0.43	0.27–0.85	1.59	1.1–2.22
3	<b>0.13</b>	0.18–0.38	<b>0.08</b>	0.18–0.37	<b>0.04</b>	0.05–0.11	0.24	0.17–0.32	0.67	0.46–0.88	1.21	0.66–2.25
4	<b>0.24</b>	0.45–1.05	<b>0.06</b>	0.17–0.31	0.09	0.07–0.27	0.34	0.17–0.47	<b>0.95</b>	0.27–0.85	<b>0.97</b>	1.1–2.22
5	<b>0.11</b>	0.15–0.41	<b>0.01</b>	0.13–0.25	0.05	0.05–0.11	0.23	0.15–0.27	<b>0.72</b>	0.3–0.56	1.5	0.66–2.25
6	<b>0.06</b>	0.45–1.05	<b>0.08</b>	0.17–0.31	0.07	0.07–0.27	0.26	0.17–0.47	0.72	0.27–0.85	1.12	1.1–2.22
7	<b>0.08</b>	0.18–0.38	<b>0.06</b>	0.18–0.37	0.07	0.05–0.11	<b>0.38</b>	0.17–0.32	0.74	0.46–0.88	<b>1.11</b>	1.16–2.13
8	0.16	0.15–0.41	<b>0.05</b>	0.13–0.25	0.06	0.05–0.11	<b>0.44</b>	0.15–0.27	<b>1.7</b>	0.3–0.56	1.12	0.66–2.25
9	0.28	0.18–0.38	<b>0.03</b>	0.18–0.37	0.09	0.05–0.11	<b>0.38</b>	0.17–0.32	0.66	0.46–0.88	1.27	1.16–2.13
10	<b>0.11</b>	0.18–0.38	<b>0.08</b>	0.18–0.37	0.05	0.05–0.11	0.30	0.17–0.32	0.57	0.46–0.88	<b>1.7</b>	1.16–2.13
11	<b>0.07</b>	0.18–0.38	<b>0.03</b>	0.18–0.37	<b>0.04</b>	0.05–0.11	0.19	0.17–0.32	0.52	0.46–0.88	<b>0.96</b>	1.16–2.13

The reference ranges for individual patients according to age of patients are displayed in next column. Controls are constituted in the three major groups (0–2 years old; 3–18 years old and adults). Alterations in patient’s complexes activities are shown in bold. Abbreviations: CI complex I, NADH coenzyme Q reductase; CI + III complex I + III, NADH cytochrome c reductase; CII complex II, succinate:coenzyme Q reductase; CII + III complex II + III, succinate:cytochrome c oxidoreductase; CIII complex III, coenzyme Q:cytochrome c oxidoreductase; CIV complex IV, cytochrome c oxidase; CS citrate synthase

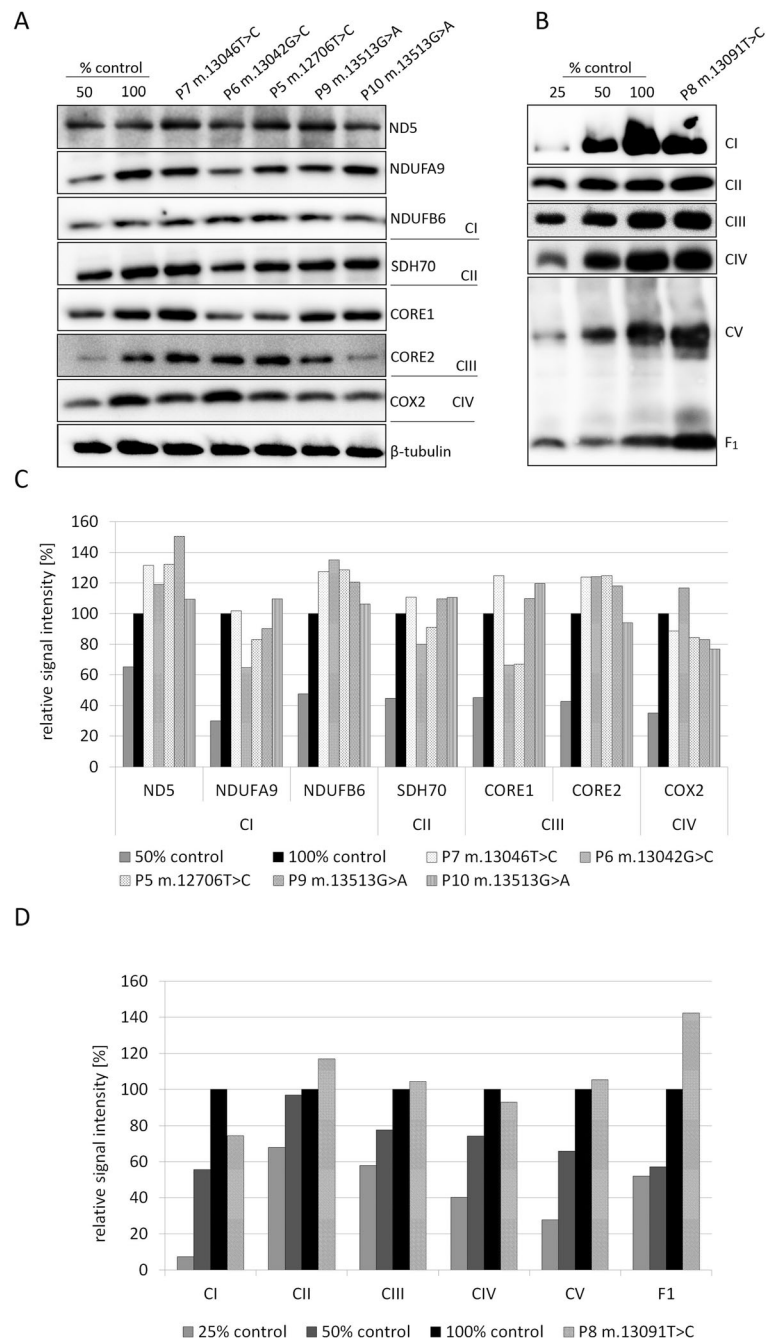


**Fig. 2** Protein analysis in six patients with heteroplasmic mutations in MT-ND5 gene. **a** Comparison of steady-state levels of several OXPHOS-related proteins in P5, P6, P7, P9 and P10 in fibroblasts using SDS-PAGE/WB. As a control was used primary dermal fibroblasts (ATCC® PCS-201-010™), 50 and 100% demonstrate loading dose of protein amount. **b** BN-PAGE/WB of OXPHOS complexes in isolated mitochondria from the muscle of P8. As a control was used human muscle mitochondria from healthy adult, 25; 50 and 100% demonstrate loading dose of protein amount. **c** The quantification of western blot signals from A by densitometric analysis. Relative signals intensity of individual OXPHOS antibodies were normalized to intensity of loading control β-tubulin. **d** The quantification of western blot signals from B by densitometric analysis

load of m.13091 T > C was present in urine, while blood, buccal smears and hair follicles were negative. The mutational load in samples from the patient's sister was below the detection limit of the method.

**Discussion**

Maternally inherited mutations in MT-ND, genes for structural subunits of CI, may be found in > 30% of patients with isolated CI deficiency [16, 17]. Most of them



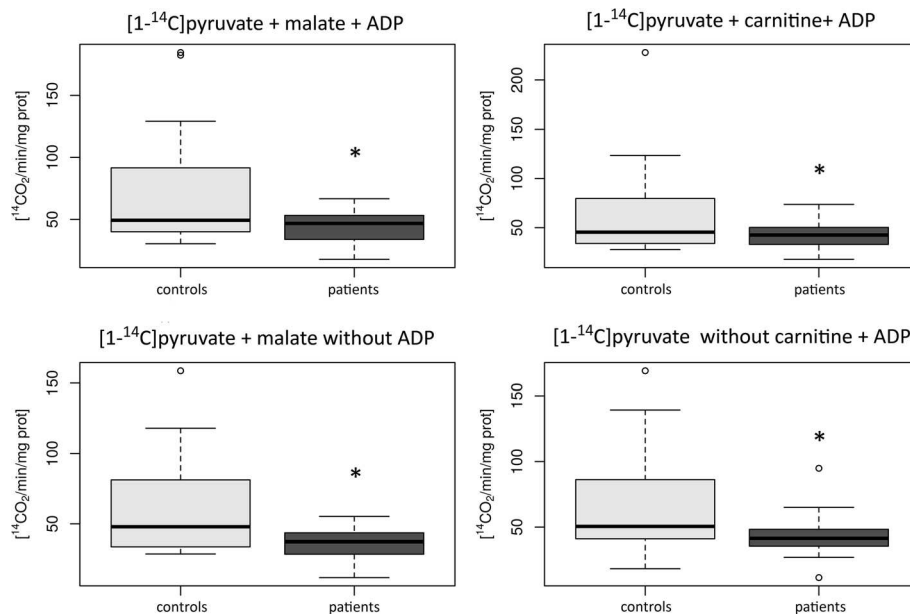


**Fig. 3** Oxidation rate of 4 different MEGS incubations containing [1-<sup>14</sup>C] pyruvate in cultivated skin fibroblasts. Patient group consists of 8 patients (P1, P2, P4, P6, P7, and P9–P11) with complex I deficiency and heteroplasmic mutations in *MT-ND1*, *MT-ND3* and *MT-ND5* genes. Control group consists of 10 age-related controls. In the group of patients, oxidation rate of all four displayed MEGS incubations are significantly decreased (\**p* < 0.05). Open circles displayed suspected outliers

have LHON syndrome with isolated optic neuropathy due to the prevalent mutations m.11777G > A in *MT-ND4*, m.3460G > A in *MT-ND1*, or m.14484 T > C in *MT-ND6*. Multisystem mitochondrial disorders are less frequent. The *MT-ND5* gene appears to be clearly a hot-spot for disease-causing mutations [18], and the m.13513G > A mutation is one of the most common [19]. Although the *MT-ND5* gene is the largest of the mtDNA-encoded genes for CI (1812 bp), this alone does not explain the increased number of mutations in this gene compared with other mitochondrial genes [20]. Still, it corresponds well with the results of molecular analyses in our families with multisystem MD, because most of them have mutations in the *MT-ND5* gene, including one girl with the novel heteroplasmic mutation m.13091 T > C. Similarly to other reports [19, 21, 22] also in our group of patients, the most frequent mutation in the *MT-ND5* gene was m.13513G > A. The second most common group of mutations in our subjects were mutations in the *MT-ND1* gene, found in three patients. One of the mutations, m.3946G > A, was the first within *MT-ND* genes associated with the MELAS syndrome phenotype [23].

The phenotype in patients with CI deficiency may have overlapping features of different mitochondrial syndromes. Our patients manifested, most frequently during childhood or adolescence, with LS with progressive motor and subsequent mental deterioration, or with MELAS syndrome, lactic acidosis and attacks of stroke-

like episodes. Less frequent was the onset of optic neuropathy followed with multisystem symptoms representing LHON/MELAS overlap syndrome. Hypertrophic CMP with or without WPW syndrome is not rare in patients with the mutation m.13513G > A [19, 21, 22, 24, 25]; we observed it in 2 patients. Severe rhabdomyolysis was observed only once, in P7.

Clinical symptoms in P8 with MELAS syndrome and the novel heteroplasmic variant m.13091 T > C in *MT-ND5* started with attacks of migraine at the age of 10 years and stroke-like episodes at the age of 26 years. In addition, she developed myopathy, optic neuropathy and secondary epilepsy. This course of the disease is compatible with our observation that any symptom from the broad phenotypic spectrum of MELAS syndrome may come first and stay isolated for a long period of time [26].

Three patients with mutations in *MT-ND1* also developed an acute encephalitic episode characterized by an acute qualitative alteration of consciousness with hyporesponsivity and profound hypotonia. This may have been caused by selective neuronal impairment due to energetic deprivation, leading to reversible ischaemic damage that lacks evidence of decreased tissue perfusion [27]. Some patients may recover to a normal or nearly normal condition as before the event [1, 19, 22]. Of some interest is the Wernicke's aphasia in P5, with mutation m.12706 T > C in *MT-ND5*, which was characterized by a difficulty of understanding written and spoken language. The cause of Wernicke's aphasia is usually an

ischaemic stroke affecting the Wernicke's area in the posterior temporal lobe of the dominant hemisphere perfused by branches of the middle cerebral artery [28]. MRI of the brain revealed a typical ischemic hyperintensity in the left temporoparietal region. In contrast, MELAS lesions do not follow vascular territories or a border zone and the cerebral angiography fails to demonstrate any steno-occlusive lesions [29]. As far as we know, only one mitochondrial patient with mtDNA mutation m.3243G > A has previously been described with Wernicke's aphasia [30].

Vascular dysfunction seems to play an important role in the pathogenesis of MD. However, the affected areas, as observed via neuroimaging, do not always correspond to classic regional vascular distributions; therefore, they are called "stroke-like" lesions. Additionally, other pathophysiological mechanisms may contribute to or be responsible for the development of stroke-like episodes. One of them is a generalized cytopathy caused by critical energy deprivation in neurons and/or glia. The cytotoxicity may lead to either temporary or permanent lesions depending on the level of energetic failure [31, 32]. It was also hypothesized that the abnormal mitochondria in the endothelium may disturb the blood–brain barrier, resulting in altered ion homeostasis, hyperexcitability and focal epileptic activity [33]. Using MRI and  $^1\text{H}$  magnetic resonance spectroscopy, different white and grey matter lesions may be found in the central nervous system of patients with CI deficiency. Caudate lesions were more common in patients with mtDNA mutations, as opposed to patients with nuclear mutations [34].

LS is characterized by symmetric involvement of the deep grey matter. The most commonly affected structures are the substantia nigra, putamen, nucleus dentatus and the brainstem; however, the thalamus, cerebellum and grey matter of the spinal cord may also be involved, and lesions in white matter structures were also described [35]. The deep grey matter lesions may result from several factors, including ATP depletion, gliosis, high lactate and excessive reactive oxygen species production [36]. In patients with MELAS syndrome, stroke-like lesions with the involvement of grey matter and subcortical white matter typically exhibit a "shifting spread" (appearance, disappearance and re-appearance). These lesions are characterized by asymmetric signal changes crossing vascular territories and an abnormally prominent lactate peak [37, 38]. Some patients also have small lesions in the deep grey matter (either less symmetrical than in LS or unilateral) and calcifications in basal ganglia.

In our patients with maternally inherited CI deficiency, MRI revealed both the involvement of deep grey matter structures and stroke-like lesions similar to other reports [4]. We also demonstrated the coexistence of LS and

stroke-like lesions in 4 of the 13 patients, suggesting that an overlap between the LS and MELAS phenotypes is not rare in patients with maternally inherited CI deficiency. Moderate cortical or periventricular atrophy was present in 4 of 13 patients, but these atrophies have been shown to be non-specific in patients with mitochondrial diseases [34].

Grey matter has been estimated to consume approximately 2.5-fold more ATP than white matter [39]. It is therefore not surprising that the majority of MDs present with predominant involvement of grey matter that may extend to secondary white matter degeneration [36], similar to what was observed in the subcortical regions in some of our patients. It was hypothesized that LS is typical in patients with very high levels of mtDNA mutation heteroplasmy [36]. However, this was only partly supported by our study, as some of our patients with high levels of heteroplasmy manifested stroke-like phenotypes. In fact, isolated LS and LS/MELAS overlap syndromes were present even in some patients with lower levels of heteroplasmy.

### Prognosis

The prognosis in most patients with multisystem MD and CI deficiency is not good. Similarly to other reports [1, 19, 22, 40], our patients with higher levels of heteroplasmy (expressed as the median of heteroplasmy from all analysed tissues) had poorer prognosis with LS phenotype and an earlier onset of the disease, whereas patients with lower heteroplasmy levels developed milder MELAS or LHON/MELAS phenotypes with a later onset [19, 20, 41, 42]. On the other hand, LS was also described in some patients with low levels of heteroplasmy [21, 43, 44]. It was shown in patients with MELAS syndrome, including m.13513G > A mutation, that L-arginine infusion during the acute phase of the stroke-like episode may reduce acute symptoms, and oral supplementation with L-arginine and/or L-citrulline may prevent further stroke-like episodes, with arginine acting as a nitric oxide donor, reversing the vasospasm [45]. A recent study at the basic research level has shown that in the induced pluripotent stem cells (iPSCs) with m.13513G > A, it is possible to decrease the level of heteroplasmy in iPSCs using transcription activator-like effector nucleases (TALENs) [46].

### Biochemical findings

The activities of CI and CI + III in isolated muscle mitochondria were decreased in most patients. Results of our study suggest that CI + III activity in muscle biopsy normalized to CS activity (serving as the control enzyme) is a good biochemical indicator for CI deficiency. This may be due to the CI assay measuring only the redox activity of the enzyme, which takes place within the peripheral

arm, while mutations in the membrane arm subunits (which includes all seven mtDNA-encoded subunits [47]), may theoretically result in ostensibly normal enzymatic activity [1]. In 4/10 patients, CII + III activity was elevated, probably as a compensatory effect of CI deficiency. A similar effect was described in patients with multiple system atrophy with altered biosynthesis of the electron carrier CoQ10 as a consequence of a mutation in the *COQ2* gene [48]. The increase of CI activity that they observed could indicate a compensatory mechanism in response to downstream reduction in CII + III activity in cerebellar and occipital white matter [48]. In comparison to spectrophotometric analyses of muscle biopsies, similar measurements in cultivated fibroblasts for the diagnosis of CI deficiency in most of our patients were less predictive. In addition, no correlation was found between the activities and amounts of CI and CI + III in the muscle biopsies or cultivated fibroblasts, and the levels of heteroplasmic mutations in *MT-ND1*, *MT-ND3* and *MT-ND5* genes, similar to several other reports [19–21, 44]. Contrarily, a correlation between the level of heteroplasmy and the level of residual CI activity was described in cybrids derived from patients with mutations m.3481G > A in *MT-ND1*, m.10158 T > C and m.10191 T > C in *MT-ND3* and m.13063G > A in *MT-ND5* [48, 49]. However, the variable expression may be caused by different nuclear backgrounds, mtDNA haplotypes, environmental factors or ageing [43].

Recently, Kopinski et al. [50] showed how the level of mtDNA heteroplasmy changed the nuclear epigenome through metabolites, in cybrid models with an altered level of m.3243A > G encoded tRNA<sup>Leu</sup> in the same nuclear background. They showed changes in nuclear gene expression via histone modification, which is modulated by the level of mitochondrially generated metabolites acetyl-CoA and  $\alpha$ -ketoglutarate. Levels of those metabolites correlate with histone modifications, which differ across the different levels of heteroplasmy. They also revealed that mtDNA heteroplasmy affects mitochondrial NAD<sup>+</sup>/NADH ratio, which correlates with nuclear histone acetylation. Meanwhile, nuclear NAD<sup>+</sup>/NADH ratio correlates with changes in nDNA and mtDNA transcription. Hence, mutations in mtDNA generate particular metabolites and epigenetic changes at different heteroplasmy levels. This could explain the phenotypic variability of mitochondrial disease [50].

Simultaneous analyses of spectrophotometric and MEGS measurements in muscle biopsies from patients with MDs have already been performed in several studies [15, 51–53]. MEGS analysis is a sensitive method for detection of OXPHOS deficiency and the deficiency of adenine nucleotide translocator or pyruvate dehydrogenase complex (PDHc) in muscle tissue [15, 52]. In our cohort, MEGS analysis revealed disturbances of OXPHOS

in all 4 patients where muscle tissue was examined. Moreover, in fibroblasts from 8 patients, MEGS analysis revealed decreased oxidation rates in 4 out of 6 incubations containing [1-<sup>14</sup>C] pyruvate, whereas the oxidation rates of incubations containing [U-<sup>14</sup>C] malate or [1, 4-<sup>14</sup>C] succinate remained within the control range. Similarly, diminished [2-<sup>14</sup>C] pyruvate oxidation was also described in 8 out of 11 fibroblast lines from patients with CI deficiency [54]. The disturbances of CI led to an increased NADH/NAD<sup>+</sup> ratio, resulting in the inhibition of PDHc activity and thus slowing down of the pyruvate oxidation rate [55, 56]. Combined evaluation of all MEGS parameters makes it possible to clearly distinguish suspicion for complex I deficiency.

The results of our study suggest that MEGS analyses may serve as a good indicator for CI deficiency and may help to accelerate the diagnostic flow. Both analyses – MEGS and spectrophotometry, especially the activity of complex I + III – are sensitive methods for the recognition of CI deficiency due to *MT-ND* mutation in muscle biopsy. In fibroblasts, MEGS seems to be more sensitive. Combining several biochemical methods may improve our understanding of the impact of individual mutations of *MT-ND* genes on mitochondrial bioenergetics.

## Conclusions

Patients with multisystem MDs due to heteroplasmic mtDNA mutations resulting in isolated CI deficiency represent approximately 11% of all families with maternally inherited MD diagnosed in our geographical region. MRI of the brain revealed the presence of LS in 6 out of 13 patients (46%), MELAS syndrome in 3/13 (23%), and an overlap between both syndromes in 4/13 (31%). All four patients with mutations in *MT-ND1* or *MT-ND3* had LS, whereas patients with *MT-ND5* mutations presented equally often with LS or MELAS. MEGS, especially oxidation of [1-<sup>14</sup>C] pyruvate might serve as a sensitive indicator of functional impairment due to *MT-ND* mutations in fibroblasts. Early onset of the disease and higher level of mtDNA mutation heteroplasmy were associated with worse prognosis.

## Supplementary information

Supplementary information accompanies this paper at <https://doi.org/10.1186/s12887-020-1912-x>.

**Additional file 1 : Table S1.** Structural and Non-Structural Nuclear Genes for Complex I disorders. **Table S2.** Composition of individual MEGS incubations.

## Abbreviations

BCVA: Best Corrected Visual Acuity; BN-PAGE: Blue Native Polyacrylamide Gel Electrophoresis; CI + III: Respiratory chain complex I + III (NADH:cytochrome c oxidoreductase); CI: Respiratory chain complex I (NADH:coenzyme Q oxidoreductase); CII + III: Respiratory chain complex II + III

(succinate:cytochrome c oxidoreductase); CII: Respiratory chain complex II (succinate:coenzyme Q oxidoreductase); CIII: Respiratory chain complex III (coenzyme Q:cytochrome c oxidoreductase); CIV: Respiratory chain complex IV (cytochrome c oxidase); CS: Citrate synthase; CSF: Cerebrospinal fluid; HCMF: Hypertrophic cardiomyopathy; iPSCs: Induced Pluripotent Stem Cells; LHON: Leber Hereditary Optic Neuropathy; LS: Leigh syndrome, symmetric necrotic lesions in basal ganglia and/or in the brain stem; MD: Mitochondrial disorders; MEGS: Mitochondrial energy-generating system; MELAS: Mitochondrial Encephalopathy, Lactic Acidosis and Stroke-like episode; mtDNA: mitochondrial DNA; OXPHOS: Oxidative phosphorylation; PDHc: Pyruvate dehydrogenase complex; RNFL: Retinal nerve fiber layer; SDS-PAGE: Sodium dodecyl sulfate polyacrylamide gel electrophoresis; TALENs: Transcription activator-like effector nucleases; WB: Western blot; WPW: Wolf-Parkinson-White syndrome

### Acknowledgements

Special thanks to Daniela Sedlackova and Suzana Knopova for their technical support and to Vaclav Capek for statistical analysis.

### Authors' contributions

TD performed MEGS, SDS-PAGE and BN-PAGE analyses, performed literature search and prepared the manuscript. HK performed the clinical part of the manuscript. JZ interpreted data and prepared the manuscript. HH performed MEGS in muscle biopsies and supervised the interpretation of OXPHOS functional data. MV and LL collected and interpreted the MRI data, VKV and KB performed mtDNA sequencing and determined heteroplasmy levels of the mutations. TH performed medical examinations of the patients. MT designed the study, interpreted data and revised the manuscript. All authors have read and approved the final manuscript as written and take responsibility for its content.

### Funding

This study was supported by research grants from the Ministry of Health of the Czech Republic (AZV 17-30965A, RVO VFN 64165), and Charles University (Progress Q26/LF1, UNCE 204064, SVV260367). The funding bodies were not involved in the design of the study, collection, analysis and interpretation of data, and in the writing of the manuscript.

### Availability of data and materials

The datasets used and/or analysed during the current study are available from the corresponding author on reasonable request.

### Ethics approval and consent to participate

The study was approved by the Ethics Committee of the General University Hospital in Prague and was conducted in agreement with institutional guidelines. Written informed consent for participation in the study was obtained from the patients and parents of affected children.

### Consent for publication

Not applicable.

### Competing interests

The authors declare that they have no competing interests.

### Author details

<sup>1</sup>Department of Pediatrics and Adolescent Medicine, First Faculty of Medicine, Charles University and General University Hospital in Prague, Ke Karlovu 2, 128 08 Praha 2, Prague, Czech Republic. <sup>2</sup>Department of Radiology, First Faculty of Medicine, Charles University and General University Hospital in Prague, Prague, Czech Republic.

Received: 27 August 2019 Accepted: 7 January 2020

Published online: 29 January 2020

### References

- Fassone E, Rahman S. Complex I deficiency: clinical features, biochemistry and molecular genetics. *J Med Genet*. 2012;49(9):578–90.
- Alston CL, Heidler J, Dibley MG, Kremer LS, Taylor LS, Fratter C, et al. Bi-allelic mutations in NDUFA6 establish its role in early-onset isolated mitochondrial complex I deficiency. *Am J Hum Genet*. 2018;103(4):592–601.
- Kolarova H, Liskova P, Tesarova M, Kucerova Vidrova V, Forgac M, Zamecnik J, et al. Unique presentation of LHON/MELAS overlap syndrome caused by m.13046T>C in *MTND5*. *Ophthalmic Genet*. 2016;37(4):419–23.
- Ng YS, Lax NZ, Maddison P, Alston CL, Blakely EL, Hepplewhite PD, et al. MT-ND5 mutation exhibits highly variable neurological manifestations at low mutant load. *EBioMedicine*. 2018;30:86–93.
- Leng Y, Liu Y, Fang X, Li Y, Yu L, Yuan Y, et al. The mitochondrial DNA 10197 G > a mutation causes MELAS/Leigh overlap syndrome presenting with acute auditory agnosia. *Mitochondrial DNA*. 2015;26(2):208–12.
- Vondrackova A, Vesela K, Hansikova H, Zajicova Docekalova D, Rozsypalova E, Zeman J, et al. High-resolution melting analysis of 15 genes in 60 patients with cytochrome-c oxidase deficiency. *J Hum Genet*. 2012;57(7):442–8.
- Makinen MW, Lee CP. Biochemical studies of skeletal muscle mitochondria. I. Microanalysis of cytochrome content, oxidative and phosphorylative activities of mammalian skeletal muscle mitochondria. *Arch Biochem Biophys*. 1968;126(1):75–82.
- Jesina P, Tesarova M, Fornuskova D, Vojtkova A, Pecina P, Kaplanova V, et al. Diminished synthesis of subunit a (ATP6) and altered function of ATP synthase and cytochrome c oxidase due to the mtDNA 2 bp microdeletion of TA at positions 9205 and 9206. *Biochem J*. 2004;383(Pt. 3):561–71.
- Rustin P, Chretien D, Bourgeron T, Gérard B, Rötig A, Saudubray JM, et al. Biochemical and molecular investigations in respiratory chain deficiencies. *Clin Chim Acta*. 1994;228(1):35–51.
- Srere PA. [1] Citrate synthase: [EC 4.1.3.7. Citrate oxaloacetate-lyase (CoA-acetylating)]. In: Lowenstein JM, editor. *Methods in Enzymology* [Internet]. Academic Press; 1969. p. 3–11. (Citric Acid Cycle; vol. 13). Available from: <http://www.sciencedirect.com/science/article/pii/007687969130050>. [cited 2015 Apr 5]
- Lowry OH, Rosebrough NJ, Farr AL, Randall RJ. Protein measurement with the Folin phenol reagent. *J Biol Chem*. 1951;193(1):265–75.
- Schägger H, von Jagow G. Blue native electrophoresis for isolation of membrane protein complexes in enzymatically active form. *Anal Biochem*. 1991;199(2):223–31.
- Fornuskova D, Brantova O, Tesarova M, Stiburek L, Honzik T, Wenchich L, et al. The impact of mitochondrial tRNA mutations on the amount of ATP synthase differs in the brain compared to other tissues. *Biochim Biophys Acta (BBA) - Mol Basis Dis*. 2008;1782(5):317–25.
- Schägger H, von Jagow G. Tricine-sodium dodecyl sulfate-polyacrylamide gel electrophoresis for the separation of proteins in the range from 1 to 100 kDa. *Anal Biochem*. 1987;166(2):368–79.
- Janssen TFM, Sengers RCA, Wintjes LTM, Ruitenbeek W, Smeitink JAM, et al. measurement of the energy-generating capacity of human muscle mitochondria: diagnostic procedure and application to human pathology. *Clin Chem*. 2006;52(5):860–71.
- Swalwell H, Kirby DM, Blakely EL, Mitchell A, Salemi R, Sugiana C, et al. Respiratory chain complex I deficiency caused by mitochondrial DNA mutations. *Eur J Hum Genet*. 2011;19(7):769–75.
- Ma Y-Y, Li X-Y, Li Z-Q, Song J-Q, Hou J, Li J-H, et al. Clinical, biochemical, and genetic analysis of the mitochondrial respiratory chain complex I deficiency. *Medicine (Baltimore)*. 2018;97(32):e11606.
- Liolitsa D, Rahman S, Benton S, Carr LJ, Hanna MG. Is the mitochondrial complex I ND5 gene a hot-spot for MELAS causing mutations? *Ann Neurol*. 2003;53(1):128–32.
- Shanske S, Coku J, Lu J, Ganesh J, Krishna S, Tanji K, et al. The G13513A mutation in the ND5 gene of mitochondrial DNA as a common cause of MELAS or Leigh syndrome: evidence from 12 cases. *Arch Neurol*. 2008;65(3):368–72.
- Blok MJ, Spruijt L, de Coo IFM, Schoonderwoerd K, Hendrickx A, Smeets HJ. Mutations in the ND5 subunit of complex I of the mitochondrial DNA are a frequent cause of oxidative phosphorylation disease. *J Med Genet*. 2007;44(4):e74.
- Sudo A, Honzawa S, Nonaka I, Goto Y. Leigh syndrome caused by mitochondrial DNA G13513A mutation: frequency and clinical features in Japan. *J Hum Genet*. 2004;49(2):92–6.
- Chol M. The mitochondrial DNA G13513A MELAS mutation in the NADH dehydrogenase 5 gene is a frequent cause of Leigh-like syndrome with isolated complex I deficiency. *J Med Genet*. 2003;40(3):188–91.
- Kirby DM. Mutations of the mitochondrial ND1 gene as a cause of MELAS. *J Med Genet*. 2004;41(10):784–9.
- Ruiter EM, Siers MH, van den Elzen C, van Engelen BG, Smeitink JAM, Rodenburg RJ, et al. The mitochondrial 13513G > a mutation is most

- frequent in Leigh syndrome combined with reduced complex I activity, optic atrophy and/or Wolff-Parkinson-white. *Eur J Hum Genet EJHG*. 2007; 15(2):155–61.
25. Wang S-B, Weng W-C, Lee N-C, Hwu W-L, Fan P-C, Lee W-T. Mutation of mitochondrial DNA G13513A presenting with Leigh syndrome, Wolff-Parkinson-white syndrome and cardiomyopathy. *Pediatr Neonatol*. 2008;49(4):145–9.
  26. Dvorakova V, Kolarova H, Magner M, Tesarova M, Hansikova H, Zeman J, et al. The phenotypic spectrum of fifty Czech m.3243A>G carriers. *Mol Genet Metab*. 2016;118(4):288–95.
  27. Tzoulis C, Bindoff LA. Acute mitochondrial encephalopathy reflects neuronal energy failure irrespective of which genome the genetic defect affects. *Brain*. 2012;135(12):3627–34.
  28. Knepper LE, Biller J, Tranel D, Adams HP, Marsh EE. Etiology of stroke in patients with Wernicke's aphasia. *Stroke*. 1989;20(12):1730–2.
  29. Kim JH, Lim MK, Jeon TY, Rha JH, Rha JH, Eo H, et al. Diffusion and perfusion characteristics of MELAS (mitochondrial myopathy, encephalopathy, lactic acidosis, and stroke-like episode) in thirteen patients. *Korean J Radiol*. 2011;12(1):15–24.
  30. Napolitano A, Salvetti S, Vista M, Lombardi V, Siciliano G, Giraldi C. Long-term treatment with idebenone and riboflavin in a patient with MELAS. *Neurol Sci Off J Ital Neurol Soc Ital Soc Clin Neurophysiol*. 2000; 21(5 Suppl):S981–2.
  31. Ito H, Mori K, Kagami S. Neuroimaging of stroke-like episodes in MELAS. *Brain and Development*. 2011;33(4):283–8.
  32. Sproule DM, Kaufmann P. Mitochondrial encephalopathy, lactic acidosis, and stroke-like episodes: basic concepts, clinical phenotype, and therapeutic management of MELAS syndrome. *Ann N Y Acad Sci*. 2008;1142:133–58.
  33. Iizuka T, Sakai F, Suzuki N, Hata T, Tsukahara S, Fukuda M, et al. Neuronal hyperexcitability in stroke-like episodes of MELAS syndrome. *Neurology*. 2002;59(6):816–24.
  34. Lebre AS, Rio M, Faivre d'Arcier L, Vernerey D, Landrieu P, Slama A, et al. A common pattern of brain MRI imaging in mitochondrial diseases with complex I deficiency. *J Med Genet*. 2011;48(1):16–23.
  35. Lerman-Sagie T, Leshinsky-Silver E, Watemberg N, Luckman Y, Lev D. White matter involvement in mitochondrial diseases. *Mol Genet Metab*. 2005;84(2):127–36.
  36. Lake NJ, Bird MJ, Isohanni P, Paetau A. Leigh syndrome: neuropathology and pathogenesis. *J Neuropathol Exp Neurol*. 2015;74(6):482–92.
  37. Finsterer J, Zarrouk-Mahjoub S. Cerebral imaging in paediatric mitochondrial disorders. *Neuroradiol J*. 2018;31(6):596–608.
  38. Mascalchi M, Montomoli M, Guerrini R. Neuroimaging in mitochondrial disorders. *Essays Biochem*. 2018;62(3):409–21.
  39. Harris JJ, Attwell D. The energetics of CNS white matter. *J Neurosci*. 2012; 32(1):356–71.
  40. Petruzzella V, Di Giacinto G, Scacco S, Piemonte F, Torraco A, Carozzo R, et al. Atypical Leigh syndrome associated with the D393N mutation in the mitochondrial ND5 subunit. *Neurology*. 2003;61(7):1017–8.
  41. Corona P, Antozzi C, Carrara F, D'Incerti L, Lamantea E, Tiranti V, et al. A novel mtDNA mutation in the ND5 subunit of complex I in two MELAS patients. *Ann Neurol*. 2001;49(1):106–10.
  42. Hanna MG, Nelson IP, Morgan-Hughes JA, Wood NW. MELAS: a new disease associated mitochondrial DNA mutation and evidence for further genetic heterogeneity. *J Neurol Neurosurg Psychiatry*. 1998;65(4):512–7.
  43. Brautbar A, Wang J, Abdenur JE, Chang RC, Thomas JA, Grebe TA, et al. The mitochondrial 13513G>a mutation is associated with Leigh disease phenotypes independent of complex I deficiency in muscle. *Mol Genet Metab*. 2008;94(4):485–90.
  44. Kirby DM, Boneh A, Chow CW, Ohtake A, Ryan MT, Thyagarajan D, et al. Low mutant load of mitochondrial DNA G13513A mutation can cause Leigh's disease. *Ann Neurol*. 2003;54(4):473–8.
  45. Ganetzky RD, Falk MJ. 8-year retrospective analysis of intravenous arginine therapy for acute metabolic strokes in pediatric mitochondrial disease. *Mol Genet Metab*. 2018;123(3):301–8.
  46. Yahata N, Matsumoto Y, Omi M, Yamamoto N, Hata R, et al. *Sci Rep*. 2017; 7(1):15557.
  47. Angerer H, Zwicker K, Wumaier Z, Sokolova L, Heide H, Steger M, et al. A scaffold of accessory subunits links the peripheral arm and the distal proton-pumping module of mitochondrial complex I. *Biochem J*. 2011; 437(2):279–88.
  48. Malfatti E, Bugiani M, Invernizzi F, de Souza CF-M, Farina L, Carrara F, et al. Novel mutations of ND genes in complex I deficiency associated with mitochondrial encephalopathy. *Brain*. 2007;130(7):1894–904.
  49. McFarland R, Kirby DM, Fowler KJ, Ohtake A, Ryan MT, Amor DJ, et al. De novo mutations in the mitochondrial ND3 gene as a cause of infantile mitochondrial encephalopathy and complex I deficiency. *Ann Neurol*. 2004; 55(1):58–64.
  50. Kopinski PK, Janssen KA, Schaefer PM, Trefely S, Perry CE, Potluri P, et al. Regulation of nuclear epigenome by mitochondrial DNA heteroplasmy. *Proc Natl Acad Sci U S A*. 2019;116(32):16028–35.
  51. Hoefs SJG, Dieteren CEJ, Distelmaier F, Janssen RJRJ, Epplen A, Swarts HGP, et al. NDUFA2 complex I mutation leads to Leigh disease. *Am J Hum Genet*. 2008;82(6):1306–15.
  52. Janssen AJM, Schuelke M, Smeitink JAM, Trijbels FJM, Sengers RCA, Lucke B, et al. Muscle 3243A-->G mutation load and capacity of the mitochondrial energy-generating system. *Ann Neurol*. 2008;63(4):473–81.
  53. Smits P, Antonicka H, van Hasselt PM, Weraarpachai W, Haller W, Schreurs M, et al. Mutation in subdomain G' of mitochondrial elongation factor G1 is associated with combined OXPHOS deficiency in fibroblasts but not in muscle. *Eur J Hum Genet*. 2011;19(3):275–9.
  54. Cameron JM, Levandovskiy V, MacKay N, Robinson BH. Respiratory chain analysis of skin fibroblasts in mitochondrial disease. *Mitochondrion*. 2004; 4(5–6):387–94.
  55. Patel MS, Korotchkina LG. Regulation of the pyruvate dehydrogenase complex. *Biochem Soc Trans*. 2006;34(Pt 2):217–22.
  56. Harris RA, Bowker-Kinley MM, Huang B, Wu P. Regulation of the activity of the pyruvate dehydrogenase complex. *Adv Enzym Regul*. 2002;42:249–59.

## Publisher's Note

Springer Nature remains neutral with regard to jurisdictional claims in published maps and institutional affiliations.

**Ready to submit your research? Choose BMC and benefit from:**

- fast, convenient online submission
- thorough peer review by experienced researchers in your field
- rapid publication on acceptance
- support for research data, including large and complex data types
- gold Open Access which fosters wider collaboration and increased citations
- maximum visibility for your research: over 100M website views per year

**At BMC, research is always in progress.**

Learn more [biomedcentral.com/submissions](https://biomedcentral.com/submissions)



1 **Table S1:** Structural and Non-Structural Nuclear Genes for Complex I disorders

	<b>structural genes</b>	<b>references</b>
1	<i>NDUFS1</i>	(Bé nit et al., 2001)
2	<i>NDUFS2</i>	(Loeffen et al., 2001)
3	<i>NDUFS3</i>	(Bé nit et al., 2004)
4	<i>NDUFS4</i>	(van den Heuvel et al., 1998)
5	<i>NDUFS6</i>	(Kirby et al., 2004, p. 6; Spiegel et al., 2009, p. 6)
6	<i>NDUFS7</i>	(Smeitink and van den Heuvel, 1999)
7	<i>NDUFS8</i>	(Loeffen et al., 1998)
8	<i>NDUFB3</i>	(Calvo et al., 2012)
9	<i>NDUFB8</i>	(Piekutowska-Abramczuk et al., 2018)
10	<i>NDUFB9</i>	(Haack et al., 2012)
11	<i>NDUFB10</i>	(Friederich et al., 2017)
12	<i>NDUFB11</i>	(Kohda et al., 2016)
13	<i>NDUFV1</i>	(Smeitink and van den Heuvel, 1999)
14	<i>NDUFV2</i>	(Bé nit et al., 2003)
15	<i>NDUFA1</i>	(Fernandez-Moreira et al., 2007; Potluri et al., 2009)
16	<i>NDUFA2</i>	(Hoefs et al., 2008)
17	<i>NDUFA6</i>	(Alston et al., 2018)
18	<i>NDUFA9</i>	(van den Bosch et al., 2012)
19	<i>NDUFA10</i>	(Hoefs et al., 2011)
20	<i>NDUFA11</i>	(Berger et al., 2008)
21	<i>NDUFA12</i>	(Ostergaard et al., 2011)
22	<i>NDUFA13</i>	(Angebault et al., 2015)
	<b>non-structural genes</b>	<b>references</b>
1	<i>NDUFAF1</i>	(Dunning et al., 2007)
2	<i>NDUFAF2</i>	(Ogilvie et al., 2005)
3	<i>NDUFAF3</i>	(Saada et al., 2009)
4	<i>NDUFAF4</i>	(Saada et al., 2008)
5	<i>NDUFAF5</i>	(Gerards et al., 2010)
6	<i>NDUFAF6</i>	(Bianciardi et al., 2016)
7	<i>NUBPL</i>	(Calvo et al., 2010)
8	<i>FOXRED1</i>	(Calvo et al., 2010)
9	<i>ACAD9</i>	(Haack et al., 2010)
10	<i>TIMMDC1</i>	(Kremer et al., 2017)
11	<i>TMEM126B</i>	(Sánchez-Caballero et al., 2016)

## 2 **References:**

- 3 Alston, C.L., Heidler, J., Dibley, M.G., Kremer, L.S., Taylor, L.S., Fratter, C., French, C.E.,  
4 Glasgow, R.I.C., Feichtinger, R.G., Delon, I., Pagnamenta, A.T., Dolling, H., Lemonde, H.,  
5 Aiton, N., Bjørnstad, A., Henneke, L., Gärtner, J., Thiele, H., Tauchmannova, K.,  
6 Quaghebeur, G., Houstek, J., Sperl, W., Raymond, F.L., Prokisch, H., Mayr, J.A.,  
7 McFarland, R., Poulton, J., Ryan, M.T., Wittig, I., Henneke, M., Taylor, R.W., 2018. Bi-  
8 allelic Mutations in NDUFA6 Establish Its Role in Early-Onset Isolated Mitochondrial  
9 Complex I Deficiency. *Am. J. Hum. Genet.* 103, 592–601.  
10 <https://doi.org/10.1016/j.ajhg.2018.08.013>
- 11 Angebault, C., Charif, M., Guegen, N., Piro-Megy, C., Mousson de Camaret, B., Procaccio, V.,  
12 Guichet, P.-O., Hebrard, M., Manes, G., Leboucq, N., Rivier, F., Hamel, C.P., Lenaers, G.,  
13 Roubertie, A., 2015. Mutation in NDUFA13/GRIM19 leads to early onset hypotonia,  
14 dyskinesia and sensorial deficiencies, and mitochondrial complex I instability. *Hum. Mol.*  
15 *Genet.* 24, 3948–3955. <https://doi.org/10.1093/hmg/ddv133>
- 16 Bénit, P., Beugnot, R., Chretien, D., Giurgea, I., De Lonlay-Debeney, P., Issartel, J.-P., Corral-  
17 Debrinski, M., Kerscher, S., Rustin, P., Rötig, A., Munnich, A., 2003. Mutant NDUFV2  
18 subunit of mitochondrial complex I causes early onset hypertrophic cardiomyopathy and  
19 encephalopathy. *Hum. Mutat.* 21, 582–586. <https://doi.org/10.1002/humu.10225>
- 20 Bénit, P., Chretien, D., Kadhom, N., de Lonlay-Debeney, P., Cormier-Daire, V., Cabral, A.,  
21 Peudenier, S., Rustin, P., Munnich, A., Rötig, A., 2001. Large-scale deletion and point  
22 mutations of the nuclear NDUFV1 and NDUFV2 genes in mitochondrial complex I  
23 deficiency. *Am. J. Hum. Genet.* 68, 1344–1352. <https://doi.org/10.1086/320603>
- 24 Bénit, P., Slama, A., Cartault, F., Giurgea, I., Chretien, D., Lebon, S., Marsac, C., Munnich, A.,  
25 Rötig, A., Rustin, P., 2004. Mutant NDUFV3 subunit of mitochondrial complex I causes  
26 Leigh syndrome. *J. Med. Genet.* 41, 14–17.
- 27 Berger, I., Hershkovitz, E., Shaag, A., Edvardson, S., Saada, A., Elpeleg, O., 2008. Mitochondrial  
28 complex I deficiency caused by a deleterious NDUFA11 mutation. *Ann. Neurol.* 63, 405–  
29 408. <https://doi.org/10.1002/ana.21332>
- 30 Bianciardi, L., Imperatore, V., Fernandez-Vizarra, E., Lopomo, A., Falabella, M., Furini, S.,  
31 Galluzzi, P., Grosso, S., Zeviani, M., Renieri, A., Mari, F., Frullanti, E., 2016. Exome  
32 sequencing coupled with mRNA analysis identifies NDUFV3 as a Leigh gene. *Mol. Genet.*  
33 *Metab.* 119, 214–222. <https://doi.org/10.1016/j.ymgme.2016.09.001>
- 34 Calvo, S.E., Compton, A.G., Hershman, S.G., Lim, S.C., Lieber, D.S., Tucker, E.J., Laskowski,  
35 A., Garone, C., Liu, S., Jaffe, D.B., Christodoulou, J., Fletcher, J.M., Bruno, D.L.,  
36 Goldblatt, J., Dimauro, S., Thorburn, D.R., Mootha, V.K., 2012. Molecular diagnosis of  
37 infantile mitochondrial disease with targeted next-generation sequencing. *Sci. Transl. Med.*  
38 4, 118ra10. <https://doi.org/10.1126/scitranslmed.3003310>
- 39 Calvo, S.E., Tucker, E.J., Compton, A.G., Kirby, D.M., Crawford, G., Burt, N.P., Rivas, M.,  
40 Guiducci, C., Bruno, D.L., Goldberger, O.A., Redman, M.C., Wiltshire, E., Wilson, C.J.,  
41 Altshuler, D., Gabriel, S.B., Daly, M.J., Thorburn, D.R., Mootha, V.K., 2010. High-

- 42 throughput, pooled sequencing identifies mutations in NUBPL and FOXRED1 in human  
43 complex I deficiency. *Nat. Genet.* 42, 851–858. <https://doi.org/10.1038/ng.659>
- 44 Dunning, C.J.R., McKenzie, M., Sugiana, C., Lazarou, M., Silke, J., Connelly, A., Fletcher, J.M.,  
45 Kirby, D.M., Thorburn, D.R., Ryan, M.T., 2007. Human CIA30 is involved in the early  
46 assembly of mitochondrial complex I and mutations in its gene cause disease. *EMBO J.* 26,  
47 3227–3237. <https://doi.org/10.1038/sj.emboj.7601748>
- 48 Fernandez-Moreira, D., Ugalde, C., Smeets, R., Rodenburg, R.J.T., Lopez-Laso, E., Ruiz-Falco,  
49 M.L., Briones, P., Martin, M.A., Smeitink, J.A.M., Arenas, J., 2007. X-linked NDUFA1  
50 gene mutations associated with mitochondrial encephalomyopathy. *Ann. Neurol.* 61, 73–83.  
51 <https://doi.org/10.1002/ana.21036>
- 52 Friederich, M.W., Erdogan, A.J., Coughlin, C.R., Elos, M.T., Jiang, H., O'Rourke, C.P., Lovell,  
53 M.A., Wartchow, E., Gowan, K., Chatfield, K.C., Chick, W.S., Spector, E.B., Van Hove,  
54 J.L.K., Riemer, J., 2017. Mutations in the accessory subunit NDUFB10 result in isolated  
55 complex I deficiency and illustrate the critical role of intermembrane space import for  
56 complex I holoenzyme assembly. *Hum. Mol. Genet.* 26, 702–716.  
57 <https://doi.org/10.1093/hmg/ddw431>
- 58 Gerards, M., Sluiter, W., van den Bosch, B.J.C., de Wit, L.E.A., Calis, C.M.H., Frentzen, M.,  
59 Akbari, H., Schoonderwoerd, K., Scholte, H.R., Jongbloed, R.J., Hendrickx, A.T.M., de  
60 Coo, I.F.M., Smeets, H.J.M., 2010. Defective complex I assembly due to C20orf7 mutations  
61 as a new cause of Leigh syndrome. *J. Med. Genet.* 47, 507–512.  
62 <https://doi.org/10.1136/jmg.2009.067553>
- 63 Haack, T.B., Danhauser, K., Haberberger, B., Hoser, J., Strecker, V., Boehm, D., Uziel, G.,  
64 Lamantea, E., Invernizzi, F., Poulton, J., Rolinski, B., Iuso, A., Biskup, S., Schmidt, T.,  
65 Mewes, H.-W., Wittig, I., Meitinger, T., Zeviani, M., Prokisch, H., 2010. Exome sequencing  
66 identifies ACAD9 mutations as a cause of complex I deficiency. *Nat. Genet.* 42, 1131–  
67 1134. <https://doi.org/10.1038/ng.706>
- 68 Haack, T.B., Madignier, F., Herzer, M., Lamantea, E., Danhauser, K., Invernizzi, F., Koch, J.,  
69 Freitag, M., Drost, R., Hillier, I., Haberberger, B., Mayr, J.A., Ahting, U., Tiranti, V., Rötig,  
70 A., Iuso, A., Horvath, R., Tesarova, M., Baric, I., Uziel, G., Rolinski, B., Sperl, W.,  
71 Meitinger, T., Zeviani, M., Freisinger, P., Prokisch, H., 2012. Mutation screening of 75  
72 candidate genes in 152 complex I deficiency cases identifies pathogenic variants in 16 genes  
73 including NDUFB9. *J. Med. Genet.* 49, 83–89. <https://doi.org/10.1136/jmedgenet-2011-100577>
- 75 Hoefs, S.J.G., Dieteren, C.E.J., Distelmaier, F., Janssen, R.J.R.J., Epplen, A., Swarts, H.G.P.,  
76 Forkink, M., Rodenburg, R.J., Nijtmans, L.G., Willems, P.H., Smeitink, J.A.M., van den  
77 Heuvel, L.P., 2008. NDUFA2 complex I mutation leads to Leigh disease. *Am. J. Hum.*  
78 *Genet.* 82, 1306–1315. <https://doi.org/10.1016/j.ajhg.2008.05.007>
- 79 Hoefs, S.J.G., van Spronsen, F.J., Lenssen, E.W.H., Nijtmans, L.G., Rodenburg, R.J., Smeitink,  
80 J.A.M., van den Heuvel, L.P., 2011. NDUFA10 mutations cause complex I deficiency in a



- 81 patient with Leigh disease. *Eur. J. Hum. Genet.* 19, 270–274.  
82 <https://doi.org/10.1038/ejhg.2010.204>
- 83 Kirby, D.M., Salemi, R., Sugiana, C., Ohtake, A., Parry, L., Bell, K.M., Kirk, E.P., Boneh, A.,  
84 Taylor, R.W., Dahl, H.-H.M., Ryan, M.T., Thorburn, D.R., 2004. NDUFS6 mutations are a  
85 novel cause of lethal neonatal mitochondrial complex I deficiency. *J. Clin. Invest.* 114, 837–  
86 845. <https://doi.org/10.1172/JCI20683>
- 87 Kohda, M., Tokuzawa, Y., Kishita, Y., Nyuzuki, H., Moriyama, Y., Mizuno, Y., Hirata, T.,  
88 Yatsuka, Y., Yamashita-Sugahara, Y., Nakachi, Y., Kato, H., Okuda, A., Tamaru, S., Borna,  
89 N.N., Banshoya, K., Aigaki, T., Sato-Miyata, Y., Ohnuma, K., Suzuki, T., Nagao, A.,  
90 Maehata, H., Matsuda, F., Higasa, K., Nagasaki, M., Yasuda, J., Yamamoto, M., Fushimi,  
91 T., Shimura, M., Kaiho-Ichimoto, K., Harashima, H., Yamazaki, T., Mori, M., Murayama,  
92 K., Ohtake, A., Okazaki, Y., 2016. A Comprehensive Genomic Analysis Reveals the  
93 Genetic Landscape of Mitochondrial Respiratory Chain Complex Deficiencies. *PLoS Genet.*  
94 12, e1005679. <https://doi.org/10.1371/journal.pgen.1005679>
- 95 Kremer, L.S., Bader, D.M., Mertes, C., Kopajtich, R., Pichler, G., Iuso, A., Haack, T.B., Graf, E.,  
96 Schwarzmayr, T., Terrile, C., Koňáriková, E., Repp, B., Kastenmüller, G., Adamski, J.,  
97 Lichtner, P., Leonhardt, C., Funalot, B., Donati, A., Tiranti, V., Lombes, A., Jardel, C.,  
98 Gläser, D., Taylor, R.W., Ghezzi, D., Mayr, J.A., Rötig, A., Freisinger, P., Distelmaier, F.,  
99 Strom, T.M., Meitinger, T., Gagneur, J., Prokisch, H., 2017. Genetic diagnosis of Mendelian  
100 disorders via RNA sequencing. *Nat. Commun.* 8, 15824.  
101 <https://doi.org/10.1038/ncomms15824>
- 102 Loeffen, J., Elpeleg, O., Smeitink, J., Smeets, R., Stöckler-Ipsiroglu, S., Mandel, H., Sengers, R.,  
103 Trijbels, F., van den Heuvel, L., 2001. Mutations in the complex I NDUFS2 gene of patients  
104 with cardiomyopathy and encephalomyopathy. *Ann. Neurol.* 49, 195–201.
- 105 Loeffen, J., Smeitink, J., Triepels, R., Smeets, R., Schuelke, M., Sengers, R., Trijbels, F., Hamel,  
106 B., Mullaart, R., van den Heuvel, L., 1998. The first nuclear-encoded complex I mutation in  
107 a patient with Leigh syndrome. *Am. J. Hum. Genet.* 63, 1598–1608.  
108 <https://doi.org/10.1086/302154>
- 109 Ogilvie, I., Kennaway, N.G., Shoubridge, E.A., 2005. A molecular chaperone for mitochondrial  
110 complex I assembly is mutated in a progressive encephalopathy. *J. Clin. Invest.* 115, 2784–  
111 2792. <https://doi.org/10.1172/JCI26020>
- 112 Ostergaard, E., Rodenburg, R.J., van den Brand, M., Thomsen, L.L., Duno, M., Batbayli, M.,  
113 Wibrand, F., Nijtmans, L., 2011. Respiratory chain complex I deficiency due to NDUFA12  
114 mutations as a new cause of Leigh syndrome. *J. Med. Genet.* 48, 737–740.  
115 <https://doi.org/10.1136/jmg.2011.088856>
- 116 Piekutowska-Abramczuk, D., Assouline, Z., Mataković, L., Feichtinger, R.G., Koňáriková, E.,  
117 Jurkiewicz, E., Stawiński, P., Gusic, M., Koller, A., Pollak, A., Gasperowicz, P., Trubicka,  
118 J., Ciara, E., Iwanicka-Pronicka, K., Rokicki, D., Hanein, S., Wortmann, S.B., Sperl, W.,  
119 Rötig, A., Prokisch, H., Pronicka, E., Płoski, R., Barcia, G., Mayr, J.A., 2018. NDUFB8  
120 Mutations Cause Mitochondrial Complex I Deficiency in Individuals with Leigh-like

- 121 Encephalomyopathy. *Am. J. Hum. Genet.* 102, 460–467.  
122 <https://doi.org/10.1016/j.ajhg.2018.01.008>
- 123 Potluri, P., Davila, A., Ruiz-Pesini, E., Mishmar, D., O’Hearn, S., Hancock, S., Simon, M.,  
124 Scheffler, I.E., Wallace, D.C., Procaccio, V., 2009. A novel NDUFA1 mutation leads to a  
125 progressive mitochondrial complex I-specific neurodegenerative disease. *Mol. Genet.*  
126 *Metab.* 96, 189–195. <https://doi.org/10.1016/j.ymgme.2008.12.004>
- 127 Saada, A., Edvardson, S., Rapoport, M., Shaag, A., Amry, K., Miller, C., Lorberboum-Galski, H.,  
128 Elpeleg, O., 2008. C6ORF66 is an assembly factor of mitochondrial complex I. *Am. J.*  
129 *Hum. Genet.* 82, 32–38. <https://doi.org/10.1016/j.ajhg.2007.08.003>
- 130 Saada, A., Vogel, R.O., Hoefs, S.J., van den Brand, M.A., Wessels, H.J., Willems, P.H.,  
131 Venselaar, H., Shaag, A., Barghuti, F., Reish, O., Shohat, M., Huynen, M.A., Smeitink,  
132 J.A.M., van den Heuvel, L.P., Nijtmans, L.G., 2009. Mutations in NDUFAF3 (C3ORF60),  
133 encoding an NDUFAF4 (C6ORF66)-interacting complex I assembly protein, cause fatal  
134 neonatal mitochondrial disease. *Am. J. Hum. Genet.* 84, 718–727.  
135 <https://doi.org/10.1016/j.ajhg.2009.04.020>
- 136 Sánchez-Caballero, L., Ruzzenente, B., Bianchi, L., Assouline, Z., Barcia, G., Metodiev, M.D.,  
137 Rio, M., Funalot, B., van den Brand, M.A.M., Guerrero-Castillo, S., Molenaar, J.P., Koolen,  
138 D., Brandt, U., Rodenburg, R.J., Nijtmans, L.G., Rötig, A., 2016. Mutations in Complex I  
139 Assembly Factor TMEM126B Result in Muscle Weakness and Isolated Complex I  
140 Deficiency. *Am. J. Hum. Genet.* 99, 208–216. <https://doi.org/10.1016/j.ajhg.2016.05.022>
- 141 Smeitink, J., van den Heuvel, L., 1999. Human mitochondrial complex I in health and disease.  
142 *Am. J. Hum. Genet.* 64, 1505–1510. <https://doi.org/10.1086/302432>
- 143 Spiegel, R., Shaag, A., Mandel, H., Reich, D., Penyakov, M., Hujeirat, Y., Saada, A., Elpeleg, O.,  
144 Shalev, S.A., 2009. Mutated NDUF6 is the cause of fatal neonatal lactic acidemia in  
145 Caucasus Jews. *Eur. J. Hum. Genet. EJHG* 17, 1200–1203.  
146 <https://doi.org/10.1038/ejhg.2009.24>
- 147 van den Bosch, B.J.C., Gerards, M., Sluiter, W., Stegmann, A.P.A., Jongen, E.L.C., Hellebrekers,  
148 D.M.E.I., Oegema, R., Lambrichs, E.H., Prokisch, H., Danhauser, K., Schoonderwoerd, K.,  
149 de Coo, I.F.M., Smeets, H.J.M., 2012. Defective NDUFA9 as a novel cause of neonatally  
150 fatal complex I disease. *J. Med. Genet.* 49, 10–15. <https://doi.org/10.1136/jmedgenet-2011-100466>
- 152 van den Heuvel, L., Ruitenbeek, W., Smeets, R., Gelman-Kohan, Z., Elpeleg, O., Loeffen, J.,  
153 Trijbels, F., Mariman, E., de Bruijn, D., Smeitink, J., 1998. Demonstration of a new  
154 pathogenic mutation in human complex I deficiency: a 5-bp duplication in the nuclear gene  
155 encoding the 18-kD (AQDQ) subunit. *Am. J. Hum. Genet.* 62, 262–268.  
156 <https://doi.org/10.1086/301716>

**Table S2:** Composition of individual MEGS incubations.

incubation	Substrates
1	[1- <sup>14</sup> C]pyruvate + malate + ADP
2	[1- <sup>14</sup> C]pyruvate + carnitine + ADP
3	[1- <sup>14</sup> C]pyruvate + malate <b>without</b> ADP
4	[1- <sup>14</sup> C]pyruvate + malate <b>without</b> ADP + CCCP
4a	[1- <sup>14</sup> C]pyruvate <b>without</b> carnitine + ADP
5	[1- <sup>14</sup> C]pyruvate + malate + ADP + atractyloside
6	[U- <sup>14</sup> C]malate + pyruvate + malonate + ADP
7	[U- <sup>14</sup> C]malate + acetylcarnitine + malonate + ADP
8	[U- <sup>14</sup> C]malate + acetylcarnitine + arsenite + ADP
9	[1,4- <sup>14</sup> C]succinate + acetylcarnitine + ADP

## **A rare variant m.4135T>C in the *MT-ND1* gene leads to LHON and altered OXPHOS supercomplexes**

Rákosníková Tereza<sup>1</sup>, Kelifová Silvie<sup>1</sup>, Štufková Hana<sup>1</sup>, Lišková Petra<sup>2</sup>, Kousal Bohdan<sup>2</sup>,  
Martínek Václav<sup>3</sup>, Honzík Tomáš<sup>1</sup>, Hansíková Hana<sup>1</sup>, Tesařová Markéta<sup>1</sup>

<sup>1</sup>Department of Paediatrics and Inherited Metabolic Disorders, Charles University, First Faculty of Medicine and General University Hospital in Prague, Prague, Czech Republic.

<sup>2</sup>Department of Ophthalmology, First Faculty of Medicine, Charles University and General University Hospital in Prague, Prague, Czech Republic.

<sup>3</sup>Department of Biochemistry, Faculty of Science, Charles University, Prague, Czech Republic.

## INTRODUCTION

Respiratory chain complex I (CI, NADH: coenzyme Q oxidoreductase, EC 1.6.5.3) is the largest enzyme of the oxidative phosphorylation system (OXPHOS) and is consisting of 44 different protein subunits. Seven of them are encoded by mitochondrial DNA (mtDNA) and the rest 37 are encoded by the nuclear genome. CI is composed of three different functional and structural modules - N-module (NADH dehydrogenase), where NADH is oxidized and electrons are passed through the iron-sulfur clusters to the Q-module, where ubiquinone is subsequently reduced, and the transmembrane part of the enzyme, the P-module (proton-pumping) which pumps 4 protons for every two electrons. The mtDNA encoded membrane core subunits (ND1 – ND6 and ND4L) are localised in the P-module. The assembly of CI is an intricate process in which numerous assembly intermediates are formed in several parallel steps to produce a fully assembled CI. Moreover, CI also forms supercomplexes (SCs) with a complex III (CIII)-dimer (I+III<sub>2</sub>) or with CIII-dimer and one or two copies of complex IV (CIV) (I+III<sub>2</sub>+IV<sub>1-2</sub>).

Pathogenic point variant in the *MT-ND1* gene can result in either isolated symptoms, such as Leber hereditary optic neuropathy (LHON), or multi-system syndromes, such as mitochondrial encephalomyopathy, lactic acidosis, and stroke-like episodes (MELAS). Currently, 6 genetic point variants of *MT-ND1* are confirmed as pathogenic in the MITOMAP database (1). Those variants are associated with LHON, LHON/MELAS overlap, MELAS, Leigh syndrome, myopathy, progressive encephalomyopathy, or Leigh-like phenotype (1).

Herein, we present a rare missense variant m.4135T>C in the *MT-ND1* gene identified in a patient manifesting LHON and a significant impact on CI activity and SC formation.

## **MATERIAL AND METHODS**

The study was approved by the Ethics Committee of the General University Hospital in Prague and was conducted in agreement with institutional guidelines. Written informed consent for participation in the study was obtained from the patient and his brother.

A description of the laboratory methods is given in the Supplementary information.

## **RESULTS**

### **Patient**

The male patient was referred to the Department of Paediatrics and Inherited Metabolic Disorders at the age of 38 years with a history of fluctuating declines of visual acuity bilaterally occurring only during physical exercise, or higher ambient temperature, i.e. Uthoff phenomenon) in the past 12 months. He was not able to distinguish which eye was initially affected. His medical history was uneventful including ocular history, reportedly before the start of current symptoms he could see well. He has been a heavy smoker (15 cigarettes a day) since the age of 15.

Family history revealed that his father suffers from colour vision deficiency and one of his two brothers died of a heart defect not closely specified at the age of 15; his mother and older brother are healthy. The older brother is also a smoker but has been smoking since the age of 18 and reports fewer cigarettes smoked per day (seven). His ophthalmic examination at the age of 42 did not reveal any pathology apart from colour vision impairment which was attributed to other genetic causes.

Ocular examination performed one year after the onset of visual symptoms revealed best-corrected visual acuity (BCVA) 0.32 (0.50 logMAR) in the right eye and 0.5 (0.30 logMAR) in the left eye and marked bilateral colour vision impairment. Static perimetry (M700, Medmont International, Nunawading, Australia) showed bilateral centrocecal scotoma with corresponding retinal nerve fiber layer (RNFL) thinning as measured by spectral-domain optical coherence tomography and decreased central vision. Fundus examination revealed pallor of the optic disc bilaterally (Figure 1). No other ocular or systemic pathology was found. Selective metabolic screening showed only mild intermittent hyperalaninaemia (maximum 591  $\mu\text{mol/l}$ ; controls 150

– 500  $\mu\text{mol/l}$ ), lactate concentration in blood and urine and urine organic acids were repeatedly normal. A metabolic examination was also performed on the older brother with normal findings.

Because of subacute painless onset of visual impairment, LHON was suspected, therefore the patient was recommended idebenone treatment (900 mg/day) which was started one year and three months after the onset, later genetic testing confirmed the variant in the subunit of CI therefore supporting our previous decision. Nearly 2 years (21 months) after the disease manifestation BCVA was 0.25 (0.60 logMAR) and 0.5 (0.3 logMAR) in the right and left eye, respectively. Visual field defects remained stable as well as the reduction of RNFL in temporal fields bilaterally (Figure 1).

Subjectively persisted Uhthoff phenomenon, typically seen in multiple sclerosis characterized by vision fluctuation and worsening during physical activity, stress, or higher ambient temperature.

### **Genetics**

The mtDNA sequencing in the patient's blood revealed a heteroplasmic variant m.4135T>C in the *MT-ND1* gene resulting in amino acid substitution p.Tyr277His. The presence of the variant was confirmed in other tissues and heteroplasmy levels were determined (93% in muscle, 92% in buccal swabs, 90% in blood and urinary epithelial cells, and 89% in fibroblasts). The variant m.4135T>C was found in the blood of the patient's older brother at the heteroplasmy level of only 24%. Unfortunately, no samples from the patient's mother were available for the variant testing. Exome sequencing in patient's DNA revealed no other variant(s) that could explain his phenotype.

### **Position of the variant**

The affected ND1 subunit is localised in the membrane part of the CI close to the matrix part of the enzyme (Figure 2A). Human ND1 has eight transmembrane helices (TMH) and Tyr277 is located at the matrix end of TMH7 (Figure 2B). Tyr277 is highly conserved across mammals, but in a larger group of organisms (including prokaryotes), position 277 is conserved for hydrophobic residues (Supplementary Figure 1). Using the MitImpact (2), 11 out of 16 pathogenicity predictors evaluate the m.4135T>C variant as pathogenic.

To predict the effect of the missense variant m.4135T>C (p.Tyr277His) in the *MT-ND1* gene on the structure and function of CI, we used DynaMut software (3). DynaMut integrates their graph-based signatures along with normal mode dynamics to generate a consensus prediction of the impact of a variant on protein stability, thus allowing prediction of both stabilizing and destabilizing effects of the missense variant on the protein. Tyr277His mutation is predicted to be destabilizing ( $\Delta\Delta G = -0.226$  kcal/mol) using the cryoEM structure of the mouse mitochondrial CI in the active state (PDB:6G2J) (4). Interestingly the mouse mitochondrial CI in the inactive state (PDB:6G72) is predicted to be slightly stabilized ( $\Delta\Delta G = 0.046$  kcal/mol) by the Tyr277His mutation. The inactive form stabilisation effect of the mutation could be explained by forming the new inter-subunit H-bond between His277 (subunit ND1) with Asn232 of the subunit NDUFS2 (Figure 2C). The mouse Asn232 of the NDUFS2 protein corresponded to the Asn265 in the human NDUFS2 subunit.

### **Functional characterisation**

To characterize the impact of the m.4135T>C (p.Tyr277His) variant on the structure and function of the OXPHOS system, we performed the analysis of steady-state levels of OXPHOS protein complexes in isolated mitochondria from muscle and fibroblasts (Figure 2). The amount of CI holoenzyme was decreased to approx. 80% in muscle and 90% in fibroblasts. In fibroblasts, CI was detected by three different antibodies (NDUFA9 (Q-module), NDUFV1 (N-module), and NDUFS3 (Q-module)). Immunodetection of DDM-solubilised mitochondria did not reveal an accumulation of CI assembly intermediates. The amount of CIV was decreased below 80 % of control values in both tissues and the amount of CV (ATP synthase) is elevated. Analysis of DIG-solubilised mitochondria reveals the decreased amount of CI-containing SCs and increased CIII-dimer in fibroblasts. Due to the limited amount of obtained tissue, analysis of SCs from muscle was not performed.

While the amount of CI was decreased only to approx. 80–90%, its activity is decreased to approx. 60% and CI+III to 80% of the lower limit of control values in muscle (Table1). Decreased activity of CI and CI+III leads to significantly increased CII (>300%), CII+III (>200%), CIII and CIV (170%) activities and CS activity is slightly elevated (Table 1). Histochemistry in the skeletal muscle biopsy revealed focal subsarcolemmal accumulation of the SDH reaction product in approx. 5% of muscle fibres.



In fibroblasts, CI+III activity was below the lower limit of control. Activities of other analysed enzymes (CI, CII, CIV, and CS) remain in the control range (Table 1).

## DISCUSSION

The clinical manifestation of our patient was rather unique in comparison to a classic LHON manifestation. He suffered from a typical bilateral painless decrease of VA, however, the BCVA at nadir did not decline to a level that would cause as significant visual loss as seen in patients with LHON - their visual outcome is usually worse than 20/200 BCVA (5,6). The patient was referred to our Clinic at the later stage of the disease, so we do not know if an acute phase was present during disease onset. Clinically interesting is also the Uhthoff's phenomenon in our patient, which is rather rare in LHON, described only in four cases by Riordan-Eva et al. in 1995 (7).

The pathogenic variants, both homoplasmic and heteroplasmic, in *MT-ND* genes, over the years have been associated with LHON phenotype. Over 90% of LHON patients are carriers of one of the most frequent pathogenic variants: m.11778G>A (p.Arg340His) (*MT-ND4*), m.14484T>C (p.Met64Val) (*MT-ND6*), and m.3460G>A (p.Ala53Thr) (*MT-ND1*) (8). These variants are necessary but not sufficient to cause blindness and other environmental factors (e.g. smoking (9)) are necessary to trigger retinal ganglion cells degeneration. In the patient with an LHON-like phenotype, we found the heteroplasmic variant m.4135T>C (p.Tyr277His) in the *MT-ND1* gene. Although the variant was present with 0.032%–0.046% frequency in public databases (Mitomap update July 1, 2022; GnomAD 3.1; and Helix) (1,10,11) similar to the frequency of the most common LHON variant m.11778G>A, we provide compelling evidence supporting the causal role of the variant m.4135T>C in the patient's phenotype.

Using ACMG/AMP criteria adapted for mitochondrial variants (12), the variant was classified as pathogenic since functional analysis in two tissues demonstrated its damaging effect on CI (PS3), its level of heteroplasmy segregates with the phenotype in the family (PP1), the *in silico* analyses (2) support its damaging effect on the protein (PP3), and the phenotype suggests a single gene aetiology (PP4).

The heteroplasmic m.4135T>C (p.Tyr277His) variant in the *MT-ND1* gene leads to only a slightly decreased amount of CI but the formation of SCs and activity of the enzyme are

disturbed markedly. Disturbed CI function results in a compensatory effect on other OXPHOS enzyme activities, which are elevated. Disrupted formation of SCs leads to increased CIII-dimer and decreased amount of CIV. The increased amount of CIII-dimer and elevated CII, II+III, III, and CS enzyme activities were also reported in 143B cybrids carrying a homoplasmic m.3571dupC (p.Leu89Profs\*13) in the *MT-ND1* gene (13) or L929dt mouse fibroblasts carrying two homoplasmic variants (m.4206C>T (p.Thr98Met) and m.4859C>T (p.His316Tyr)) in *MT-ND2* gene (14). In fibroblasts derived from three patients with compound-heterozygous variants in TMEM126B, encoding a CI assembly factor, a mild increase in CIII<sub>2</sub>+IV SC was observed (15). While CIII-dimer remains stable in the absence of the formation of CI-containing SC, the steady-state level of CIV decreased, probably due to reduced stability in the absence of SCs formation (13). Recently, a novel m.3955G>A variant in *MT-ND1* was found (16) in two patients with Leigh syndrome. Analysis of cybrid cells with mutation loads of 87% and 98% respectively showed a decreased amount of ND1 protein subunit and a significantly reduced amount of mature CI. CI-containing SC was significantly decreased in both cybrid cell lines when detected by NDUFS2 antibody, but in UQCRC2 or COXIV detections, similar signals across wild-type and mutant cybrid cell lines were found. The activity of CI was significantly reduced, but CII, CII+III, CIII, and CIV activities remain in the control range (16).

We hypothesised that the *MT-ND1* p.Tyr277His missense variant stabilizes the inactive form of CI. Substitution of hydrophobic Tyr to hydrophilic His at position 277 may alter CI structure and therefore formation of SCs is disrupted. The reduction of ubiquinone still occurs, since the CI+III activity is only partially disturbed. Due to decreased ability to form SCs, cells preferred alternative electrons to flow through CII (elevated CII and CII+III activities) and probably also through other pathways which we did not study (e.g. SQOR). Secondly, because of stabilizing effect of the variant on the inactive form of CI, where ubiquinone does not bind to the ubiquinone binding cavity of CI, CI-containing SC is not assembled. Instead, other pathways with a source of electrons for ubiquinone (CII, SQOR) are boosted and activities of remaining respiratory chain complexes are elevated. Thirdly, the mutation could destabilize the natural equilibrium between mentioned CI-containing SC states, by increasing the population of the inactive conformation and perhaps altering natural mechanism of allosteric regulation of the respiration chain activity.

The site of mutation is 11 Å from the ubiquinone molecule therefore it can also affect Q<sub>10</sub> binding channel. Up to 14 Å electron donor–acceptor distance is sufficient to facilitate efficient electron transfer between the two redox centers embedded in a protein medium (17).

## **CONCLUSION**

In patient with m.4135T>C variant in the *MT-ND1* gene, it was shown that albeit the CI is successfully assembled, the activity of CI and CI+III and the ability to form SCs is decreased, probably due to the stabilisation role of the mutation m.4135T>C (p.Tyr277His) in the inactive form of CI.

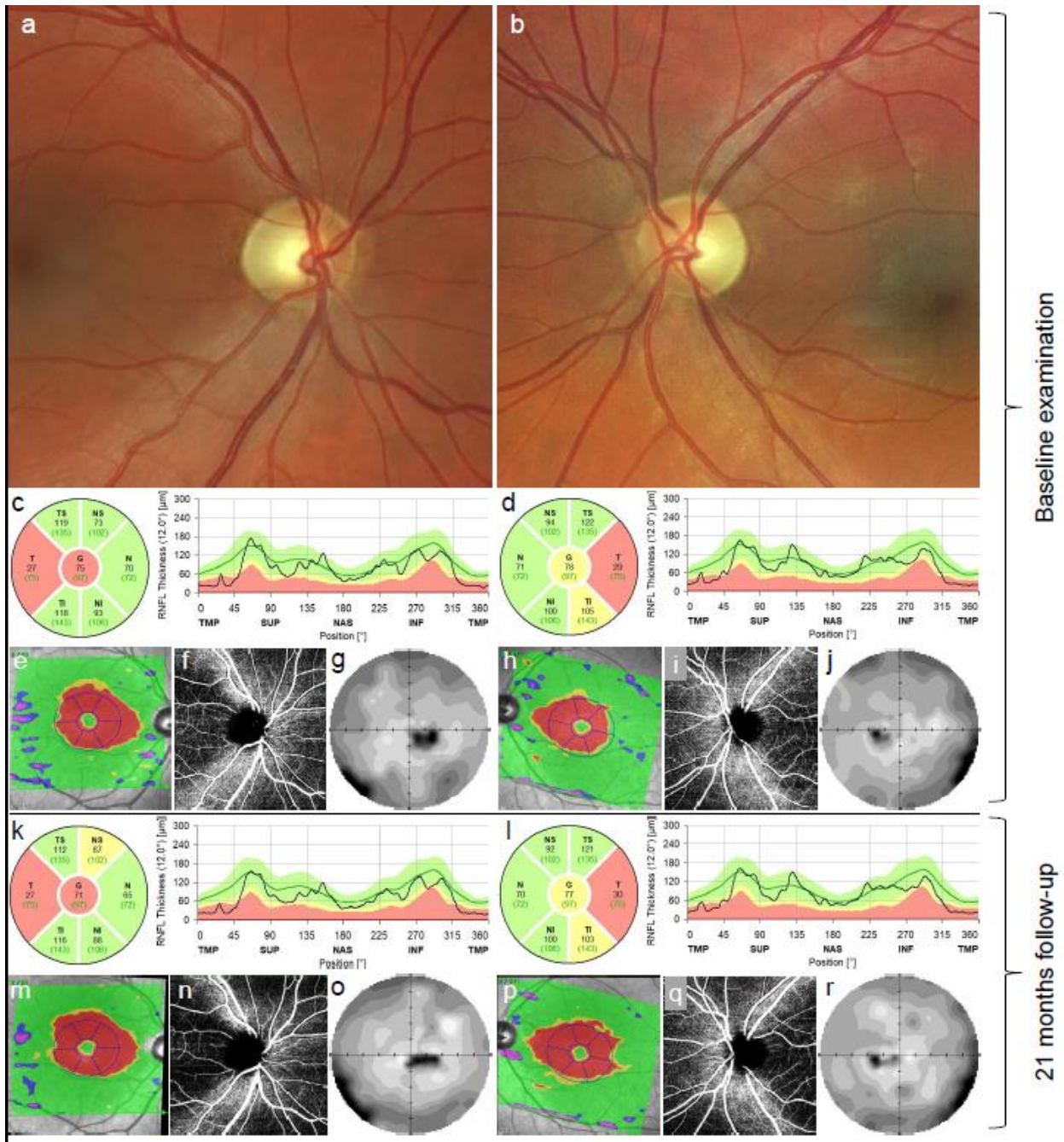


**Figure 1:** Ocular findings in the case carrying m.4135T>C fundus photograph of the right (a) and left eye (b) documenting pallor (atrophy) of the optic discs. Thinning of the retinal nerve fiber layer in the right (c) and left (d) eye in the temporal quadrants at baseline examination corresponding to thinning of the ganglion cell layer (red areas) (e, h) in the macular region, peripapillary capillary dropout (f, i) and centrocecal scotoma more pronounced on the right (g), less pronounced on the left (j) eye. Follow-up examination 21 months later, retinal nerve fibre layer in the right (k) and left (l) eye, ganglion cell layer in the right (m) and left (p) eye, bilateral peripapillary capillary dropout (n, q) and visual field defect in the right (o) and left (r) eye, no marked progression was observed.

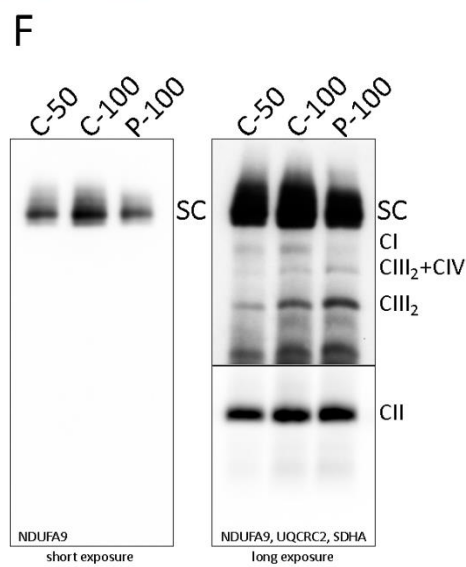
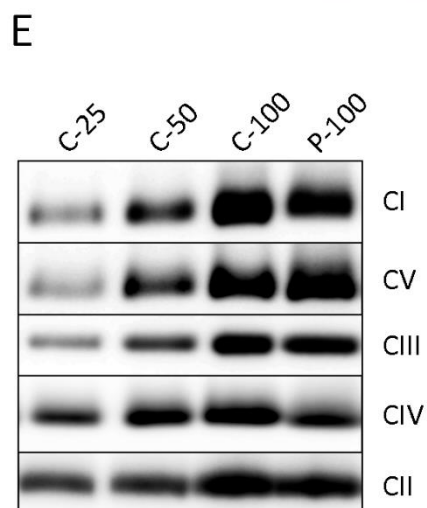
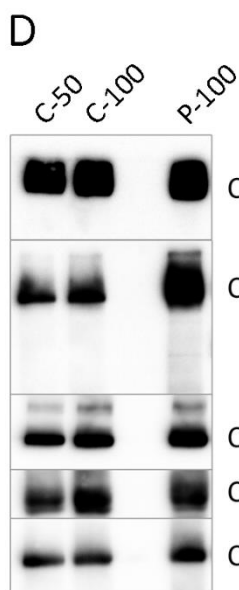
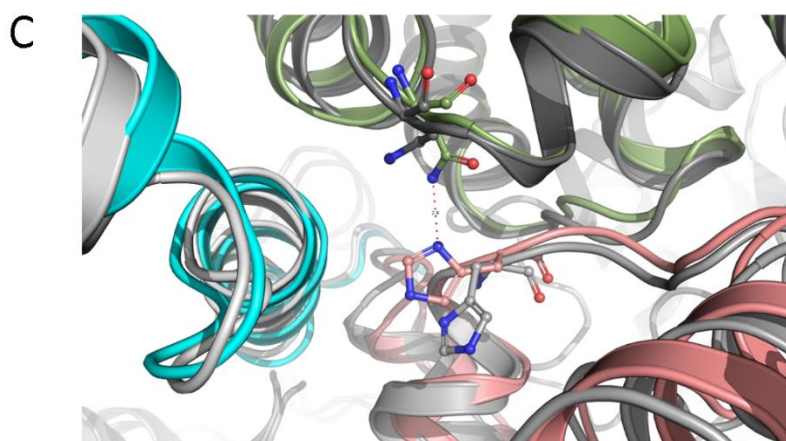
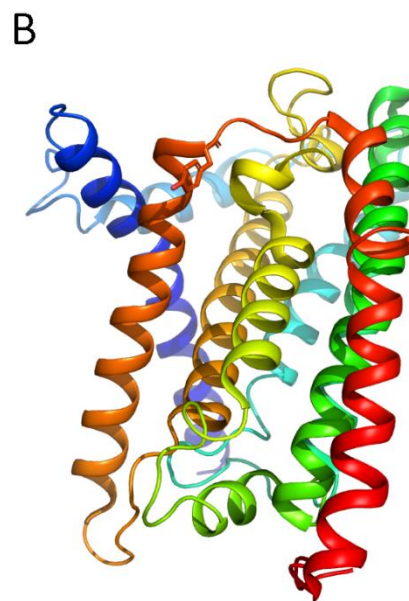
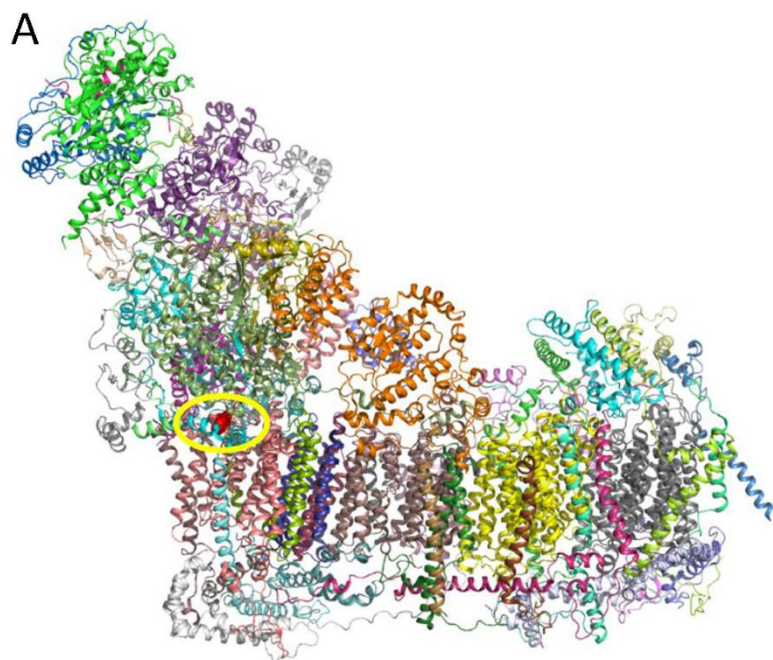


**Figure 2:** A) Human respiratory Complex I. Individual protein molecules in the cartoon representation are shown in various colours. Subunit ND1 is shown in pink and atoms of tyrosin residue 277 (Tyr277) are rendered as red spheres. B) Structure of the ND1 subunit is composed of eight transmembrane helices (TMHs), individual helices in the cartoon representation are shown in rainbow color (blue in the N- terminus and red in the C-terminus). Tyr277 is located at the end of TMH7 (dark orange). C) Difference in histidine position and interactions in ND1<sup>Tyr277His</sup> mutant. Mutated active form is shown in greyscale and inactive state in color (ND1 in pink, NDUFS2 in green and NDUFS8 in blue). In the inactive form, His277 forms H-bond with side chain of Asn232 of the NDUFS2 subunit (mouse model). D) BN-PAGE analysis of dodecylmaltoside-solubilized mitochondria from control and patient's muscle and E) cultivated skin fibroblasts. F) BN-PAGE/WB analysis of digitonin-solubilized mitochondria from control and patient's fibroblast. The numbers 25, 50, and 100 show the loading dose of the protein. Relative signal intensity was normalized to the intensity of complex II by densitometric analysis. C: control, CI – CV: complex I – V, P: patient, SC: supercomplexes (I+III<sub>2</sub>, I+III<sub>2</sub>+IV, I+III<sub>2</sub>+IV<sub>2</sub>), CIII<sub>2</sub>+IV: supercomplex containing CIII-dimer and CIV, CIII<sub>2</sub>: CIII-dimer.

**Table 1:** The activities of respiratory chain complexes in isolated mitochondria from muscle and fibroblasts.

	isolated muscle mitochondria		fibroblasts	
	patient	age-related controls	patient	age-related controls
CI	<b>63.3</b>	110 – 290	31.92	12 – 66
CI+III	<b>102.1</b>	126 – 316	<b>9.18</b>	10 – 30
CII	<b>312.4</b>	21 – 93	13.6	5 – 29
CII+III	<b>532.4</b>	82 – 251	ND	ND
CIII	<b>935.6</b>	>200	ND	ND
CIV	<b>2673.3</b>	658 – 1552	14.29	5 – 26
CS	<b>1395.9</b>	435 – 1234	23.7	13 – 46

Abbreviations: CI complex I, NADH coenzyme Q reductase; CI+III complex I + III, NADH cytochrome c reductase; CII complex II, succinate coenzyme Q reductase; CII+III complex II+III, succinate cytochrome c reductase; CIII complex III, coenzyme Q cytochrome c oxidoreductase; CIV complex IV, cytochrome c oxidase; CS citrate synthase

## REFERENCES

1. MITOMAP: A Human Mitochondrial Genome Database. [cited 2022 Jul 13];2019. Available from: <http://www.mitomap.org>
2. Castellana S, Biagini T, Petrizzelli F, Parca L, Panzironi N, Caputo V, et al. MitImpact 3: modeling the residue interaction network of the Respiratory Chain subunits. *Nucleic Acids Res.* 2021 Jan 8;49(D1):D1282–8.
3. Rodrigues CH, Pires DE, Ascher DB. DynaMut: predicting the impact of mutations on protein conformation, flexibility and stability. *Nucleic Acids Res.* 2018 Jul 2;46(W1):W350–5.
4. Agip ANA, Blaza JN, Bridges HR, Viscomi C, Rawson S, Muench SP, et al. Cryo-EM structures of complex I from mouse heart mitochondria in two biochemically defined states. *Nat Struct Mol Biol.* 2018 Jul;25(7):548–56.
5. Newman NJ, Carelli V, Taniel M, Yu-Wai-Man P. Visual Outcomes in Leber Hereditary Optic Neuropathy Patients With the m.11778G>A (MTND4) Mitochondrial DNA Mutation. *J Neuro-Ophthalmol Off J North Am Neuro-Ophthalmol Soc.* 2020 Dec;40(4):547–57.
6. Chun BY, Rizzo JF. Dominant Optic Atrophy and Leber’s Hereditary Optic Neuropathy: Update on Clinical Features and Current Therapeutic Approaches. *Semin Pediatr Neurol.* 2017 May;24(2):129–34.
7. Riordan-Eva P, Sanders MD, Govan GG, Sweeney MG, Da Costa J, Harding AE. The clinical features of Leber’s hereditary optic neuropathy defined by the presence of a pathogenic mitochondrial DNA mutation. *Brain J Neurol.* 1995 Apr;118 ( Pt 2):319–37.
8. Carelli V, Ross-Cisneros FN, Sadun AA. Mitochondrial dysfunction as a cause of optic neuropathies. *Prog Retin Eye Res.* 2004 Jan;23(1):53–89.
9. Kirkman MA, Yu-Wai-Man P, Korsten A, Leonhardt M, Dimitriadis K, De Coo IF, et al. Gene–environment interactions in Leber hereditary optic neuropathy. *Brain.* 2009 Sep;132(9):2317–26.
10. Laricchia KM, Lake NJ, Watts NA, Shand M, Haessly A, Gauthier L, et al. Mitochondrial DNA variation across 56,434 individuals in gnomAD. *Genome Res.* 2022 Jan 3;32(3):569–82.
11. Helix’s mitochondrial variant database, HelixMTdb. [cited 2022 Jul 13]; Available from: [Helix.com/MILO](https://www.helix.com/MILO)
12. McCormick EM, Lott MT, Dulik MC, Shen L, Attimonelli M, Vitale O, et al. Specifications of the ACMG/AMP standards and guidelines for mitochondrial DNA variant interpretation. *Hum Mutat.* 2020;41(12):2028–57.
13. Lim SC, Hroudová J, Van Bergen NJ, Lopez Sanchez MIG, Trounce IA, McKenzie M. Loss of mitochondrial DNA-encoded protein ND1 results in disruption of complex I biogenesis during early stages of assembly. *FASEB J Off Publ Fed Am Soc Exp Biol.* 2016 Jun;30(6):2236–48.
14. Marco-Brualla J, Al-Wasaby S, Soler R, Romanos E, Conde B, Justo-Méndez R, et al. Mutations in the ND2 Subunit of Mitochondrial Complex I Are Sufficient to Confer Increased Tumorigenic and Metastatic Potential to Cancer Cells. *Cancers.* 2019 Jul 21;11(7):1027.
15. Sánchez-Caballero L, Ruzzenente B, Bianchi L, Assouline Z, Barcia G, Metodiev MD, et al. Mutations in Complex I Assembly Factor TMEM126B Result in Muscle Weakness and Isolated Complex I Deficiency. *Am J Hum Genet.* 2016 Jul;99(1):208–16.

16. Xu M, Kopajtich R, Elstner M, Li H, Liu Z, Wang J, et al. Identification of a novel m.3955G > A variant in MT-ND1 associated with Leigh syndrome. *Mitochondrion*. 2022 Jan;62:13–23.
17. Page CC, Moser CC, Chen X, Dutton PL. Natural engineering principles of electron tunnelling in biological oxidation-reduction. *Nature*. 1999 Nov 4;402(6757):47–52.
18. Burska D, Stiburek L, Krizova J, Vanisova M, Martinek V, Sladkova J, et al. Homozygous missense mutation in UQCRC2 associated with severe encephalomyopathy, mitochondrial complex III assembly defect and activation of mitochondrial protein quality control. *Biochim Biophys Acta BBA - Mol Basis Dis*. 2021 Aug 1;1867(8):166147.
19. Danhelovska T, Kolarova H, Zeman J, Hansikova H, Vaneckova M, Lambert L, et al. Multisystem mitochondrial diseases due to mutations in mtDNA-encoded subunits of complex I. *BMC Pediatr*. 2020 Jan 29;20(1):41.
20. Daňhelovská T, Zdražilová L, Štufková H, Vanišová M, Volfová N, Křížová J, et al. Knock-Out of ACBD3 Leads to Dispersed Golgi Structure, but Unaffected Mitochondrial Functions in HEK293 and HeLa Cells. *Int J Mol Sci*. 2021 Jul 6;22(14):7270.
21. Stiburek L, Vesela K, Hansikova H, Pecina P, Tesarova M, Cerna L, et al. Tissue-specific cytochrome c oxidase assembly defects due to mutations in SCO2 and SURF1. *Biochem J*. 2005 Dec 15;392(Pt 3):625–32.
22. Guo R, Zong S, Wu M, Gu J, Yang M. Architecture of Human Mitochondrial Respiratory Megacomplex I2III2IV2. *Cell*. 2017 Sep 7;170(6):1247-1257.e12.
23. Ashkenazy H, Abadi S, Martz E, Chay O, Mayrose I, Pupko T, et al. ConSurf 2016: an improved methodology to estimate and visualize evolutionary conservation in macromolecules. *Nucleic Acids Res*. 2016 Jul 8;44(W1):W344–50.



## SUPPLEMENTARY INFORMATION

### METHODS

#### *Mitochondrial DNA mutation analysis*

Genomic DNA (gDNA) from all available samples was isolated according to the manufacturer's instructions (Qiagen, Hilden, Germany) using the following kits: Genra Puregene Blood Kit (blood samples), QIAamp DNA Micro Kit (buccal swabs, urine epithelial cells), and QIAamp DNA Mini Kit (muscle biopsy, fibroblasts).

A complete mtDNA genome sequence in blood, muscle, and fibroblast cells was analysed using SeqCap EZ Design: Mitochondrial Genome Design (Roche NimbleGen, Pleasanton, CA, USA) enrichment kit, followed by analysis on MiSeq (Illumina, San Diego, CA, USA) system. Cambridge Reference Sequence (NC\_012920) was used for mtDNA variant annotation. The heteroplasmy was determined as the percentage of reads with the mutated variant. To determine heteroplasmy levels in buccal swabs and urine epithelial cells, mtDNA region m.3803 – m.4410 was amplified by PCR followed by analysis on MiSeq sequencer. No significant differences were found in heteroplasmy levels between the methods as tested in blood samples. The detection limit of both methods is 3%.

Exome sequencing was performed in genomic DNA isolated from blood as described previously (18).

#### *Isolation of mitochondria*

*Musculus triceps surae* muscle biopsy was obtained in local anaesthesia and mitochondria were isolated as described previously (19).

Studied skin fibroblasts were cultivated under the standard condition as described previously (20) and did not exceed passage 10. For Blue Native Polyacrylamide Gel Electrophoresis (BN-PAGE), mitochondria were isolated by standard differential centrifugation (21).

#### *Native electrophoresis and western blotting*

To analyse the steady-state levels of mitochondrial oxidative phosphorylation system (OXPHOS) protein complexes, BN-PAGE (DDM) solubilized isolated mitochondria was used (final ratio 4.8 or 6 mg DDM/mg muscle or fibroblasts protein respectively). Protein concentration was determined by BCA assay (Thermo Fisher Scientific, Waltham, MA, USA).

A total of 10–20 µg of protein was loaded per lane and separated by 6–15% or 4–14% (w/v) polyacrylamide gradient gels (MinProtean<sup>®</sup> 3 system; Bio-Rad, Hercules, CA, USA). A study of SCs was performed using BN-PAGE of digitonin (DIG) solubilised isolated mitochondria (final ratio 7 mg DIG/mg protein). A total of 15 µg of protein was loaded per lane and separated by NativePAGE<sup>™</sup> 3-12% Bis-Tris Mini Protein gels (Thermo Fisher Scientific). BN-PAGE gels were transferred onto Immobilon-P PVDF Membrane (Millipore, Burlington, MA, USA) by semi-dry electroblotting using the Hoefer semi-dry transfer unit (Hoefer, Harvard Bioscience, Holliston, MA, USA).

Primary detection of BN-PAGE blots was performed using mouse monoclonal antibodies against CI subunits NDUFA9 and NDUFB6, complex II (CII) subunit SDHA, CIII subunit UQCRC2, CIV subunits MTCO1 and MTCO2 and ATPB antibody was used for detection of ATP synthase, all from Abcam (Abcam, Cambridge, UK). The immunoblots were detected with peroxidase-conjugated secondary antibodies and Supersignal West Femto Maximum Sensitivity Substrate (Thermo Fisher Scientific) using G:Box (Syngene, Cambridge, UK) and analysed by ImageJ (Wayne Rasband, National Institutes of Health, Bethesda, Maryland, USA).

### ***Spectrophotometry***

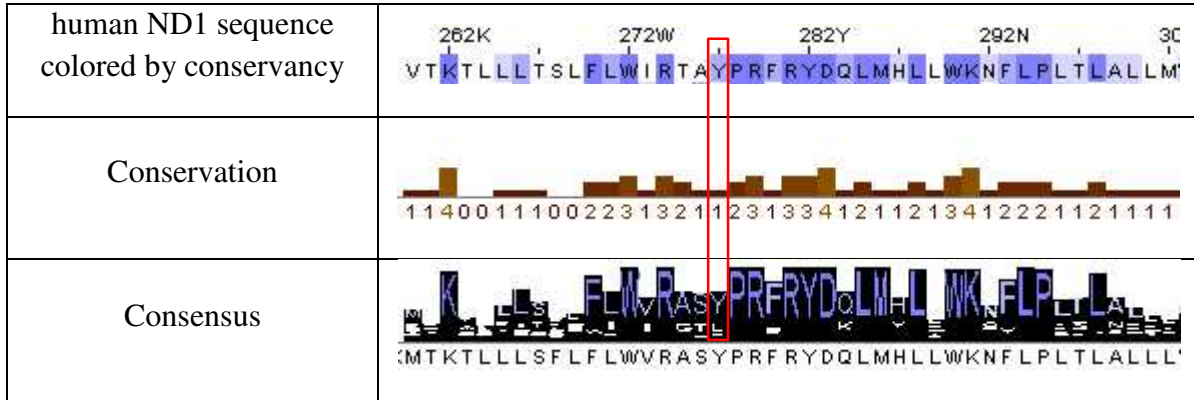
The activities of respiratory chain complexes and citrate synthase were analysed as described previously (19).

### **Computational structural analyses**

The visualisations respiratory complexes and their components were rendered by PyMol software, using atomic coordinates of human CI (PDB ID: 5XTD) and coordinates of active and inactive forms of mouse CI (PDB ID: 6G2J and 6G72, respectively) (22) The effect of mutations on protein structure and stability was predicted using DynaMut software (3).

Multiple sequence alignment was performed using the ConSurf server (23). The Resulting alignment contains 2000 unique sequences that in equal intervals sampled the representative homologous sequences, sharing identity between 50 and 95% with the human ND1 (see Supplementary file “alignment.zip”).

SUPPLEMENTARY FIGURE



**Supplementary Figure 1:** Conservation of the human ND1 protein. Position 277 is conserved for tyrosine across mammals, but across large group of organism (including prokaryotes), position 277 is semi-conserved, meaning that position is conserved for hydrophobic residue.

# **Metabolic adaptation of human skin fibroblasts to ER stress caused by glycosylation defect in PMM2-CDG**

**Zdrazilova L.<sup>1</sup>, Rakosnikova T.<sup>1</sup>, Ondruskova N.<sup>1</sup>, Pasak M.<sup>1</sup>, Vanisova M.<sup>1</sup>, Volfova N.<sup>1</sup>, Honzik T.<sup>1</sup>, Thiel C.<sup>2</sup>, Hansikova H.<sup>1</sup>**

1 Department of Pediatrics and Inherited Metabolic Disorders, First Faculty of Medicine, Charles University and General University Hospital in Prague, Czech Republic

2 Heidelberg University Hospital, Heidelberg, Germany

Hana Hansikova

[hana.hansikova@lf1.cuni.cz](mailto:hana.hansikova@lf1.cuni.cz)

Address:

Laboratory for Study of Mitochondrial Disorders

Department of Pediatrics and Inherited Metabolic Disorders, First Faculty of Medicine, Charles University and General University Hospital in Prague, Czech Republic

Ke Karlovu 2

12808 Prague 2

## Abstract

PMM2-CDG is the most prevalent type of congenital disorders of glycosylation (CDG). It is caused by pathogenic mutations in the gene encoding phosphomannomutase 2, which converts mannose-6-phosphate to mannose-1-phosphate and thus activates this saccharide for further glycosylation processes. Defective glycosylation can lead to an abnormal accumulation of unfolded proteins in endoplasmic reticulum and cause its stress.

Endoplasmic reticulum is a key compartment for glycosylation processes and its connection and communication with mitochondria has been described extensively in literature. Their crosstalk is important for cell proliferation, calcium homeostasis, apoptosis, mitochondrial fission regulation, bioenergetics, autophagy, lipid metabolism, inflammasome formation and unfolded protein response.

Therefore, present study refers to questions, whether defective glycosylation leads to bioenergetic disruption. Our data reveal possible chronic stress in ER and activated unfolded protein response via PERK pathway in PMM2-CDG fibroblasts leading to bioenergetics reorganization and increased assembly of respiratory chain complexes into supercomplexes presumably in order to compensate for compromised glycolysis in PMM2-CDG patient cells. These changes lead to alterations in Krebs cycle, which is tightly connected to electron transport system in mitochondria. In summary, we present data showing metabolic adaptation of cells to glycosylation defect caused by various mutations in *PMM2*.

## Keywords

PMM2-CDG, ER stress, glycolysis, glycosylation, ATP-production, bioenergetic metabolism, fibroblasts, mitochondria,

## Abbreviation

I, II, III, IV- respiratory chain complex I, II, III, IV; ,  $\alpha$ -KG -  $\alpha$ -ketoglutarate;  $\alpha$ -KGDH -  $\alpha$ -ketoglutarate dehydrogenase; ATF4 - activating transcription factor 4; ATF6 - activating transcription factor 6; BN-PAGE - Blue Native Polyacrylamide Gel Electrophoresis; CI+CII+FAO-respiration after addition of substrates for complexes I, II and added octanoyl carnitine; CII control state – respiratory chain complex II dependent state; CII+GpDH - respiratory state obtained from CII and respiratory stimulation by glycerophosphate; CDG- congenital disorders of glycosylation; DMEM-Dulbecco's modified Eagle medium; ECAR – extracellular acidification rate; eIF2 $\alpha$  - eukaryotic initiation factor 2 alpha; ER- endoplasmic reticulum; ET capacity – electron transfer capacity; FCR - flux control ratio; fructose; Glc-glucose; *HPRT1* - gene encoding hypoxanthine-guanine phosphoribosyltransferase; IRE- inositol-requiring 1; man-mannose; MEGS - the mitochondrial energy generating system capacity analysis; MPI- mannose phosphate isomerase; mRNA - mitochondrial RNA; MTCO1 - mitochondrially encoded cytochrome c oxidase I a subunit of respiratory chain complex IV; NDUFA9 - NADH dehydrogenase [ubiquinone] 1 alpha subcomplex subunit 9; OAA-oxalacetate; OXPHOS (CI) - capacity of mitochondria in the ADP-activated state of oxidative phosphorylation; P – P value; P1-11 - patient 1-11; PDH - pyruvate dehydrogenase complex; PERK - double-stranded RNA-dependent protein kinase (PRK)-like ER kinase; PGI- phosphoglucose isomerase; PMM2-phosphomannomutase 2; PMM2-CDG - congenital disorder of glycosylation caused by defective phosphomannomutase 2; Pyr- pyruvate; ROUTINE- routine respiration; SC - supercomplexes; SCAF1 - supercomplex assembly factor 1; SDHA- succinate dehydrogenase complex subunit A; TCA – Krebs cycle; UQCRC2 - Cytochrome b-c1 complex a subunit 2 subunit of respiratory chain complex III; V - ATP-synthase;

## Introduction

PMM2-CDG is the most prevalent type of congenital disorders of glycosylation (CDG). It is caused by pathogenic mutations in the gene encoding phosphomannomutase 2. This enzyme is important for converting mannose-6-phosphate to mannose-1-phosphate and thus activates this saccharide for further glycosylation processes <sup>1,2</sup>.

Recent studies have shown that certain disorders are manifest alterations in both mitochondrial bioenergetics and glycosylation <sup>3,4,5,6</sup>. They showed that cellular *N*-linked deglycosylation capacity is shown to be a significant factor in mitochondrial respiratory chain disease pathogenesis across divergent evolutionary species <sup>5</sup>.

Interestingly, patients with mitochondrial diseases manifest with overlapping symptoms as patients suffering from CDG. They both belong to the group of multisystem disorders. Very common symptoms for both types of disorders are muscle weakness, developmental delay and hypotonia (reviews for symptoms in mitochondrial diseases: <sup>7</sup> and in CDG:<sup>8</sup>)

The connection between mitochondria and endoplasmic reticulum (ER), as a key compartment for glycosylation processes, has a multifaceted nature and has been described extensively in literature <sup>9,10</sup>. Crosstalk between the mitochondria and the ER is important for cell proliferation, calcium homeostasis, apoptosis, mitochondrial fission regulation, bioenergetics, autophagy, lipid metabolism, inflammasome formation and unfolded protein response <sup>9,11</sup>.

Many factors such as UV radiation, reactive oxygen species, hypoxia, protein mutations, nutrient starvation <sup>12</sup> and, importantly, defective glycosylation <sup>13</sup> can lead to accumulation of unfolded proteins in ER and cause ER stress. Therefore, cells have evolved a pathway called the unfolded protein response (UPR), which is responsible for ER homeostasis reestablishment <sup>14</sup>. If UPR fails to balance the ER stress, the cell initiates the process of apoptosis <sup>15</sup>. The UPR relies mainly on three ER stress sensors: double-stranded RNA-dependent protein kinase (PRK)-like ER kinase (PERK), inositol-requiring 1 (IRE1) and activating transcription factor (ATF6) <sup>16</sup>. The activation of IRE1 mostly supports protein folding by stimulation of ER molecular chaperones expression <sup>17,18</sup>, similarly to ATF6, which

after activation migrates to the nucleus to induce the transcription of ER molecular chaperones<sup>19</sup>. PERK can selectively interact with misfolded proteins and induce ER stress signaling via phosphorylating eukaryotic initiation factor 2 alpha (eIF2 $\alpha$ ), leading to global protein translation suppression<sup>12,20</sup>, while increasing the specific translation of ATF4<sup>21</sup>. ATF4 induces the expression of genes involved in amino acid metabolism, reduction-oxidation control and proteostasis<sup>22</sup>. The ATF4 pathway activation can be also initiated by mitochondrial stress<sup>23</sup>. It has been found that the PERK arm of the UPR stimulates respiratory chain supercomplexes (SC) assembly via upregulating supercomplex assembly factor 1(SCAF1) expression and thus increase mitochondrial respiration efficiency under ER and nutrient stress conditions<sup>24</sup>. The ER stress was previously already described in PMM2-CDG fibroblasts carrying different mutations than those present in our patients' cohort<sup>25</sup>.

Our study reveals increased assembly of respiratory chain complexes into supercomplexes in fibroblasts from PMM2-CDG patients and suggests that this might be due to the presence of chronic ER stress. Moreover, our results confirm activated PERK pathway in PMM2-CDG fibroblasts. Stimulated SC assembly occurs presumably to compensate for compromised glycolysis in PMM2-CDG patient cells to meet the energetic and metabolic demands. These changes lead to alterations in Krebs cycle (TCA), which is tightly connected to electron transport system in mitochondria. All together, we present data showing metabolic adaptation of cells to glycosylation defect caused by various mutations in *PMM2*.

## **Material and methods**

### ***Cells***

### ***Controls***

Two human dermal fibroblast cell lines were purchased, HDF 1 (Primary Dermal Fibroblast Normal; Human, Neonatal HDFn, PCS\_201\_010, ATCC, NHDF-Neo), and HDF 2 (Human Dermal Fibroblasts, Neonatal, CC-2509, Lonza East Port. Four of human dermal fibroblast cell lines were derived from individuals in whom no metabolic disease had been confirmed.



## Patients

Fibroblast cell lines from 11 patients with PMM2-CDG (Table 1) were used in present study. Skin biopsy was obtained after informed parentals' consent ethics committee General Hospital in Prague approval N° 92/18 (18.10.2018) for the project GAUK (Grant Agency of Charles University 110119). Cell lines were cultured in Dulbecco's modified Eagle medium (DMEM, Pan Biotech) with 25 mM glucose, 10 % fetal bovine serum and 1 % antibiotics-antimycotics 100X at 37 °C under 5 % CO<sub>2</sub> atmosphere. Fibroblast cultures at passage number 7 to 15 were grown to approximately 80 % confluence. Suspended cells were counted by a Handheld Automated Cell Counter (Millipore). Cells were harvested by incubation in trypsin 0.05 % w/V with Ethylenediaminetetraacetic Acid Tetrasodium Salt 0.02 %, w/V for 5 min at 37 °C, washed, and centrifuged at 300 g (5 min, 24 °C). Unless otherwise stated, pellets of cells were stored at -80°C until analyses.

**Table 1. Cohort of PMM2-CDG patients included in this study.**

Patient	genotype	age	gender	PMM2 activity (%)	phenotype
P1	c.395T>C/c.422G>A	2y	M	26.32	moderate
P2	c.338C>T/c.422G>A	5y	F	4.61	moderate
P3	c.338C>T/c.422G>A	8y	F	55.26	moderate
P4	c.338C>T/c.422G>A	7y	F	26.32	moderate
P5	c.357C>A/c.422G>A	1.5y	M	69.08	severe
P6	c.357C>A/c.422G>A	10y	F	32.89	severe
P7+	c.422G>A / c.691G>A	2m	M	7.89	severe
P8	c.338C>T / c.422G>A	11m	M	nd	severe
P9	c.178+3A>T/422G>A	13y	M	39.47	severe
P10	c.24delC/c.338C>T	1y	M	nd	severe
P11+	c.447+3dupA/c.691G>A	3m	M	nd	severe

+.. died, nd- not defined

## Transmission electron microscopy

Cultured skin fibroblasts were cultivated to 80% confluence and fixed in phosphate-buffered saline (PBS, BioWhittaker, Lonza, Walkersville, MD) containing 2% (w/v) potassium permanganate for 15 min at room temperature (RT). After fixation, cells were dehydrated by ethanol series (for 10 min in 50%,

70% and 90% ethanol, for 30 min in 100% ethanol). Samples were incubated in propylene oxide (2 x 15 min) and embedded in Durcupan Epon (Durcupan Epon: Propylene oxide 1:1 for 2 hours, Durcupan Epon: Propylene oxide 1:3 overnight). Polymerized blocks were sectioned by Ultracut Reichert microtome. 600-900 Å thick slices were stained with lead citrate and uranyl acetate <sup>26</sup>(Brantova et al., 2006). Images were acquired with transmission electron microscope (JEOL JEM 1200 EX, JEOL, Peabody, MA).

### ***Western blot analyses***

Western blot (WB) analyses were performed according to Ondruskova et al, 2020 <sup>27</sup>. Tricine SDS-PAGE separation was performed using 12% gels. The concentration and catalog number of used antibodies are summarized in Table S1 in supplementary data.

### ***qPCR***

Reverse transcription and quantitative RT-PCR was performed according to Ondruskova et al, 2020 <sup>27</sup>. TaqMan-FAM probes ATF4 probe (Hs00909569\_g1, Thermo Fisher Scientific) and HPRT1 probe (Hs01003267\_m1, Thermo Fisher Scientific) were employed for the measurement using 7300 Real-Time PCR System (Applied Biosystems). Delta Ct method was used for *ATF4* gene expression analysis and data were normalized to the expression of *HPRT1*.

### ***Glycolytic function measurements***

#### **Glucose starvation pretreatment:**

To the flask with cells with confluence around 70% and without medium was added Dulbecco's modified Eagle's medium (DMEM, P04-04510, Pan Biotech) without glucose, but containing antibiotics-antimycotics (XC-A4110/100, Biosera) and dialyzed fetal bovine serum (P30-2102, Pan Biotech). After one day, the cells were seeded into the Seahorse XF24 cell culture microplate and 24 hours later, after changing the DMEM medium to starvation DMEM 5030 (Sigma, Aldrich, DMEM5030 was the basis of DMEM respiration medium with addition of 3.9 mM glutamate, 5 mM glucose and 2 mM pyruvate, adjusted to pH 7.4 at 37°C), glycolytic function of cells was measured in Agilent Seahorse XF Analyzer (XF24).

### Extracellular acidification rate

Extracellular acidification rate was measured in the Agilent Seahorse XF Analyzer (XF24) according to Zdrzilova et al, 2022 <sup>28</sup> with following modifications of the performed protocol: 10 mM glucose was added to cartridge port A, 2 μM oligomycin to port B, 0,7 μM Carbonyl cyanide-p-trifluoromethoxyphenylhydrazone to port C, 2 μM rotenone, 1 μM antimycin A and 100 mM 2-deoxy-D-glucose to port D.

### ***Level of metabolites in cell culture media***

Metabolites in cell culture media were assayed by tandem mass spectrometry combined with gas chromatography GC-MS/MS (ITQ 1100, Thermo Scientific, USA). All metabolites were quantified after an ethyl acetate extraction from urine and ethoxime-trimethylsilyl derivatization according to Chalmers and Lawson, 1982 <sup>29</sup>.

### ***Pyruvate dehydrogenase activity***

The basal activity of the pyruvate dehydrogenase (PDH) complex was measured according to Sheu et al, 1981 <sup>30</sup> as the production of <sup>14</sup>CO<sub>2</sub> produced by decarboxylation of [<sup>1-14</sup>C]-pyruvate (Perkin –Elmer, USA) with incubation time 20 min. Protein was estimated according to Lowry et al, 1951 <sup>31</sup>.

### ***Activities of mitochondrial enzymes***

The activities of the mitochondrial respiratory chain complexes NADH:ubiquinone oxidoreductase (CI)- rotenone sensitive, succinate:CoQ reductase (SQR, CII), ubiquinol:cytochrome c oxidoreductase (QCCR, CIII), cytochrome c oxidase (COX, CIV), were measured spectrophotometrically at 37°C in using a Shimadzu 2401 UV-VIS spectrophotometer according to Rustin et al 1994 <sup>32</sup>. Approximately 100 μg of cell suspension was used for one assay. The activities were expressed as nmol of substrate converted per minute and normalized to the protein content in the reaction (nmol.min<sup>-1</sup>.mg prot.<sup>-1</sup>).

### ***The mitochondrial energy generating system capacity (MEGS) analysis***

The mitochondrial energy generating system capacity was measured according to Janssen et al., 2006<sup>33</sup> with minor modifications described by Vanisova et al, 2022<sup>34</sup>. The analysis was performed with [<sup>1-14</sup>C] pyruvate, [<sup>U-14</sup>C]malate and [<sup>1-14</sup>C]succinate as substrates. The composition of individual incubations is summarized in Table S2 (Supplementary material).

### ***Analysis of mitochondrial DNA content***

The expression of mitochondrial DNA was measured by real-time PCR according to Pejznochova et al. 2010<sup>35</sup>.

### ***Respiratory measurements***

Mitochondrial respiration measurement in Oxygraph O2k was performed according to Zdrzilova et al, 2022<sup>28</sup> with modified protocol: endogenous ROUTINE respiration was recorded after cell addition, subsequently it was inhibited by digitonine addition (10 µg/mL), which permeabilized cell membrane and facilitated the entry of mitochondrial substrates. Next, pyruvate (5 mM), malate (2 mM) and ADP (2.5 mM) were added to investigate OXPHOS state. The following uncoupler titration (CCCP, 3.5 µM) revealed the electron transfer capacity. Afterwards, glutamate (10 mM) and succinate (10 mM) addition stimulated respiration, enabling us to obtain noncoupled electron transfer state. Inhibition of respiratory chain complex I with rotenone (0.5 µM) was followed by glycerolphosphate addition (10 mM) to investigate glycerolphosphate dehydrogenase -linked pathway. Then, the inhibitor of respiratory complex III, antimycin A (2.5 µM), was added to create a residual oxygen consumption (*Rox*) state and finally ascorbate (2 mM), TMPD (0.5mM) and azide (200 mM) were injected to investigate respiratory chain complex IV status.

### ***Cellular ATP production***

CellTiter-Glo Luminiscent Cell Viability Assay (G7570) from Promega was used for determining cellular ATP production. Protocol was performed according to the manual.

### ***Blue Native Polyacrylamide Gel Electrophoresis (BN-PAGE)***

For Blue Native Polyacrylamide Gel Electrophoresis (BN-PAGE), mitochondria were isolated by standard differential centrifugation according to Danhelovska et al, 2020<sup>36</sup>. To analyse the steady-state levels of mitochondrial oxidative phosphorylation system (OXPHOS) protein complexes, BN-PAGE of n-dodecyl  $\beta$ -d-maltoside (DDM) solubilized isolated mitochondria was used at final ratio 6 mg DDM/mg protein. Protein concentration was determined by BCA assay (Thermo Fisher Scientific, Waltham, MA, USA). A total of 10–25  $\mu$ g of protein was loaded per lane and separated by 6-15%, 4-14% or 8-16% (w/v) polyacrylamide gradient gels (MinProtean<sup>®</sup> 3 system; Bio-Rad, Hercules, CA, USA). A study of SCs was performed using BN-PAGE of digitonin solubilised isolated mitochondria (final ratio 7 mg DIG/mg protein). A total of 15  $\mu$ g of protein was loaded per lane and separated by NativePAGE™ 3-12% Bis-Tris Mini Protein gels (Thermo Fisher Scientific). BN-PAGE gels were transferred onto Immobilon-P PVDF Membrane (Millipore, Burlington, MA, USA) by semi-dry electroblotting using the Hoefer semi-dry transfer unit (Hoefer, Harvard Bioscience, Holliston, MA, USA). Primary detection of BN-PAGE blots was performed using mouse monoclonal antibodies against CI subunits NDUFA9 and NDUF6, complex II (CII) subunit SDHA and SDHB, CIII subunit UQCRC2, CIV subunits MTCO1, ATPB antibody was used for detection of ATP synthase, all from Abcam (Abcam, Cambridge, UK). The immunoblots were detected with peroxidase-conjugated secondary antibodies and Supersignal West Femto Maximum Sensitivity Substrate (Thermo Fisher Scientific) using G:Box (Syngene, Cambridge, UK) and analyzed by Quantity One software (Bio-Rad). The concentration and catalog number of used antibodies are summarized in Table S1 in supplementary data.

### ***Statistics***

The activity of enzymes was statistically analyzed using Wilcoxon test. The rest of the data was statistically analyzed using multiple comparison test and graphs were generated in GraphPad Prism 8.3.0.

## Results

### Confirmation of induced stress in endoplasmic reticulum

Ultrastructural investigation showed dilatation of endoplasmic reticulum together with abnormal ER cisternae and, presumably, accumulation of proteins in 4 PMM2-CDG patients' fibroblasts (P1, P2, P9, P10) (representative image in Figure 1A). Protein level of the stress factor ATF4 (Figure 1C) was increased to approximately 150%, which was accompanied by the finding of 3-fold increased expression of the corresponding gene *ATF4* (Figure 1B).

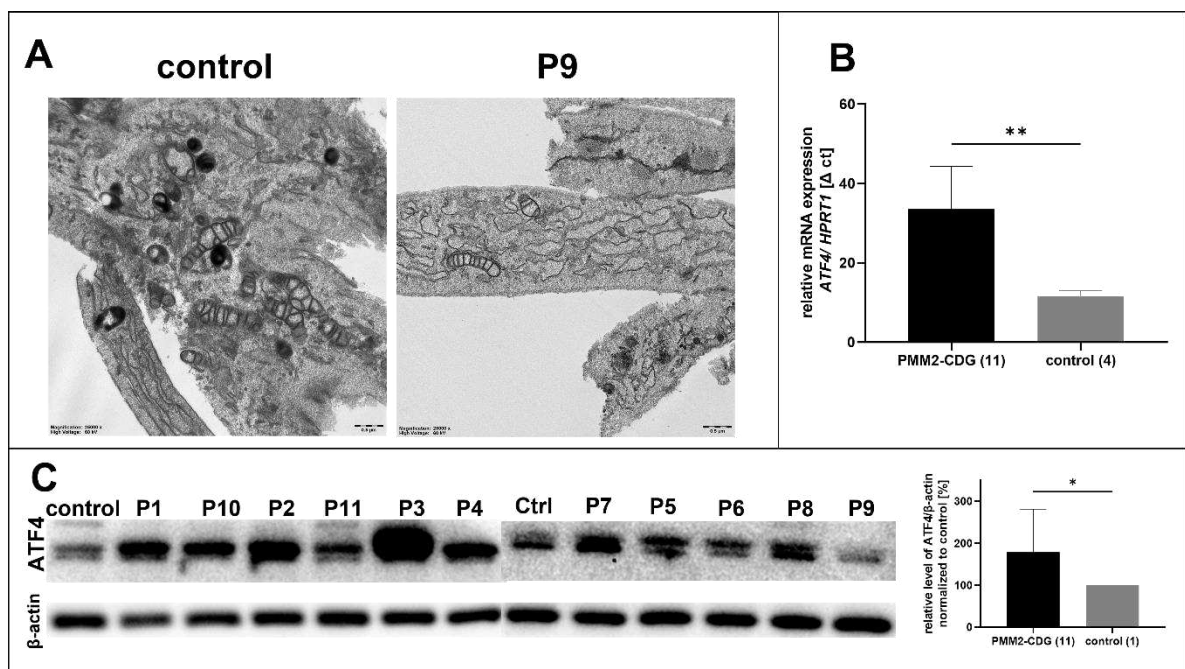


**Figure 1: Confirmation of ER stress in PMM2-CDG fibroblasts.** **A)** ER dilatation in PMM2-CDG fibroblasts captured by transmission electron microscopy (25 000 x magnification). ER dilatation, abnormal ER cisternae and seeming protein accumulation was detected in 4 PMM2-CDG patients out of 10 tested. **B)** Relative mRNA expression of ATF4 normalized to the expression of HPRT1 gene measured by qPCR showed significant increase ( $p=0.0016$ ). **C)** Steady-state level of ATF4 protein in PMM2-CDG fibroblasts measured by SDS-PAGE/WB. 10  $\mu$ g of protein was loaded per well. The intensity of signal was normalized to the loading control  $\beta$ -actin. Protein level of ATF4 was on average increased to 178% ( $p=0.02$ ).  $P$  –  $P$  value; P1-11 - patient 1-11; ATF4 - Activating transcription factor 4; PMM2-CDG - congenital disorder of glycosylation caused by defective phosphomannomutase 2; mRNA - mitochondrial RNA; HPRT1 - gene encoding hypoxanthine-guanine phosphoribosyltransferase.

## Reduced glycolytic function

Glycolytic function showed reduced glycolysis and glycolytic capacity in the patients in comparison to the controls (Figure 2A). After cell starvation (48 hours without glucose), the glycolysis parameter returned to level comparable to controls (Figure 2B). The level of pyruvate in cell culture media was reduced (Figure 2D), but lactate remained unchanged (Figure 2E). Pyruvate dehydrogenase complex activity showed a slightly decreased trend (Figure 2C).

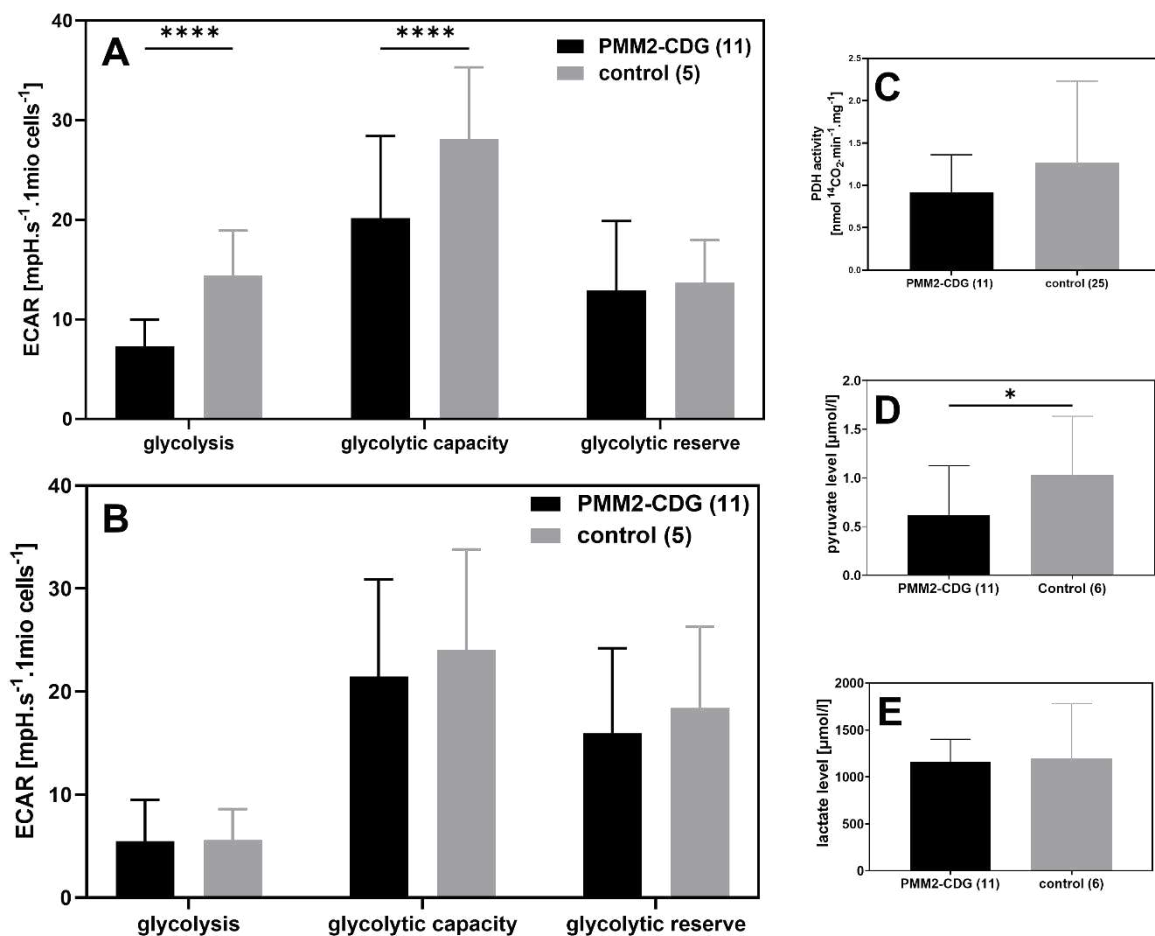


**Figure 2: PMM2-CDG fibroblasts exhibited slightly diminished glycolytic parameters. A)** Glycolytic function in PMM2-CDG patients' fibroblasts measured by Seahorse Bioanalyzer. Glycolysis and glycolytic capacity was significantly reduced ( $P < 0.0001$ ); **B)** Glycolytic function in PMM2-CDG patients' fibroblasts after 48 hours of glucose starvation measured in Seahorse Bioanalyzer showed equal glycolysis rate compared to controls; **C)** Pyruvate dehydrogenase (PDH) activity measured by spectrophotometric method was slightly, but non-significantly reduced; **D)** Level of pyruvate in the cell culture media from 11 PMM2-CDG patients' fibroblasts measured by tandem mass spectrometry was reduced ( $P=0.0492$ ), **E:** Level of lactate in cell culturing media

from 11 PMM2-CDG patients' fibroblasts measured by tandem mass spectrometry was unchanged. ECAR – extracellular acidification rate; *P* – *P* value; PMM2-CDG – congenital disorder of glycosylation caused by defective phosphomannomutase 2.

### Reorganization of Krebs cycle

To dissect mitochondrial bioenergetics in more detail, Krebs (TCA) cycle was investigated due to its direct connection to the respiratory chain. Citrate synthase level and activity were lowered, suggesting changes in the citrate flow (Figure 3A and B). The level of  $\alpha$ -ketoglutarate in cell culture media was significantly reduced while measured by tandem mass spectrometry (Figure 3C).  $\alpha$ -ketoglutarate dehydrogenase ( $\alpha$ -KGDH) complex dependent state (7/8 ratio) measured by MEGS analysis was slightly increased suggesting its stimulation (Figure 3D).

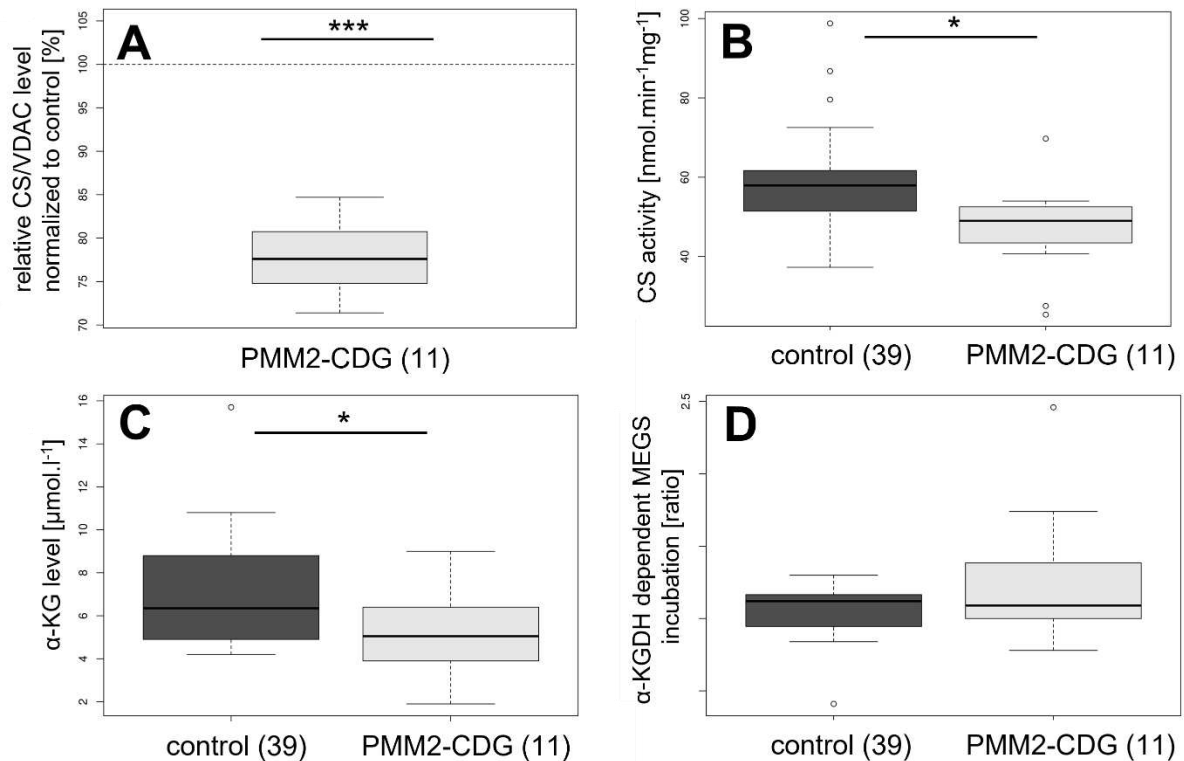


**Figure 3: Alteration of Krebs cycle in PMM2-CDG fibroblasts.** **A)** Citrate synthase steady state level in PMM2-CDG patients' fibroblasts measured by SDS/WB was significantly decreased compared to a control. **B)** Decreased citrate synthase activity in PMM2-CDG patients measured by spectrophotometric method. **C)** Level of  $\alpha$ -ketoglutarate in cell cultivation media from 11 PMM2-CDG patients' fibroblasts measured by LC-MS/MS was significantly decreased ( $P=0.0221$ ). **D)** The mitochondrial energy generating system capacity analysis ratio ( $[U-^{14}C]$  Malate+Acetylcarnitine+Malonate+ADP/ $[U-^{14}C]$  Malate+Acetylcarnitine+Artenite+ADP) showing  $\alpha$ -ketoglutarate dehydrogenase complex dependent state slightly upregulated.



## Functional changes of cellular bioenergetics

The activities of respiratory chain complexes were significantly increased for complexes I (CI) and II (CII) and decreased for complex IV (CIV) in PMM2-CDG cells (Figure 4). When evaluating the relationship between PMM2 activity and the activity of respiratory chain complexes I, II and IV, a significant correlation was found for the complex II activity (Figure S1).

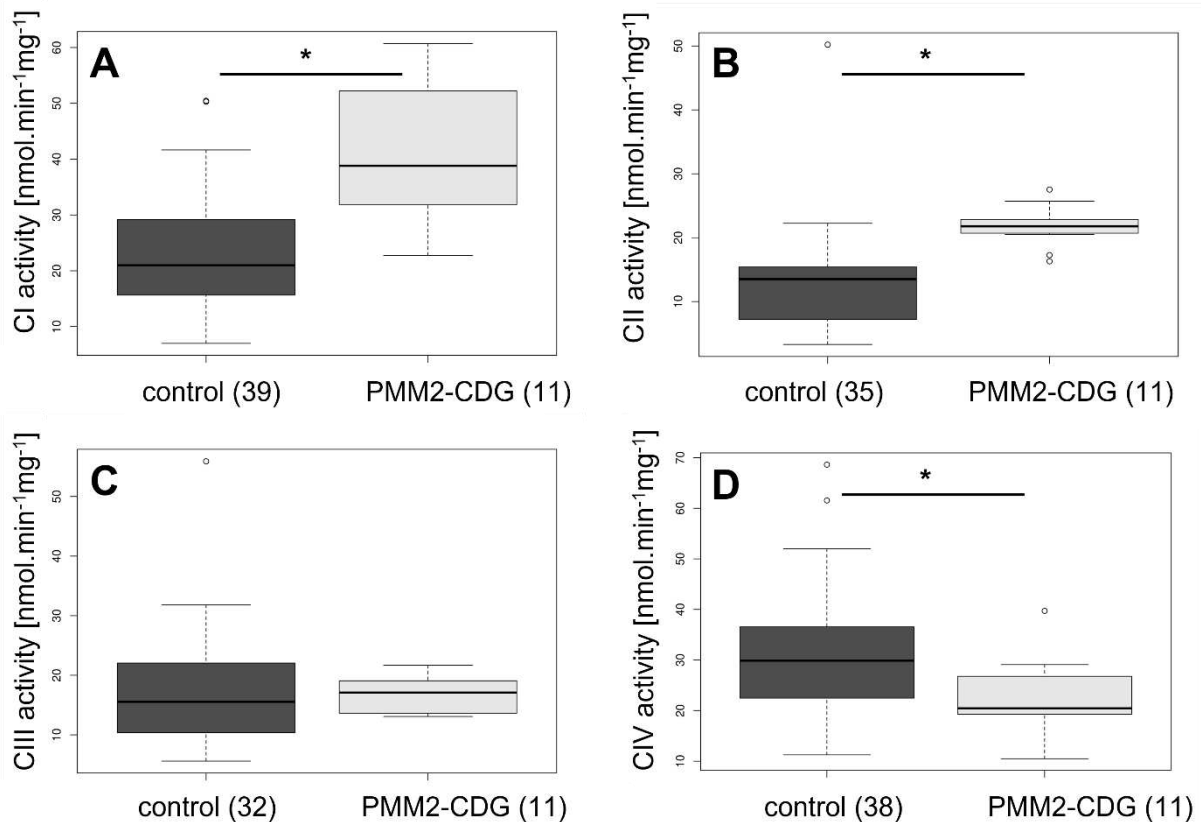


**Figure 4: Impairment of the respiratory chain complexes' activities in PMM2-CDG fibroblasts.** **A)** Activity of complex I was significantly increased in comparison to controls. **B)** Complex II activity was significantly increased in comparison to controls, **C)** Complex III, **D)** Complex IV activity was significantly decreased in comparison to controls. \*  $P < 0.005$ .  $\text{nmol}\cdot\text{min}^{-1}\cdot\text{mg}^{-1}$  PMM2-CDG- congenital disorder of glycosylation caused by defective phosphomannomutase 2.

## Increased level of the supercomplexes

Blue native PAGE electrophoresis performed in selected patients' samples (P1, P7, P8) revealed increased level of supercomplexes when detected by antibodies against NDUFA9, CORE2 and COXI. A considerable increase of up to 150% was

detected using NDUFA9 and COXI antibodies, (Figure 6). SDS/WB analyses of selected subunits of the individual OXPHOS complexes (NDUFA9 and NDUFB8 for CI, SDHA and SDHB for CII, CORE II for CIII, COX II and COX IV for CIV, ATP5a for CV) did not show uniform changes in comparison with controls (data not shown).

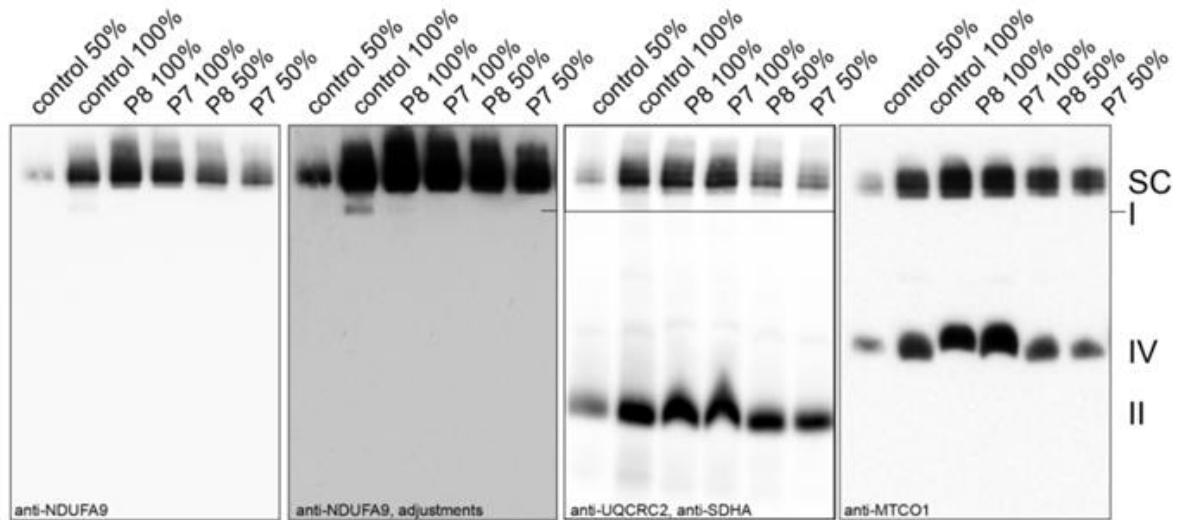


**Figure 5: Level of respiratory chain complexes and increased supercomplexes in PMM2-CDG fibroblasts.** Representative results of the steady state levels of respiratory chain complexes determined by BN-PAGE/WB with 6-15%, 4-14% or 8-16% (w/v) polyacrylamide gradient gels (MinProtean® 3 system; Bio-Rad, Hercules, CA, USA) in patients 7 and 8. Patients' fibroblasts showed increased level of supercomplexes of up to 150%. The highest increase was in complex I containing SCs. SC- supercomplex; SDHA- succinate dehydrogenase complex subunit A; NDUFA9- NADH dehydrogenase [ubiquinone] 1 alpha subcomplex subunit 9; UQCRC2 - Cytochrome b-c1 complex a subunit 2 subunit of respiratory chain complex III; MTCO1 - mitochondrially encoded cytochrome c oxidase I a subunit of respiratory chain complex IV; I, II, IV - respiratory chain complexes I, II, IV.

### **Mitochondrial characterization**

Cellular ATP production was slightly increased compared to the controls (Figure 6C) similarly to MEGS analysis, where the 1/3 reaction ratio, reflecting the coupling state of oxidation and phosphorylation in mitochondria was also slightly increased (Figure 6D). Analysis of the data obtained from respiratory measurements showed reduced profile in majority of measured states but after relative normalization (*FCR*) no significant differences between the controls and patients, were observed showing sustained mitochondrial quality and capacity

(Figure 6A and B). Moreover, mitochondrial DNA content measured by qPCR was unchanged (Figure 6E).

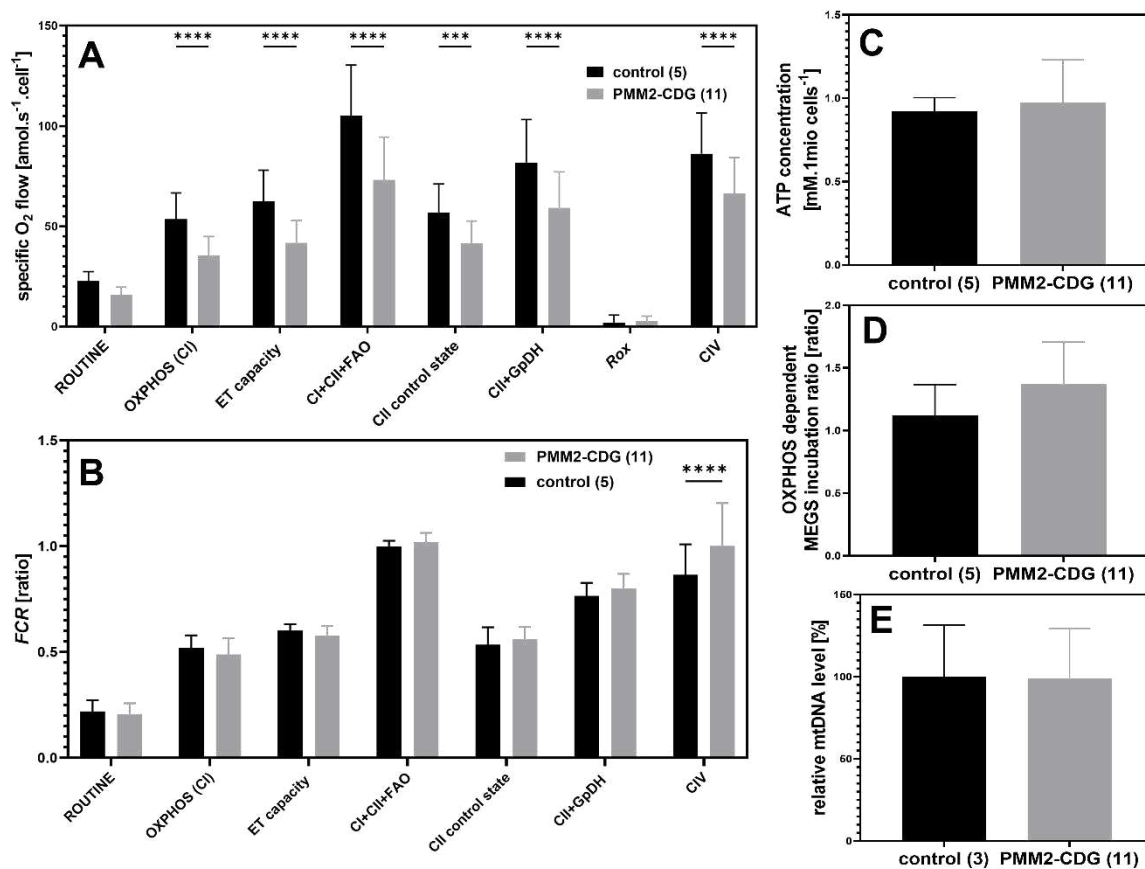


**Figure 6: Mitochondrial parameters' profile in 11 PMM2-CDG fibroblast cell lines showed sustained mitochondrial quality and function.** **A)** Specific O<sub>2</sub> flow of mitochondrial respiration showed reduced measured respiratory states **B)** Flux control ratio of mitochondrial respiration in 11 PMM2-CDG patients' fibroblasts and controls showed sustained mitochondrial quality. Respiratory chain complex activity IV was significantly increased compared to controls (\*= P<0.0001). **C)** Cellular ATP production measured by luminometry was unchanged **D)** The mitochondrial energy generating capacity system analysis. The reaction 1 consists of: [1-<sup>14</sup>C] Pyruvate+Malate+ADP, 3: [1-<sup>14</sup>C] Pyruvate+Malate-ADP. The 1/3 ratio was non-significantly increased compared to controls. **E)** Relative mitochondrial DNA level was not altered in the patients' fibroblasts. FCR - flux control ratio, it provides an internal normalization, expressing respiratory control independent of mitochondrial content and thus independent of a marker for mitochondrial amount; ROUTINE-routine respiration, showing energetic demand of the cell under normal conditions using endogenous substrates and available substrates in media; OXPHOS (CI) - capacity of mitochondria in the ADP-activated state of oxidative phosphorylation, at saturating concentrations of ADP and inorganic phosphate, with added substrates for respiratory complex I (pyruvate, malate); ET capacity - maximum rate of O<sub>2</sub> consumption reflecting the electron transfer capacity ("maximal respiration") in the noncoupled state; CI+CII+FAO-respiration after addition of substrates for complexes I, II and added octanoyl carnitine to test the fatty acid oxidation influence on

*respiration; CII control state - state after complex I inhibition showing the respiratory capacity of complex II; CII+GpDH - respiratory state obtained from CII and respiratory stimulation by the addition of glycerophosphate. PMM2-CDG - congenital disorder of glycosylation caused by defective phosphomannomutase 2.*

## **Discussion**

Mitochondria tightly communicate and interact with endoplasmic reticulum (ER), and ER is a key organelle for the process of glycosylation. Transmission electron microscopy revealed ER dilatation, abnormal ER cisternae and visible, presumably, protein accumulation in 4 PMM2-CDG cell lines (P1, P2, P9, P10) (Figure 1). We hypothesized that these ultrastructural changes could be due to induced ER stress, as it had been already described previously in a yeast model by Bernales et al 2006 <sup>37</sup>. Together with the finding of increased ATF4 both at the protein and mRNA level (Figure 1), our data suggest the induction of ER stress in PMM2-CDG patients' fibroblasts (Figure 7A). ER stress can be triggered by accumulation of misfolded proteins in ER due to a defective glycosylation, and result in unfolded protein response (UPR). The UPR initiates a compensatory mechanism leading to the attenuation of general protein expression and upregulation of stress factors expression <sup>14,16</sup>. Non-ER specific processes such as amino acid metabolism, mitochondrial function (and thus energy production) and others are then transcriptionally regulated by an induced UPR (<sup>19</sup>Rutkowski and Kaufman, 2007). The PERK and ATF6 arm of UPR has been confirmed to be activated in CDG type I patients <sup>13,25</sup>. Accumulated misfolded proteins are subsequently degraded by proteasomes to single amino acids, which were found to be increased in PMM2-CDG fibroblasts (Thiel et al, 2022). Ubiquitin proteasome system is also known to be regulated by UPR <sup>38</sup>.

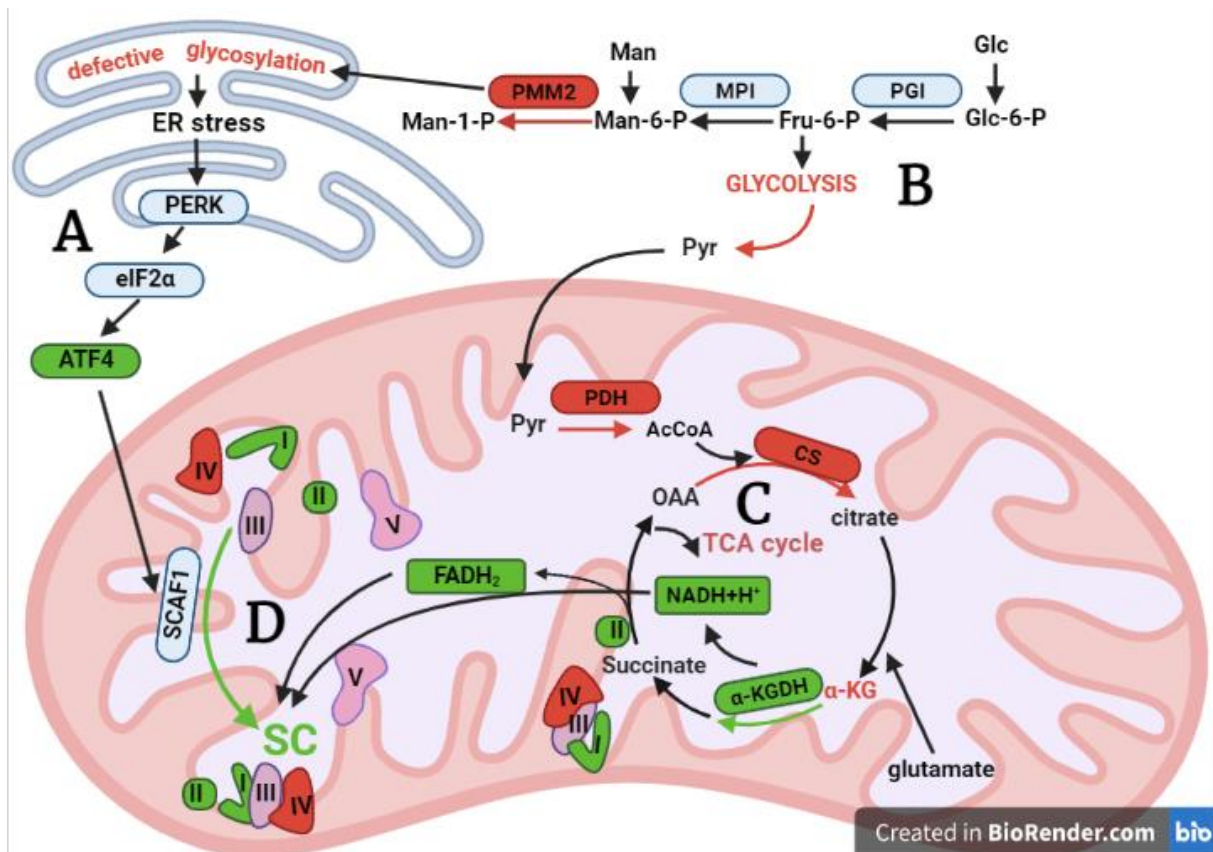


**Figure 7: Bioenergetic reorganization of PMM2 deficient cells.** **A)** Defective glycosylation leads to accumulation of unfolded proteins in ER and induces ER stress response. That initiates the PERK pathway and ATF4 activation. **B)** The glucose bioenergetics is suppressed leading to reduced glycolysis, lower pyruvate level and pyruvate dehydrogenase activity, together with the reduced activity and level of citrate synthase. **C)** The disruption of Krebs cycle is confirmed not only by citrate synthase attenuation, but also by succinyl dehydrogenase activation and stimulation of  $\alpha$ -ketoglutarate dehydrogenase ( $\alpha$ -KGDH). That results in increased production of reduced coenzymes necessary for proper oxidative phosphorylation. The sources of Krebs cycle intermediates include catabolized fatty acids, one carbon metabolites or amino acids from catabolized unfolded proteins. **D)** Increased assembly of respiratory chain complexes into supercomplexes caused by ER stress via PERK pathway activation. Red colour: down regulated, green colour: up regulated. I, II, III, IV- respiratory chain complex I, II, III, IV; V - ATP-synthase;  $\alpha$ -KG -  $\alpha$ -ketoglutarate;  $\alpha$ -KGDH -  $\alpha$ -ketoglutarate dehydrogenase; ATF4 - activating transcription factor; eIF2 $\alpha$  - eukaryotic initiation factor 2 alpha; ER - endoplasmic reticulum; Fru – fructose; Glc – glucose; SC - Supercomplex, TCA cycle – Krebs cycle; Man – mannose; MPI - mannose phosphate isomerase; OAA – oxalacetate; PERK - double-stranded RNA-dependent protein kinase (PRK)-like ER kinase; PGI - phosphoglucose isomerase; PMM2 - phosphomannomutase 2; Pyr – pyruvate; SCAF1- supercomplex assembly factor 1.

We inquired whether the activated ER stress has a detrimental impact on the cellular energy production, or, on the contrary, if it stimulates bioenergetic

reorganization in order to compensate for the consequences of a glycosylation defect. Surprisingly, a significant reduction in glycolysis together with glycolytic capacity (Figure 2) in PMM2-CDG fibroblasts was observed. The reduced utilization of glucose for the energy production could explain a slight decrease in pyruvate dehydrogenase (PDH) activity together with reduced pyruvate level in cell culture media (Figure 7B). Pyruvate level in primary PMM2-CDG fibroblast cells was found to be significantly increased (Thiel et al, 2022) supporting our findings of reduced PDH activity leading to pyruvate accumulation and suggesting an increase in pyruvate production by other pathways than glycolysis, such as metabolism of selected amino acids: alanine, glycine, threonine, which were found to be increased in PMM2-CDG fibroblasts but unchanged in patients' serum (Thiel et al, 2022).

We propose two possible explanations for the observed attenuation of glycolysis. One hypothesis starts with biotinidase (personal communication, Christian Thiel, CDG conference), which is an *N*-glycosylated enzyme that releases the coenzyme biotin necessary for the proper function of five carboxylases<sup>39,40</sup>. It has been published that mutation in biotinidase at the glycosylation site of the protein had an impact on its activity, which was reduced to 10 %<sup>41</sup>. Defective function of biotin containing propionyl CoA carboxylase leads to the accumulation of propionyl CoA, which can interact with oxalacetate and create methyl citrate<sup>42</sup>. Methyl citrate is known to inhibit one step in glycolysis, specifically phosphofructokinase activity<sup>43</sup>. Increased level of methyl citrate would explain not only reduced glycolysis in the patients' fibroblasts, but also reduced activity of citrate synthase (Figure 3B). We can only speculate whether methyl citrate is increased in PMM2-CDG patients' cells and whether it could be a cause of the metabolic reorganization that we have found, namely the reduction in glycolysis and reorganization of TCA cycle enzymes activities (described below). If that is true, there could be a new biomarker for PMM2-CDG possibly detectable from urine by mass spectrometry.

Another plausible mechanism underlying abnormal glycolysis is that the ER stress, which via UPR adjusts the extent of protein translation, might direct the flow of metabolites from glycolysis and the TCA cycle to the serine biosynthesis and to one-carbon metabolism to generate ATP<sup>44,45</sup>. 3-phosphoglycerate from glycolysis is used for serine biosynthesis to produce NADH via one-carbon metabolism.

Enzymes of serine biosynthesis are known to be transcriptionally induced in various stresses<sup>(46,47)</sup>. Produced NADH can then be used as an alternative fuel for complex I<sup>48</sup>. This would not only support the efficient synthesis of NADH for energy production by oxidative phosphorylation, but also ensure (via glycine synthesis) the availability of glutathione, which is needed during ER stress<sup>22,45</sup>.

Our data are in agreement with both aforementioned hypotheses.

Lower PDH (Figure 2C) probably leads to decreased acetyl CoA production, a necessary metabolite for TCA cycle and a substrate for citrate synthase (CS), which we found significantly decreased in its activity and level (Figure 3A and B, 7C). It was observed that the intracellular level of citrate is significantly higher in PMM2-CDG fibroblasts compared to controls (Thiel et al,2022), suggesting that not only citrate production via CS is reduced, but also its degradation. Noteworthy, aconitase, the enzyme converting citrate into isocitrate, was reported to be inhibited by a higher level of methyl citrate, as well as citrate synthase and isocitrate dehydrogenase<sup>43</sup>.

The ER stress was found to downregulate TCA cycle in cervical cancer cells<sup>45</sup> underpinning the requirement for alternative NADH production pathways. Our finding of boosted  $\alpha$ -KGDH activity (Figure 3) demonstrates the increased need for NADH production. It is presumably facilitated by redirection of glutamate, which is converted to  $\alpha$ -ketoglutarate by glutamate dehydrogenase, and by one-carbon metabolism<sup>45</sup>. It might explain increased respiratory chain complex I (CI) activity observed in our cells (Figure 4A) and in cells stressed by glucose starvation<sup>24</sup>.

TCA cycle is tightly connected with electron transport system. The succinate dehydrogenase (CII) plays a specific role in both pathways (Figure 7C). It was observed that with decreasing PMM2 activity (therefore also increasing severity of the disease) the Complex II activity was rising probably to compensate the defect (Figure S1). There is, to our best knowledge, yet no known correlation between CII and the UPR activation. We can expect that ER stress in PMM2-CDG is chronic, ie., not acute as was the case in most publications (such as Balsa et al, 2019<sup>24</sup>). We suggest that abnormal lipid metabolism could be involved, as it has been documented that UPR stimulates FA synthesis<sup>49</sup>. Also, higher levels of certain lipids were observed in PMM2-CDG patients' fibroblasts (Thiel et al, 2022). A shift

from glucose to fatty acids as energy sources <sup>50</sup> increases electron flux through FAD, which can lead to the CII increased activity <sup>51</sup> as observed in our cells (Figure 4B).

The decreased activity of another respiratory chain complex CIV (Figure 4D) could be due to disturbed changes in expression and assembly during ER stress <sup>52</sup>. The next explanation could be due to aforementioned biotinidase malfunction resulting in heme synthesis inhibition with subsequent reduction of respiratory chain complex IV level <sup>53</sup>.

Respiratory chain complexes can diffuse freely in the mitochondrial membrane as described by the fluid state model, but might also exist in a solid state creating supercomplexes <sup>54,55</sup>. It was described that the assembly of supercomplexes can increase mitochondrial respiration, and thus it is presumed that SCs are assembled when cells are stressed or in need to increase the mitochondrial respiration effectivity <sup>24</sup>. Our BN-PAGE investigation revealed increased level of supercomplexes of up to 150 % (Figure 6) in the PMM2-CDG fibroblasts, suggesting a requirement of higher respiratory efficiency (Figure 7D). Our findings are in concordance with the hypothesis described by Balsa et al., 2019 <sup>24</sup>, where they connect increased activity of mitochondrial respiratory chain complex I and increased level of supercomplexes (especially I and III) with ER stress. ATF4, which was confirmed to be upregulated in our cells, stimulates *SCAF1* expression <sup>24</sup>. Supercomplex assembly factor 1 (SCAF1) protein is thought to initiate assembly of SCs by connecting CIII and CIV <sup>50</sup>, however, the assembly and function of SCs together with SCAF1 role is under a great debate.<sup>56, 57,58</sup>. It is not clear whether SCAF1 is the main effector or whether other mechanisms of SCs assembly are stimulated by UPR, but increased assembly of SCs was confirmed in our PMM2-CDG patients (Figure 5).

More efficient assembly of SCs could be the reason why results of mitochondrial characterization such as cellular ATP production, MEGS analysis or mitochondrial DNA content show no difference between PMM2-CDG fibroblasts and controls (Figure 6C, D and E). Even though respiratory measurement presented reduced most of the respiratory states, the *FCR* normalization showed sustained mitochondrial quality (Figure 6A and B). The extent of compensation in other



tissues remains unknown, especially in organs with higher energetic demand, which are dominantly affected in CDG patients.

In conclusion, our findings suggest bioenergetics redirection in PMM2-CDG patients' fibroblast cell lines due to defective glycosylation leading to ER stress (see Fig 7). It results in higher supercomplexes assembly and increased activity of respiratory chain complexes I and II, together with adjustment of TCA cycle. We propose that the presented metabolic adaptation might apply to other *N*-glycosylation deficiencies. Further studies, especially in a more clinically relevant material (such as animal models) would be warranted, as well as investigation of the cellular bioenergetics in different types of glycosylation disorders.

Supported by institutional projects of Charles University (GAUK 110119 (LZ), Cooperatio - Paediatrics, SVV (LZ, TD, MV, NV), AZV MZ CR NU22-07-02-00474 (HH), GAČR-PMM2 (HH, NO, LZ), EURO-Glycanomics (HH, TH, LZ, CT), CELSA (HH).

Authors participation:

Acknowledgments:

We give a special thanks to Vaclav Capek for statistical data analysis and to Daniela Sedlackova and Petr Chrastina for technical support.

## References

1. Matthijs G, Schollen E, Pardon E, et al. Mutations in PMM2, a phosphomannomutase gene on chromosome 16p13 in carbohydrate-deficient glycoprotein type I syndrome (Jaeken syndrome). *Nat Genet.* 1997;16(1):88-92. doi:10.1038/ng0597-88
2. Matthijs G, Schollen E, Bjursell C, et al. Mutations in PMM2 that cause congenital disorders of glycosylation, type Ia (CDG-Ia). *Hum Mutat.* 2000;16(5):386-394. doi:10.1002/1098-1004(200011)16:5<386::AID-HUMU2>3.0.CO;2-Y
3. Zhang Z, Falk MJ. Integrated transcriptome analysis across mitochondrial disease etiologies and tissues improves understanding of common cellular adaptations to respiratory chain dysfunction. *Int J Biochem Cell Biol.* 2014;50:106-111. doi:10.1016/j.biocel.2014.02.012

4. Yang K, Huang R, Fujihira H, Suzuki T, Yan N. N-glycanase NGLY1 regulates mitochondrial homeostasis and inflammation through NRF1. *J Exp Med*. 2018;215(10):2600-2616. doi:10.1084/jem.20180783
5. Kong J, Peng M, Ostrovsky J, et al. Mitochondrial function requires NGLY1. *Mitochondrion*. Published online 2018. doi:10.1016/j.mito.2017.07.008
6. Pandey A, Adams JM, Han SY, Jafar-Nejad H. NGLY1 Deficiency, a Congenital Disorder of Deglycosylation: From Disease Gene Function to Pathophysiology. *Cells*. 2022;11(7):1-35. doi:10.3390/cells11071155
7. Parikh S, Goldstein A, Karaa A, et al. Patient care standards for primary mitochondrial disease: A consensus statement from the mitochondrial medicine society. *Genet Med*. 2017;19(12):1-18. doi:10.1038/gim.2017.107
8. Chang IJ, He M, Lam CT. Congenital disorders of glycosylation. *Ann Transl Med*. 2018;6(24):477. doi:10.21037/atm.2018.10.45
9. Filadi R, Theurey P, Pizzo P. The endoplasmic reticulum-mitochondria coupling in health and disease: Molecules, functions and significance. *Cell Calcium*. Published online 2017. doi:10.1016/j.ceca.2017.01.003
10. Zhang L, Yan F, Li L, et al. New focuses on roles of communications between endoplasmic reticulum and mitochondria in identification of biomarkers and targets. *Clin Transl Med*. 2021;11(11). doi:10.1002/ctm2.626
11. Rainbolt TK, Saunders JM, Wiseman RL. Stress-responsive regulation of mitochondria through the ER unfolded protein response. *Trends Endocrinol Metab*. 2014;25(10):528-537. doi:10.1016/j.tem.2014.06.007
12. Wang P, Li J, Sha B. The ER stress sensor PERK luminal domain functions as a molecular chaperone to interact with misfolded proteins. *Acta Crystallogr Sect D Struct Biol*. 2016;72(12):1290-1297. doi:10.1107/S2059798316018064
13. Lecca MR, Wagner U, Patrignani A, Berger EG, Hennet T. Genome-wide analysis of the unfolded protein response in fibroblasts from congenital disorders of glycosylation type-I patients. *FASEB J Off Publ Fed Am Soc Exp Biol*. 2005;19(2):240-242. doi:10.1096/fj.04-2397fje
14. Frakes AE, Dillin A. The UPR(ER): Sensor and Coordinator of Organismal Homeostasis. *Mol Cell*. 2017;66(6):761-771. doi:10.1016/j.molcel.2017.05.031

15. Lin JH, Li H, Yasumura D, et al. IRE1 signaling affects cell fate during the unfolded protein response. *Science*. 2007;318(5852):944-949. doi:10.1126/science.1146361
16. Senft D, Ronai ZA. UPR, autophagy, and mitochondria crosstalk underlies the ER stress response. *Trends Biochem Sci*. 2015;40(3):141-148. doi:10.1016/j.tibs.2015.01.002
17. Kang S-W, Rane NS, Kim SJ, Garrison JL, Taunton J, Hegde RS. Substrate-specific translocational attenuation during ER stress defines a pre-emptive quality control pathway. *Cell*. 2006;127(5):999-1013. doi:10.1016/j.cell.2006.10.032
18. Hollien J, Weissman JS. Decay of endoplasmic reticulum-localized mRNAs during the unfolded protein response. *Science*. 2006;313(5783):104-107. doi:10.1126/science.1129631
19. Rutkowski DT, Kaufman RJ. That which does not kill me makes me stronger: adapting to chronic ER stress. *Trends Biochem Sci*. 2007;32(10):469-476. doi:10.1016/j.tibs.2007.09.003
20. Ron D, Walter P. Signal integration in the endoplasmic reticulum unfolded protein response. *Nat Rev Mol Cell Biol*. 2007;8(7):519-529. doi:10.1038/nrm2199
21. Walter P, Ron D. The unfolded protein response: from stress pathway to homeostatic regulation. *Science*. 2011;334(6059):1081-1086. doi:10.1126/science.1209038
22. Harding HP, Zhang Y, Zeng H, et al. An integrated stress response regulates amino acid metabolism and resistance to oxidative stress. *Mol Cell*. 2003;11(3):619-633. doi:10.1016/s1097-2765(03)00105-9
23. Bao XR, Ong S-E, Goldberger O, et al. Mitochondrial dysfunction remodels one-carbon metabolism in human cells. *Elife*. 2016;5. doi:10.7554/eLife.10575
24. Balsa E, Soustek MS, Thomas A, et al. ER and Nutrient Stress Promote Assembly of Respiratory Chain Supercomplexes through the PERK-eIF2 $\alpha$  Axis. *Mol Cell*. 2019;74(5):877-890.e6. doi:10.1016/j.molcel.2019.03.031
25. Yuste-Checa P, Vega AI, Martín-Higueras C, et al. DPAGT1-CDG: Functional analysis of disease-causing pathogenic mutations and role of endoplasmic reticulum stress. *PLoS One*. 2017;12(6):e0179456. doi:10.1371/journal.pone.0179456

26. Brantová O, Tesařová M, Hansíková H, Elleder M, Zeman J, Sládková J. Ultrastructural changes of mitochondria in the cultivated skin fibroblasts of patients with point mutations in mitochondrial DNA. *Ultrastruct Pathol*. Published online 2006. doi:10.1080/01913120600820112
27. Ondruskova N, Honzik T, Kolarova H, et al. Aberrant apolipoprotein C-III glycosylation in glycogen storage disease type III and IX. *Metabolism*. 2018;82:135-141. doi:10.1016/j.metabol.2018.01.004
28. Zdrzilova L, Hansikova H, Gnaiger E. Comparable respiratory activity in attached and suspended human fibroblasts. *PLoS One*. 2022;17(3):e0264496. doi:10.1371/journal.pone.0264496
29. Lawson AM, Chalmers RA. *Organic Acids in Man: The Analytical Chemistry, Biochemistry and Diagnosis of the Organic Acidurias.*; 1982.
30. Sheu KF, Hu CW, Utter MF. Pyruvate dehydrogenase complex activity in normal and deficient fibroblasts. *J Clin Invest*. 1981;67(5):1463-1471. doi:10.1172/jci110176
31. Lowry. Lowry Protein Assay. *J Biol Chem*. Published online 1951.
32. Rustin P, Chretien D, Bourgeron T, et al. Biochemical and molecular investigations in respiratory chain deficiencies. *Clin Chim Acta*. 1994;228(1):35-51. doi:10.1016/0009-8981(94)90055-8
33. Janssen AJM, Trijbels FJM, Sengers RCA, et al. Measurement of the energy-generating capacity of human muscle mitochondria: diagnostic procedure and application to human pathology. *Clin Chem*. 2006;52(5):860-871. doi:10.1373/clinchem.2005.062414
34. Vanisova M, Stufkova H, Kohoutova M, et al. Mitochondrial organization and structure are compromised in fibroblasts from patients with Huntington's disease. *Ultrastruct Pathol*. Published online 2022. doi:10.1080/01913123.2022.2100951/SUPPL\_FILE/IUSP\_A\_2100951\_SM1658.D OCX
35. Pejznochova M, Tesarova M, Hansikova H, et al. Mitochondrial DNA content and expression of genes involved in mtDNA transcription, regulation and maintenance during human fetal development. *Mitochondrion*. 2010;10(4):321-329. doi:10.1016/j.mito.2010.01.006

36. Danhelovska T, Kolarova H, Zeman J, et al. Multisystem mitochondrial diseases due to mutations in mtDNA-encoded subunits of complex I. *BMC Pediatr.* 2020;20(1):1-13. doi:10.1186/s12887-020-1912-x
37. Bernales S, McDonald KL, Walter P. Autophagy counterbalances endoplasmic reticulum expansion during the unfolded protein response. *PLoS Biol.* 2006;4(12):2311-2324. doi:10.1371/journal.pbio.0040423
38. Darom A, Bening-Abu-Shach U, Broday L. RNF-121 is an endoplasmic reticulum-membrane E3 ubiquitin ligase involved in the regulation of beta-integrin. *Mol Biol Cell.* 2010;21(11):1788-1798. doi:10.1091/mbc.e09-09-0774
39. Wolf B, Grier RE, Secor McVoy JR, Heard GS. Biotinidase deficiency: a novel vitamin recycling defect. *J Inherit Metab Dis.* 1985;8 Suppl 1:53-58. doi:10.1007/BF01800660
40. Tong L. Structure and function of biotin-dependent carboxylases. *Cell Mol Life Sci.* 2013;70(5):863-891. doi:10.1007/s00018-012-1096-0
41. Pomponio RJ, Yamaguchi A, Arashima S, Hymes J, Wolf B. Mutation in a putative glycosylation site (N489T) of biotinidase in the only known Japanese child with biotinidase deficiency. *Mol Genet Metab.* 1998;64(2):152-154. doi:10.1006/mgme.1998.2706
42. Ando T, Rasmussen K, Wright JM, Nyhan WL. Isolation and identification of methylcitrate, a major metabolic product of propionate in patients with propionic acidemia. *J Biol Chem.* 1972;247(7):2200-2204. doi:10.1016/s0021-9258(19)45512-9
43. Cheema-Dhadli S, Leznoff CC, Halperin ML. Effect of 2-methylcitrate on citrate metabolism: implications for the management of patients with propionic acidemia and methylmalonic aciduria. *Pediatr Res.* 1975;9(12):905-908. doi:10.1203/00006450-197512000-00008
44. Kalhan SC, Hanson RW. Resurgence of serine: an often neglected but indispensable amino acid. *J Biol Chem.* 2012;287(24):19786-19791. doi:10.1074/jbc.R112.357194
45. Rendleman J, Cheng Z, Maity S, et al. New insights into the cellular temporal response to proteostatic stress. *Elife.* 2018;7:1-37. doi:10.7554/eLife.39054

46. Zhao E, Ding J, Xia Y, et al. KDM4C and ATF4 Cooperate in Transcriptional Control of Amino Acid Metabolism. *Cell Rep.* 2016;14(3):506-519. doi:10.1016/j.celrep.2015.12.053
47. Zhou X, He L, Wu C, Zhang Y, Wu X, Yin Y. Serine alleviates oxidative stress via supporting glutathione synthesis and methionine cycle in mice. *Mol Nutr Food Res.* 2017;61(11). doi:10.1002/mnfr.201700262
48. Vazquez A, Markert EK, Oltvai ZN. Serine Biosynthesis with One Carbon Catabolism and the Glycine Cleavage System Represents a Novel Pathway for ATP Generation. *PLoS One.* 2011;6(11):25881. doi:10.1371/journal.pone.0025881
49. Jacquemyn J, Cascalho A, Goodchild RE. The ins and outs of endoplasmic reticulum-controlled lipid biosynthesis. *EMBO Rep.* 2017;18(11):1905-1921. doi:10.15252/embr.201643426
50. Lapuente-Brun E, Moreno-Loshuertos R, Acín-Pérez R, et al. Supercomplex assembly determines electron flux in the mitochondrial electron transport chain. *Science.* 2013;340(6140):1567-1570. doi:10.1126/science.1230381
51. Guarás A, Perales-Clemente E, Calvo E, et al. The CoQH2/CoQ Ratio Serves as a Sensor of Respiratory Chain Efficiency. *Cell Rep.* 2016;15(1):197-209. doi:10.1016/j.celrep.2016.03.009
52. Hori O, Ichinoda F, Tamatani T, et al. Transmission of cell stress from endoplasmic reticulum to mitochondria: Enhanced expression of Lon protease. *J Cell Biol.* 2002;157(7):1151-1160. doi:10.1083/jcb.200108103
53. Atamna H, Newberry J, Erlitzki R, Schultz CS, Ames BN. Biotin deficiency inhibits heme synthesis and impairs mitochondria in human lung fibroblasts. *J Nutr.* 2007;137(1):25-30. doi:10.1093/jn/137.1.25
54. Jha P, Wang X, Auwerx J. Analysis of Mitochondrial Respiratory Chain Supercomplexes Using Blue Native Polyacrylamide Gel Electrophoresis (BN-PAGE). *Curr Protoc Mouse Biol.* 2016;6(1):1-14. doi:10.1002/9780470942390.mo150182
55. Schon EA, Dencher NA. Heavy Breathing: Energy Conversion by Mitochondrial Respiratory Supercomplexes. *Cell Metab.* 2009;9(1):1-3. doi:10.1016/J.CMET.2008.12.011

56. Fernández-Vizarra E, Ugalde C. Cooperative assembly of the mitochondrial respiratory chain. *Trends Biochem Sci*. Published online August 2022. doi:10.1016/j.tibs.2022.07.005
57. Calvo E, Cogliati S, Hernansanz-Agustín P, et al. Functional role of respiratory supercomplexes in mice: SCAF1 relevance and segmentation of the Qpool. *Sci Adv*. 2020;6(26). doi:10.1126/sciadv.aba7509
58. Vercellino I, Sazanov LA. Structure and assembly of the mammalian mitochondrial supercomplex CIII(2)CIV. *Nature*. 2021;598(7880):364-367. doi:10.1038/s41586-021-03927-z

## Supplementary data:

**Table S1A: Used antibodies for WB-SDS/PAGE**

primary	VDAC	Abcam	14734	1:2000
	citratesynthase	Abcam	96600	1:2000
	ATF4	Proteintech	10835-1-AP	1:1000
	$\beta$ -actin	Cell Signaling	4970	1:1000
secondary	anti-rabbit IgG	Sigma Aldrich	A0545	1:2500

**Table S1B: Used antibodies for BN-PAGE**

PMM2 patients DDM-solubilized BN-PAGE (fibroblasts)	NDUFA9	Abcam	14713	1:2000
	SDHA	MitoScience	MS204	1:10000
	SDHB	Abcam	14714	1:10000
	CORE2	Abcam	14745	1:8000
	COXI	Abcam	14705	1:4000
	ATP $\beta$	Abcam	14730	1:5000
	VDAC1	Abcam	14734	1:2000
PMM2 patients DIG-solubilized BN-PAGE (fibroblasts)	NDUFA9	Abcam	14713	1:2000
	NDUFB6	Abcam	110244	1:2000
	SDH70	Abcam	14715	1:10000
	CORE2	Abcam	14745	1:8000
	COXI	Abcam	14705	1:4000

**Table S2: The list of mitochondrial energy generating system reactions with added substrates and radiolabeled substrates.**

1	[1- <sup>14</sup> C]Pyruvate+Malate+ADP
2	[1- <sup>14</sup> C]Pyruvate+Carnitine+ADP
3	[1- <sup>14</sup> C]Pyruvate+Malate-ADP
4	[1- <sup>14</sup> C]Pyruvate+Malate-ADP+CCCP
5	[1- <sup>14</sup> C]Pyruvate+Malate+ADP+Atractyloside
6	[U- <sup>14</sup> C]Malate+Pyruvate+Malonate+ADP
7	[U- <sup>14</sup> C]Malate+Acetylcarnitine+Malonate+ADP
8	[U- <sup>14</sup> C]Malate+Acetylcarnitine+Artenite+ADP
9	[1,4- <sup>14</sup> C]Sukcinate+Acetylcarnitine+ADP



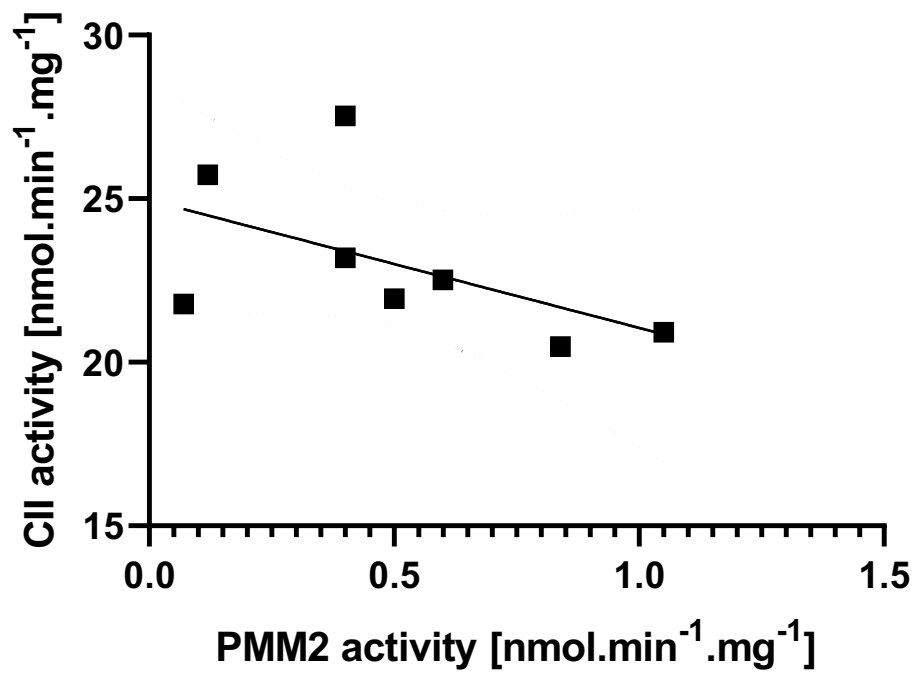


**Figure S1: Correlation between measured PMM2 activity and activity of respiratory chain Complex II.** There is a correlation between increasing Complex II activity with decreasing PMM2 activity.